NOVEL CONDUCTIVE ADHESIVES FOR ELECTRONIC PACKAGING APPLICATIONS: A WAY TOWARDS ECONOMICAL, HIGHLY CONDUCTIVE, LOW TEMPERATURE AND FLEXIBLE INTERCONNECTS

A Thesis
Presented to
The Academic Faculty

by

Rongwei Zhang

In Partial Fulfillment
of the Requirements for the Degree
Doctor of Philosophy in the
School of Chemistry and Biochemistry

Georgia Institute of Technology
May 2011

NOVEL CONDUCTIVE ADHESIVES FOR ELECTRONIC PACKAGING APPLICATIONS: A WAY TOWARDS ENCONOMICAL, HIGHLY CONDUCTIVE, LOW TEMPERATURE, AND FLEXIBLE INTERCONNECTS

Approved by:

Dr. C. P. Wong, Advisor
School of Materials Science and Engineering
Georgia Institute of Technology

Dr. Joseph Perry
School of Chemistry and Biochemistry
Georgia Institute of Technology

Dr. Jean-Luc Brédas
School of Chemistry and Biochemistry
Georgia Institute of Technology

Dr. Z. John Zhang
School of Chemistry and Biochemistry
Georgia Institute of Technology

Dr. David M. Collard
School of Chemistry and Biochemistry
Georgia Institute of Technology

Date Approved: [Mar 11, 2011]

This dissertation is dedicated to my parents, my sisters and my wife Ruijie Chai for their love, support, and encouragement

ACKNOWLEDGEMENTS

I would like to express my sincere gratitude to my advisor, Dr. C. P. Wong for his guidance, support, and encouragement throughout the course of this research. His dedication to work and expertise in electronics packaging area have been a great source of inspiration for me. I would like specially thank my previous advisor Dr. Boris Mizaikoff for his guidance and support during my second-year PhD study. I would like to extend my gratitude to Dr. Jean-Luc Brédas, Dr. David Collard, Dr. Joseph Perry and Dr. Z. John Zhang for serving on my thesis committee and providing invaluable suggestions and recommendations.

I would like to thank the following faculty, administrator and staff in the School of Chemistry & Biochemistry, the School of Materials Science & Engineering, the Office of International Education, and Microelectronics Packaging Research Center for their help and support. They are Ms. Katie Tudini, Dr. Cam Tyson, Dr. Andrew Lyon, Dr. Dennis Hess, Dr. Facundo M. Fernandez, Dr. David Bostwick, Dr. Donald F. Doyle, Dr. Uwe H. F. Bunz, Dr. Mary Peek, Dr. Meilin Liu, Mr. Rusty Edwards, Dr. Benjamin Findley, Dr. Yolande Berta, Dr. Rao Tummala, Mr. Dean Sutter, Ms. Karen H. Mayo, Ms. Nancy Pinion, Ms. Angie Beggs, Ms. Shirley Manchester, Ms. Jasmin Frett-Hodge, Ms. Jyoti Ghosh, Ms. Hope Payne and Ms. Sheri Calhoun.

I would like to thank the program managers and collaborators. They are Dr. Stefanie Lotz, Dr. Ning-Cheng Lee, Dr. David Lu, Dr. Venky Sundaram, Dr. Daniela Staiculescu, Dr. Li Yang, Ms. Giulia Orecchini, Dr. Manos Tentzeris, Dr. Hongsik

Hwang, Dr. Lee Kresge, Mr. Abhishek Choudhury, Dr. Andrew Hunt, Dr. Ganesh Venugopal, and Dr. Wenbin Xu.

I would like to acknowledge the input and help I received from my fellow co-workers, especially Dr. Kyoung-sik Moon, Dr. Yi Li, Mr. Wei Lin, and Mr. Josh Agar. I also thank the following colleagues for their help: Dr. Hongjin Jiang, Myung Jin Yim, Dr. Jiongxin Lu, Dr. Yonghao Xiu, Dr. Lingbo Zhu, Mr. Owen Hildreth, Mr. Qizhen Liang, Ms. Yan Liu, Ms. Zhuo Li, Mr. Zhiyin Lin, Mr. Wentian Gu, Ms. Fan Cai, Ms. Guseul Yun, Dr. Daoqiang Lu, Dr. Yangyang Sun, Dr. Cheng Yang, Dr. Mingxiang Chen, Dr. Yagang Yao, Dr. Jintang Shang, Dr. Christine Kranz, Dr. Seong-Soo Kim, Dr. Shuting Wei, Dr. Liqun Wang, Dr. Jean-Francois Masson, Dr. Nicola Menegazzo, Dr. Gary Dobbs, Dr. Justyna Wiedemair, Dr. Christina Young, Dr. Jong-Seok Moon, Dr. Yuliya Luzinova, and Ms. Tinsley Selina. I would like to thank the undergraduate students who worked hard with me during my PhD study. They are Mr. Kevin Lawrence, Mr. Shaun Zhang, Mr. Jeremy Moskowitz, Mr. John Guthrie, and Mr. Nick Knowles. I would like to thank my friends like Dr. Yi Gao, Mr. Yimin Zhang, Dr. Zhengchun Peng, Mr. Fengshou Zhang, and Dr. Wei Chen.

I would like to thank Intel Corporation, Nokia Corporation, Indium Corporation of America, National Science Foundation, Nanolumens, Membership Companies of Packaging Research Center at Georgia Tech, Environmental Protection Agency, and ASE Group for financial supports of this work. And I thank nGimat Corporation, Ferro Corporation, Lindau Chemicals and Technic Inc. for their supply of materials.

Special thanks go to my parents, my sisters, and my wife Ruijie Chai for their love and encouragement. Without them, this dissertation would not be possible.

TABLE OF CONTENTS

LIST OF TABLES

LIST OF FIGURES

SUMMARY

With the new emphasis on green and sustainable technologies, research into the science and engineering of interconnect materials has changed dramatically. Isotropically conductive adhesives (ICAs) have been identified as a promising lead-free interconnect material. They offer many advantages over traditional solder technology, including environmental friendliness, lower temperature processing, fewer processing steps, low stress on a substrate, flexibility and stretchability, and reduced cost. However, compared with tin/lead solder (Resistivity: $1.5\text{-}3\times10^{-5}$ Ω cm), one of the main disadvantages of ICAs is their higher resistivity (>1×10^{-4} Ω cm at 80 wt% loading of silver flakes).

This dissertation starts with an understanding of the interface between conductive fillers and the electrical conduction mechanism of ICAs (Chapter 1). The first part of this dissertation, including chapters 2-4, introduces how sintering technology reduces and eliminates the contact resistance between conductive fillers and develops highly conductive adhesives to meet specific applications. It is found that the surface residue on the surface of silver nanoparticles plays a key role in the sintering of silver nanoparticles. The surface chemistry and the thermal behavior of silver nanoparticles were studied and correlated with the electrical resistivity of the ICAs filled with these silver nanoparticles. It is found that silver nanoparticles with lower decomposition temperatures and lower content of surface residues are more promising for the development of highly conductive adhesives. Then, a further optimization of the synthesis of silver nanoparticles is conducted for the fast preparation of highly conductive ICAs. The fast preparation is compatible with the industrial reflow process. It is found the fast sintering is attributed to:

(1) the thermal decomposition of the silver carboxylate present on the surface of the incorporated silver flakes forming in situ highly reactive silver nanoparticles; (2) the surface activation of the incorporated silver nanoparticles by the removal of surface residues. As a result, ICAs prepared at 230 ^{o}C for 5 minutes, at 260 ^{o}C for 10 minutes and using a typical lead-free solder reflow process show electrical resistivities of 8.1×10^{-5}, 6.0×10^{-6} and 6.3×10^{-5} Ω cm, respectively. The problems associated with the incorporation of silver nanoparticles are resolved by in-situ reduction of silver carboxylate on the surface of silver flakes by a flexible epoxy (diglycidyl ether of prolypropylene glycol). The flexible epoxy enables the sintering between silver flakes and can be used to produce flexible highly conductive adhesives at 150 ^{o}C.

The second part of this dissertation is to replace expensive silver flakes with low cost silver-coated copper flakes (chapters 5-6). Two low cost ICAs filled with silver-coated copper flakes are developed. The first is an anhydride-cured ICA filled with silver-coated copper flakes modified with N-phenylaminopropyltrimethoxylsilane and the second is an amine-cured ICA filled with untreated silver-coated copper flakes. Compared with anhydride-cured ICAs filled with untreated silver-coated copper flakes (1.3×10^{-3} Ω cm), the two new ICAs showed a much lower resistivity (about 2×10^{-4} Ω cm). The resistivity of the two ICAs developed is comparable to that of commercial silver-filled ICAs. The anhydride-cured ICAs filled with modified silver-coated copper flakes showed a stable contact resistance on a Ni/Au surface during 85 ^{o}C/85% RH (relative humidity) aging for more than 1000 h. The amine-cured ICAs filled with untreated silver-coated copper flakes showed stable bulk resistivity during 85 ^{o}C/85% RH

aging for more than 1000 h. The origin of the much lower resistivity and better reliability of the developed ICAs are discussed.

The findings and insights in this dissertation significantly contribute to (1) the in-depth understanding of filler-filler, filler-polymer and structure-property relationships of ICAs; (2) the structural design and formulation of high performance ICAs; and (3) the wider use of ICAs in emerging applications such as printed electronics and solar cells.

CHAPTER 1

INTRODUCTION

This chapter gives a brief introduction of electronic packaging technologies. The prime objective of this chapter is to provide a fundamental understanding of isotropically conductive adhesive (ICA) technology and to identify its opportunities and challenges in electrical interconnects. This chapter summarizes the approaches to improve the electrical conductivity and to enhance the adhesion strengths on metal surfaces since these properties are key parameters for ICA applications. This chapter also includes the outline of the research goals and selected approaches to develop high performance ICAs for solder replacement.

1.1 A Brief Overview of Electronic Packaging

As microelectronics is driven towards lower cost, higher performance and portability, packaging of electronic circuits, i.e. electronic packaging, has become an increasingly important area of microelectronic technology. Electronic packaging is defined as bridge that interconnects integrated circuit (IC) and other components into a system-level board to form electronic products [1]. It provides four functions:

- Signal distribution, involving mainly topological and electromagnetic consideration;
- Power distribution, involving electromagnetic, structural and materials aspects
- Heat dissipation (cooling), involving structural and materials consideration.
- Mechanical, chemical, and electromagnetic protection of components and interconnections.

Electronic packaging is typically divided into four levels [2-3], as shown in Figure 1.1:

- Level 0: semiconductor chip level (integrated circuit (IC)).
- Level 1: chip in a carrier. In first level of packaging, an IC die is assembled into a package carrier (substrate or lead frame) with interconnection materials (such as conductive adhesives and solders) using wire bonding, tape automated bonding or flip chip assembly techniques. The IC die is protected by either a lid or encapsulated with a polymer mold.
- Level 2: the packaged IC die mounted to a printed-circuit board (PCB) or to another type of substrate.
- Level 3: board-to-board interconnects.

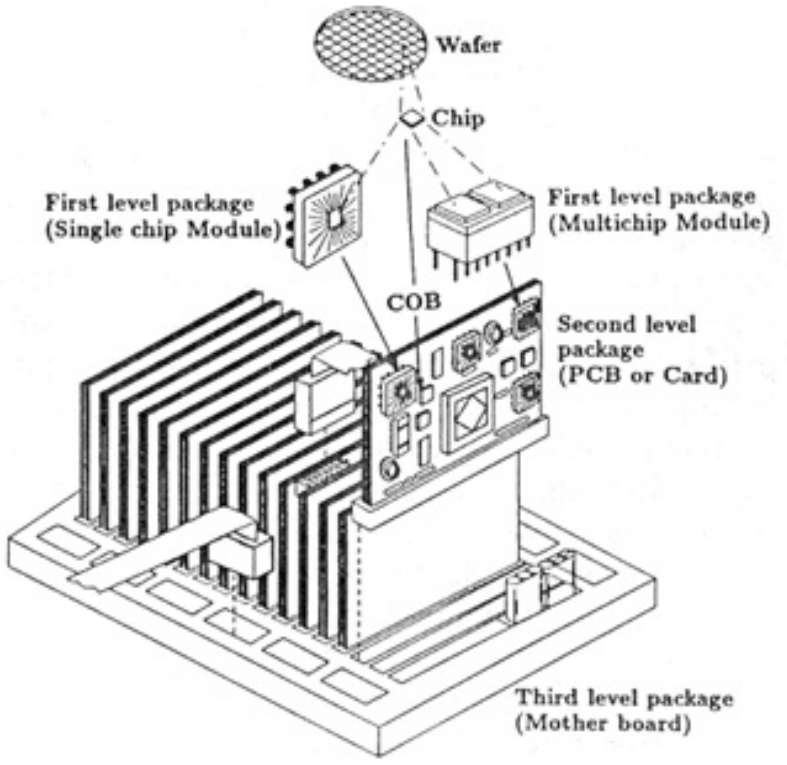

Figure 1.1 Levels of electronic packaging [3].

Electronic packaging technologies are evolving rapidly to meet the trends of lower cost, smaller form factor and higher performance. These trends require decreased pitch (the distance between two bumps), increased numbers of input/output (I/O), improved electrical performance, more effective thermal interface, software system to design and model the assembly, and most importantly, a variety of high performance packaging materials to make ever-changing requirements happen. Among these packaging materials, electrical interconnect materials are one of the most important packaging materials as they strongly affect the performance of electronic devices.

1.2 Introduction to Electrically Conductive Adhesive

The semiconductor electronic industry has made considerable advances over the past few decades, while the essential requirements for interconnects in electronic systems remained unchanged. Electrical components need to be electrically connected for power, ground and signal transmissions. In spite of the toxicity of lead, lead-containing solder, especially eutectic tin/lead (Sn/Pb) solder alloy, has been the de facto interconnect material in most areas of electronic packaging. These interconnection technologies include pin through hole (PTH), surface mount technology (SMT), ball grid array (BGA) package, chip scale package (CSP) and flip chip technology [4-6].

With the new emphasis on green and sustainable technologies, research into science and engineering of interconnect materials has changed dramatically. Research efforts have focused on two lead-free alternatives, lead-free metal solder alloys and polymer-based Electrically Conductive Adhesives (ECAs) [7-9]. A number of lead-free solder alloys have found their way in commercial products. However, these lead-free solders possess technical limits, such as processibility, wetting capability, mechanical properties,

fatigue and thermal behavior. Most significantly, current commercially available lead-free solders chosen by the majority of the US electronic industry, such as tin/silver (Sn/Ag) and tin/silver/copper (Sn/Ag/Cu), have higher melting temperatures (~220 °C) than eutectic tin-lead solder (183 °C). The higher melting temperatures result in solder reflow temperatures from 230 °C to over 260 °C. These higher processing temperatures severely limit the applicability of lead-free solders to organic/polymer packaged components and low cost printed circuit board (PCB) substrates. Moreover, the exposure of electronics to higher temperatures degrades component reliability. In addition, high reflow temperatures increase energy consumption and consequently the costs. Some low melting point lead-free alloys have been developed such as Sn/In (T_m, 120 ^oC) and Sn/Bi (T_m, 138 ^oC) [10]. However, their material properties and processibility are still of concern.

ECAs are the ideal interconnect alternative to lead containing solder materials. ECA mainly consists of a polymeric resin (epoxy, silicone, polyurethane or polyimide) that provides physical and mechanical properties such as adhesion, mechanical strength, impact strength, and metal fillers (silver, gold, nickel or copper) that conduct electricity. Depending on the filler loading level, ECAs can be categorized into isotropically conductive adhesives (ICAs) and anisotropically conductive adhesives/films (ACAs/ACFs) as shown in Figure 1.2. ICAs are electrically conductive along all the directions. In an ICA the loading level (25-30 vol%) of conductive fillers (commonly silver flakes) exceeds the percolation threshold. On the other hand, ACAs/ACFs provide unidirectional electrical conductivity in the vertical or z-axis. ACAs/ACFs have a relatively low filler loading (usually 5-10 vol%). The loading level of ACAs/ACFs is far

below the percolation threshold; the low filler loading is insufficient for inter-particle contact, which prevents conductivity in the x–y plane of the adhesives. In addition to ICAs and ACAs/ACFs, non-conductive adhesives/films (NCAs/NCFs) have also been developed recently. Instead of using electrically conductive fillers to establish the conductive joints, the direct and physical contact between two surfaces of the IC bump and the pad of substrates can be made under high bonding pressures and heat. The significant advantages of ACAs/ACFs and NCAs/NCFs lies in their fine-pitch capability. Different adhesives are being adapted as interconnect materials for surface mount technology processes, such as chip on glass (COG), chip on flex (COF) and flip-chip bonding technologies in electronic packaging industries [4-6].

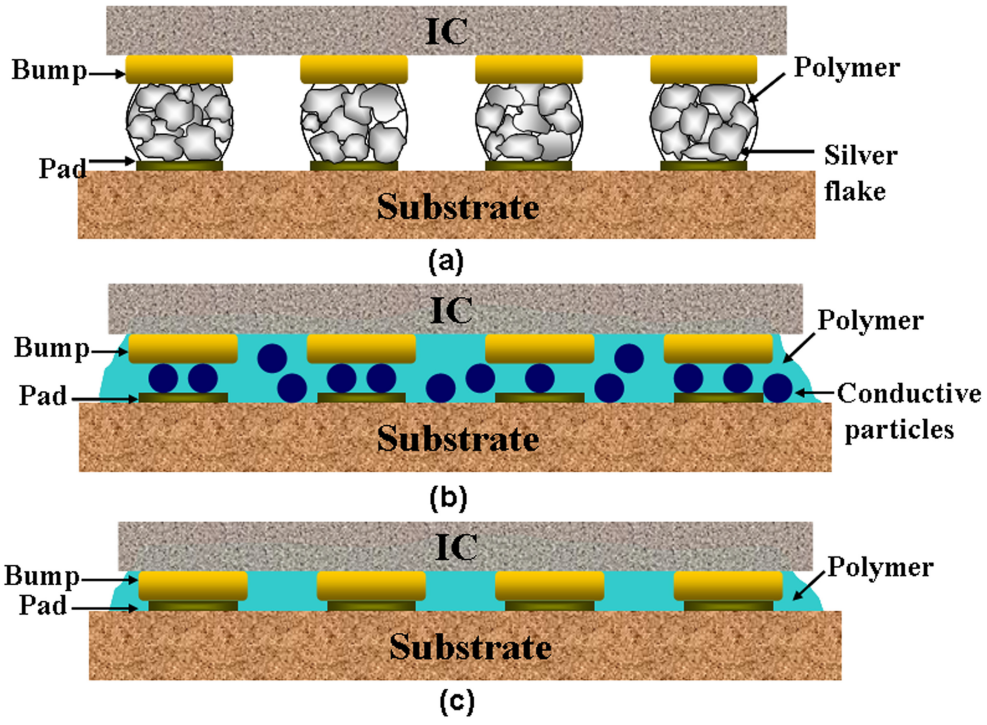

Figure 1.2 Schematic illustrations of (a) ICAs, (b) ACAs/ACFs and (c) NCFs.

Table 1.1 summarizes the advantages and limitations of both solder and conductive adhesive technologies. Although solder technology are still widely used today, in the drive toward lower costs, higher densities and further miniaturization, conductive adhesives have replaced them in many applications, especially for those where low processing temperature and flexibility of the interconnect are required [11].

Table 1.1 Comparisons of solder with conductive adhesives [11]

Connection Method	Advantages	Limitations
Solder	• Batch process • Automated dispensing or screen-printing • Automated reflow • Long history of use/mature process • Easy rework • Good electrical connections • Good thermal conductions	• Requires flux • Risk of flux residues and corrosion • Concern over toxicity of lead • Corrosion of solder in humidity, if not overcoated • Risk of voids under large component • Stress due to large CTE mismatches • High temperature exposure during solder reflow (220-260 ^{o}C) • Limited wetting and adhesion to some surface (e.g. glass)
Conductive adhesive	• Low processing temperature • Fine-pitch capability • Automated dispensing or screen-printing • Application-specific formulations • Wide variety of commercially available products to choose from • Ability to relieve stress • Excellent adhesion to most surfaces	• Lower electrical and thermal conductivities compared with solder • Risk of outgassing in enclosed packages and for space hardware • Most require moderate to long cures (1-2 h) • Limited thermal stability • Finite absorption of moisture

Table 1.1 continued

	• Snap cure types cure in seconds (160-200 ^{o}C) • Directional conductivity with anisotropic forms May be reworkable	

1.3 Isotropically Conductive Adhesive (ICA) Technology

ICAs, also called "polymer solders", are composites of a polymer matrix and conductive fillers. Compared to metal solder technology, ICAs offer numerous advantages, such as environmental friendliness (elimination of lead usage and flux cleaning), mild processing conditions, fewer processing steps (reducing processing cost), and low stress on the substrates [4-6]. However, like all other lead-free materials, ICAs have some limitations, such as lower electrical and thermal conductivities compared to solder joints, conductivity fatigue in reliability tests, limited current carrying capability, poor impact performance, etc. [4-6]. Table 1.2 shows a general comparison between tin-lead solder and generic commercialized ICAs [8]. Note that the performance of ICAs is strongly dependent on the filler loading level, polymer matrix, the interaction between fillers and polymer matrix, processing conditions, etc. In recognition of the importance and challenges of ICAs, worldwide efforts have been devoted to research and development of various high performance ICAs.

Table 1.2 Conductive adhesives compared with solder [8]

Characteristic	Sn/Pb solder	ICA
Volume resistivity (Ω cm)	0.000015	0.00035
Typical junction R (mΩ)	10-15	<25

Table 1.2 continued

Thermal conductivity (W/m K)	30	3.5
Shear strength (psi)	>2200	2000
Finest pitch (mil)	12	<6-8
Minimum processing temperature (^{o}C)	215	150-170
Environmental impact	Negative	Very minor
Thermal fatigue	Yes	Minimal

1.3.1 Basic Compositions of ICAs

The formulation of ICAs may involve resin, curing agent, catalyst, conductive filler and various additives. These additives include antioxidants, corrosion inhibitors, adhesion promoters, rheological additives and wetting agents. However, there are two basic compositions: adhesive matrix and conductive filler.

1.3.1.1 Adhesive Matrices

Polymer matrices are used to form mechanical bonds at an interconnection. Both thermosetting and thermoplastic polymers have been used in ICA formulations. Thermoplastic polymers are rigid materials at temperatures below their glass transition temperature (T_g). Above the T_g, these polymers exhibit flow characteristics. Thus, the T_g of polymer matrices for ICAs must be sufficiently high to avoid polymer flow during the application conditions. Furthermore, the T_g of polymer matrice for ICAs must also be low enough to prevent thermal damage associated with chip carrier and devices during assembly. The main thermoplastic resin used in ICA formulations is polyimide resin. Thermoplastic polymers are particularly advantageous in their ease of processibility and reworkability. A major drawback of thermoplastic ICAs is the degradation of adhesion at high temperatures. Another drawback of polyimide-based ICAs is that they generally contain solvents. During heating, voids are formed when the solvent evaporates.

Thermosetting polymers are cross-linked polymers that have an extensive three-dimensional molecular structure. The three-dimensional structure is a result of curing reactions between resins and hardeners under specific conditions such as heat, UV light, microwave, moisture, etc. During the curing process, volumetric shrinkage occurs as the distance between molecules changing from van der Waals distance to a covalent distance. The shrinkage during the curing process causes the intimate contact between conductive fillers, contributing to improved electrical conductivity. The ability to maintain strength at high temperatures and robust adhesive bonds are the principal advantages of these materials. However, because the cure reaction is not reversible, rework or repair of interconnections is not an option [12-13].

Epoxy resins, such as glycidyl ether of bisphenol F (DGEBF, Figure 1.3), are the most widely used in thermosetting ICA formulations due to their superior combined properties such as excellent adhesion, chemical and heat resistance and excellent mechanical properties. Epoxy resins can be cured with either hardeners such as carboxylic anhydrides (such as 4-methylhexahydrophthalic anhydride (MHHPA, Figure 1.3), cycloaliphatic or aromatic amines, polyphenols, dicyandiamides, and isocyanates at a curing temperature of beyond 120 ^{o}C or hardeners such as primary or secondary aliphatic amines, polyaminoamides or thiols at a temperature between room temperature and 120 ^{o}C [14]. Among these hardeners, carboxylic acid anhydrides exhibit excellent properties such as low exotherms and shrinkage during curing, low moisture absorption and almost stress-free systems after curing [14]. The disadvantage of anhydride-cured epoxy is that they require high curing temperatures to initiate the curing reactions to achieve desired mechanical properties and thermal stabilities.

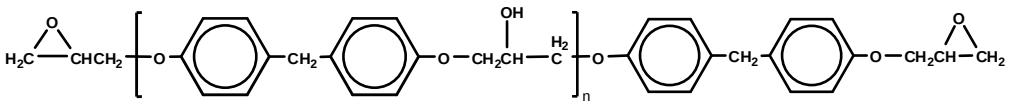

(a) DGEBF

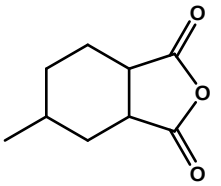

(b) MHHPA

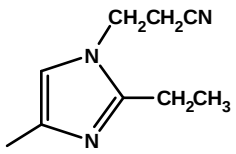

(c) 2E4MZCN

Figure 1.3 Molecular structures of DGEBF, MHHPA and 2E4MZCN.

The curing mechanism of epoxy-anhydride systems remains unclear due to several competing reactions which can occur, especially in the presence of tertiary amines as catalysts [14-21]. In the absence of tertiary amines, the uncatalyzed reaction mechanism is shown in Figure 1.4, as proposed by Fisch et al. [16-17]. First, the OH group present in the backbone of an epoxy resin donates its proton and thus open the anhydride ring, generating an ester group and a carboxylic acid group. Then, the carboxylic acid group reacts with another epoxy resin to form di-ester-alchohol, which can continue the polymerization by the alternating addition of anhydride and epoxy or by etherification until termination occurs through the condensation of one terminal carboxylic acid and alcohol to an ester linkage. As a result of the occurrence of etherification reaction, only 0.85 equivalents of anhydride, instead of one equivalent of anhydride in stoichiometry are required to provide optimum cross-link densities and desired properties.

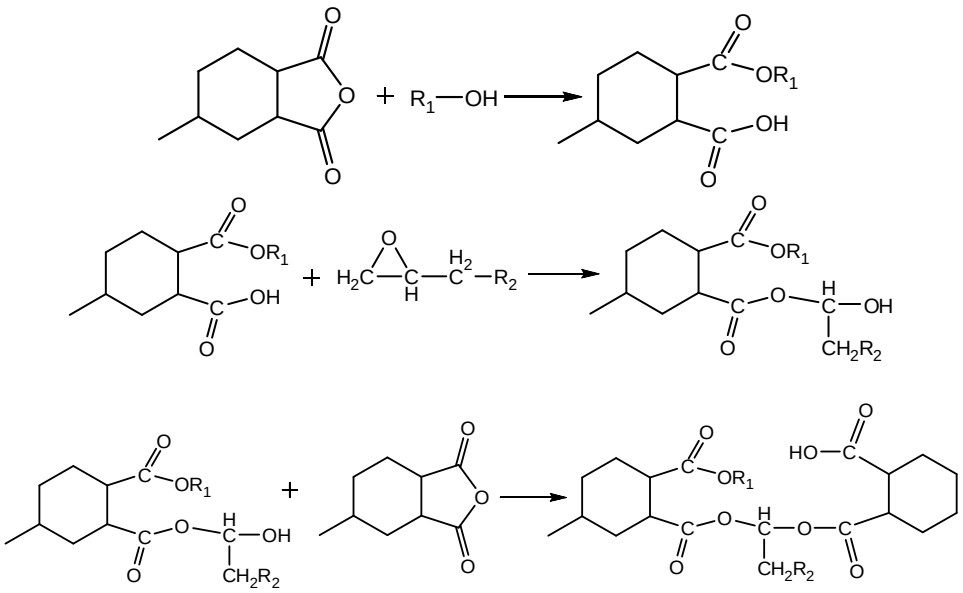

Figure 1.4 Schematic mechanism of the uncatalyzed anhydride-epoxy curing [16-17].

To accelerate the curing reaction of epoxy resins with cyclic carboxylic acid anhydrides, strong Lewis bases, such as tertiary amines, imidazoles or ammonium salts are usually incorporated into a formulation. In the presence of catalyst, such as 1-cyanoethyl-2-ethyl-4-methylimidazole (2E4MZ-CN, Figure 1.3), several possible initiation mechanisms have been proposed, as shown in Figures 1.5 and 1.6. In Figure 1.5, initiation of the curing reaction involves the reaction between the tertiary amine reacts with an epoxy resin that forms a zwitterion containing a quaternary nitrogen atom and an alkoxide anion. The alkoxide anion reacts with an anhydride group and generates a carboxylate anion. This carboxylate anion reacts with an epoxy group yielding a new alkoxide anion. Etherification between an epoxy resin and an alkoxide anion is a competing reaction resulting in an ether linkage. Another mechanism suggested by Fisch

seems to be the one being widely accepted at present [16-17]. In this mechanism (Figure 1.6), Lewis bases open anhydride rings through a nucleophilic attack and form internal salts containing a quaternary nitrogen atom and a carboxylate anion. This carboxylate anion reacts with epoxide groups to yield alkoxide esters, which react with anhydride to form new carboxylate anion esters. These carboxylate anion esters can further react with epoxide groups and this alternating reaction continues until the termination reaction occurs through the combination of two living polymers.

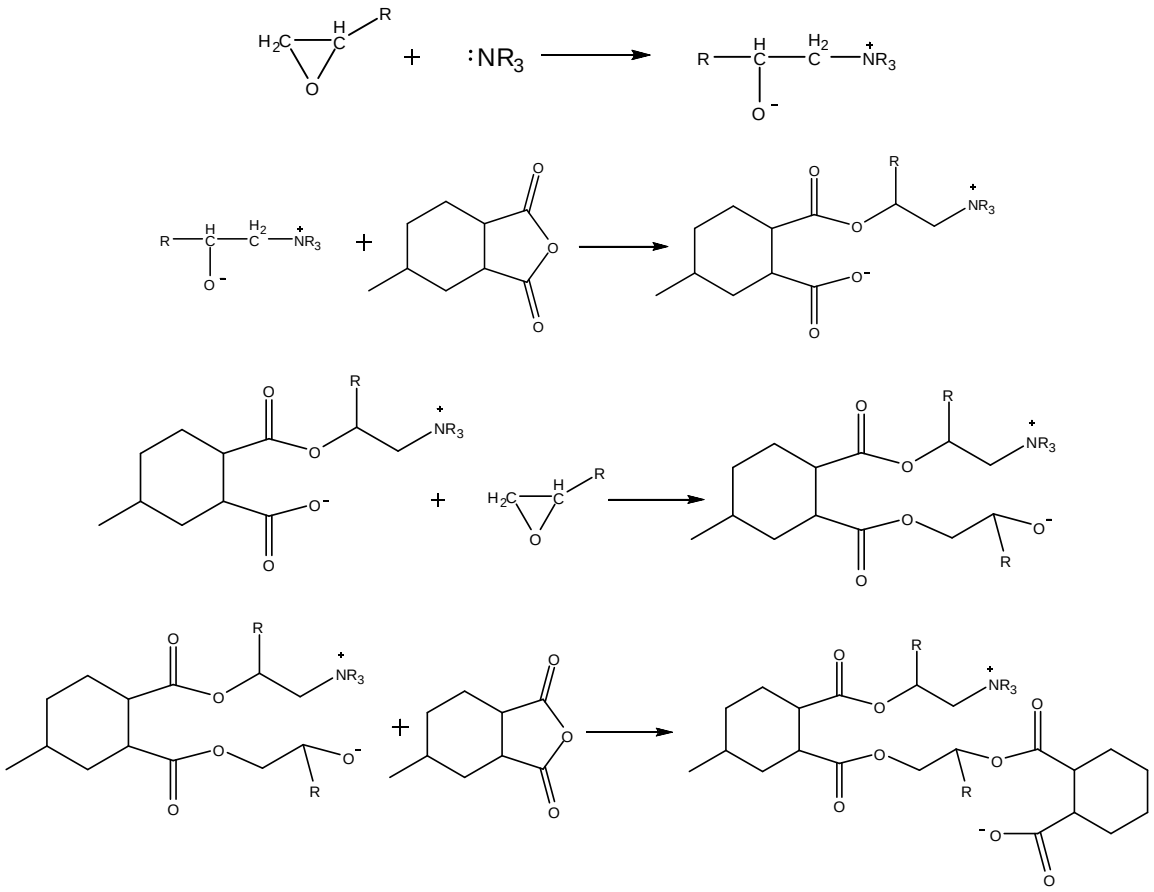

Figure 1.5 Schematic mechanism of the anhydride-epoxy reaction catalyzed by tertiary amines [14-15, 18-20].

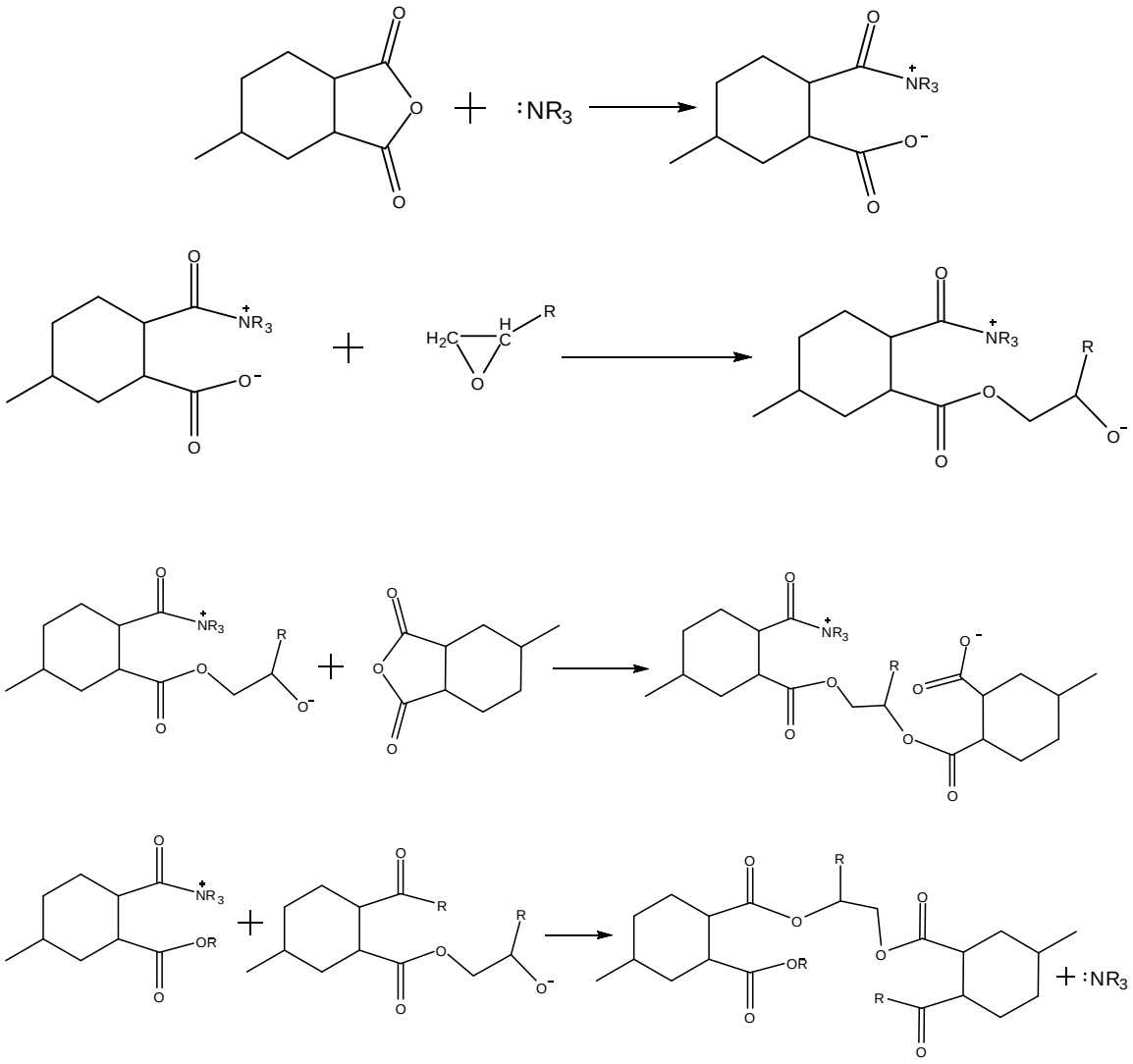

Figure 1.6 Schematic mechanism of the anhydride-epoxy reaction catalyzed by tertiary amines [14, 18-21].

The curing of an epoxy resin with an anhydride leads to the linear growth of polymer chains that then start to branch and cross-link. As the reaction proceeds, the polymer chains are linked to each other to form an infinite polymer network. The transformation from a viscous liquid to an elastic gel marks the first appearance of the infinite polymer network. The gel point is defined as the time or temperature at which the

formation of infinite polymer network occurs. Gelation typically occurs at 55-80% conversion [9]. After the gel point, the curing reaction can proceed further. Vitrification is another important phenomenon that occurs during the curing reaction. As the curing reaction proceeds, if the glass transition temperature of the growing polymer chains reaches to the curing temperature, then the transformation from a viscous liquid or elastic gel to a glass begins to occur. The vitrification point is defined as the point at which further curing reaction is prohibited due to the formation of a rigid glass. The isothermal time-temperature-transformation (TTT) cure diagram, as described by Gillham et al. (Figure 1.7) [22], is generally used to study the curing process of epoxy systems. T_{g0} is the glass transition temperature of an uncured epoxy resin and below this temperature, reaction occurs very slowly as it is confined to the solid state. Gel T_g is the temperature where gelation and vitrification occurs simultaneously. At the curing temperature between T_{g0} and Gel T_g, an epoxy resin will react and vitrification occurs as the rising glass transition temperature of the polymers equals to the curing temperature. $T_{g\infty}$ is defined as the maximam T_g of the system. At the curing temperature between gel T_g and $T_{g\infty}$, the gelation occurs before the vitrification. Above $T_{g\infty}$, gelation occurs while vitrification does not occur. In order to achieve a complete curing, it is necessary to avoid the vitrification during curing since the curing reaction changes from the chemically kinetically control to a diffusion control. It is also recommended to cure above the $T_{g\infty}$ to cross-link an epoxy resin completely and develop the desired mechanical properties of the system [9].

Table 1.3 Comparison of adhesive matrices for electronic applications [11].

Materials	Advantages	Disadvantages
Epoxies	High-temperature use; Good moisture and chemical resistance; High purity; Low outgassing	Longer cure cycles with anhydride hardeners; Degassing required for two-component systems; Exotherms in large quantities for amine-curing agents
Silicones	Highest purity; Stress absorbing; High and low temperature stability	Migrate to other circuit elements; Low surface energy; Swelled by non-polar solvents
Polyurethanes	Good flexibility at low temperatures; Stress absorbing; Highly versatile chemistry	Lower thermal stability and service temperature than epoxies (150-163 ^{o}C); Average bond strength unless primer is used
Polyimides	Higher temperature stability compared to epoxies; High ionic purity; Reduced bleedout	Trapped solvent can produce voids under large ICs; Multi-step curing required to volatilize solvent; High-stress materials; May absorb moisture in cured condition; Cannot be B-staged
Cyanate esters	High adhesion strength; High thermal stability; High T_g; Low CTE	High-moisture absorption; "Popcorn" susceptibility during solder reflow

1.3.1.2 Electrically Conductive Fillers

Electrically conductive fillers are incorporated into a polymer matrix to render the composite highly electrically conductive. Possible conductive fillers include silver (Ag), gold (Au), nickel (Ni), copper (Cu) and carbon in various shapes and sizes [9]. Despite its high cost and electrochemical activity, silver is the most popular conductive filler for ICAs due to its unique properties. These unique properties include the highest electrical and thermal conductivities of all metals, easy processing into ideal shapes and significantly higher conductivity of its oxides than those of other metals [9]. Although Au does not form oxide at ambient conditions, it is too expensive to be used in ICAs. Nickel- and copper-based conductive adhesives generally do not have good conductivity stability

because these conductive fillers are easily oxidized. Even with corrosion inhibitors, copper-based conductive adhesives show a dramatic increase in volume resistivity following aging, especially under elevated temperatures and relative humidities [23]. Silver-plated copper fillers have shown better resistance than copper fillers, but typically ICAs filled with silver-coated copper fillers show increased resistance under aging [24-26]. This could be due to the incomplete plating of copper with silver, which leads to the oxidation/corrosion of silver-coated copper fillers in the polymer matrix and thus the increased electrical resistivity. Silver-filled ICAs typically show stable (or decreased) bulk resistivity when exposed to elevated temperatures/relative humidities or thermal cycling tests. Carbon materials such as carbon black [27-28], graphite/graphene [29-30] and carbon nanotubes (CNTs) [31-34] have also been widely used as conductive fillers for conductive polymer composites. To improve the electrical conductivity of conductive polymer composites, carbon materials have been coated with metals as fillers, such as silver-plated CNTs [35-36], silver-plated carbon fibers [37], silver-coated graphite [38-40], nickel-coated carbon fibers [41] and nickel-coated graphite [42]. In addition, to improve electrical and mechanical properties, low-melting-point fillers have been used in ICA formulations. Conductive filler powders are coated with a low-melting-point metal. The conductive powder is selected from the group consisting of Au, Cu, Ag, Al, Pd, and Pt. The low-melting-point metal is selected from the group of fusible metals, such as Bi, In, Sn, Sb, and Zn. The filler particles coated with the low-melting-point metal can be fused to achieve metallurgical joints between adjacent particles, and between particles and the bond pads that are joined using the adhesive material [43-49].

Metal particles or carbon materials in various shapes and different sizes have been investigated as electrically conductive fillers for ICAs, including micron-sized silver (or Cu, Ni etc.) flakes, nano/micron-sized silver spherical particles, silver nanowires, porous nano-sized silver particles, spherical carbon black, micron-sized carbon fibers, carbon nanotubes, nano/micron-sized graphite/graphene. Compared with spherical fillers, higher aspect ratio fillers, especially nanowires/nanotubes, reduce the percolation threshold of conductive polymer composites significantly. Obtaining a low percolation threshold is advantageous in minimizing the filler loading and obtaining ideal mechanical properties of conductive polymer composites. The particle size of ICA fillers generally ranges from 1 to 20 μm. Incorporation of larger particles tend to produce ICAs with a higher electrical conductivity and lower viscosity [50]. During the preparation of ICAs, a bi-modal mixture of fillers is typically used to increase the packing density and thus the electrical conductivity at a given metal loading. Among these conductive fillers, silver flakes are the most widely used conductive fillers for ICAs. This is because flakes tend to have a larger contact area and thus a lower contact resistance than spherical fillers.

To obtain good processability stable dispersions of silver flakes in a polymer matrix are required. Fatty acids (such as stearic acid) are typically used as a lubricant and compatibilizer to enhance the processability and stability of ICAs. This lubricant layer plays an important role in the dispersion of silver flakes, viscosity and the electrical conductivity of ICAs. Therefore, understanding the behavior of lubricants on the surface of silver flakes is essential for developing high performance ICAs. Lu et al. characterized silver flakes and investigated the thermal decomposition of silver flake lubricants in detail [51-52]. It was found that (i) silver flakes lubricated with fatty acids of different

chain lengths have exothermic DSC peaks and mass losses at different temperatures. Silver flakes lubricated with longer chained fatty acids showed exothermic DSC peaks at higher temperatures and started to lose mass at higher temperatures than those lubricated with shorter fatty acids; (ii) the lubricant on silver flake surfaces is a salt formed between the acid and silver; (iii) exothermic DSC peaks (in air) of a lubricated silver flake is probably due to the oxidation of lubricant layer on the silver flake surface; (iv) the decomposition of the lubricant—silver salt of fatty acid—includes the release of the fatty acid, formation of short-chain acids by decomposition of hydrocarbon moiety of the fatty acid, and formation of alcohols through decarbonation of the short chain acids; (v) most common solvents such as methanol, tetrahydrofuran, and acetone do not cause significant desorption of the lubricants; (vi) addition of a small amount of two short chain acids, acetic acid and adipic acid, strongly affects the interaction between the silver flake and the resin, leading to a significant increase in the viscosity of the ICAs.

The lubricant layer improves the dispersion of silver flakes within an epoxy resin, which is beneficial to improvement of electrical conductivity of ICAs. However, the lubricant layer is composed of organic molecules and thus direct metal-metal contact is prohibited. The presence of the lubricant layer increases the tunneling resistance. Removal of lubricants before curing causes the aggregation of silver flakes. Therefore, it is desired to remove or replace the lubricants with short-chain acids during the curing process. The removal or replacement of the lubricants enables more intimate or direct metal-metal contact between silver flakes, improving the electrical conductivity of ICAs.

1.3.2 Conduction Mechanisms

The formation of electrical conductive paths in ICAs is generally understood by percolation theory. Figure 1.8 shows the dependence of the resistivity of an ICA on the volume fraction of electrically conductive fillers. Increasing filler volume fraction at low filler volume fractions decreases the resistivities of ICAs gradually. As the volume fraction increases a critical volume fraction, i.e. percolation threshold, is reached. At a percolation threshold, conductive fillers come into "contact" and form a continuous linkage between conductive fillers. Consequently, the ICA transforms from an insulator to a conductor. The continuous linkage between conductive fillers should be thought as a series of resistors, as shown in Figure 1.9. The resistance of an ICA is the sum of filler resistances (R_f) and inter-particle contact resistances. The contact resistance is composed of constriction resistance (R_c) and tunneling resistance (R_t). Constriction resistance occurs as the current must squeeze through the small area of contact. Tunnel resistance is due to the intermediate layer between the metal surfaces. Therefore, a total resistance of an ICA, R_{total}, could be written as [53-59]:

$$R_{total} = R_f + R_c + R_t \qquad (1)$$

Where

$$R_f = \frac{\rho}{\pi d} \ln \frac{d + \sqrt{d^2 - D^2}}{d - \sqrt{d^2 - D^2}} \qquad (2)$$

$$R_c = \frac{\rho}{d} \qquad (3)$$

$$R_t = \frac{\rho_t}{\pi (\frac{d}{2})^2} \qquad (4)$$

$$\rho_t(s,\Phi,\varepsilon) = \frac{10^{-22}}{2}\frac{A^2}{1+AB}e^{AB} \qquad (5)$$

$$A = 7.32\times10^{-5}(s - \frac{7.2}{\Phi}) \qquad (6)$$

$$B = 1.265\times10^{-6}\sqrt{\Phi - \frac{10}{s\varepsilon}} \qquad (7)$$

In Equations (2) and (3), ρ is the intrinsic resistivity of conductive fillers, d is the particle diameter and D is the contact diameter. In Equations (4)-(7), ρ_t is the tunneling resistivity, s is the thickness of a thin film that separates the conductive fillers, ε is the dielectric of the thin film, and Φ is the work function of the metal fillers.

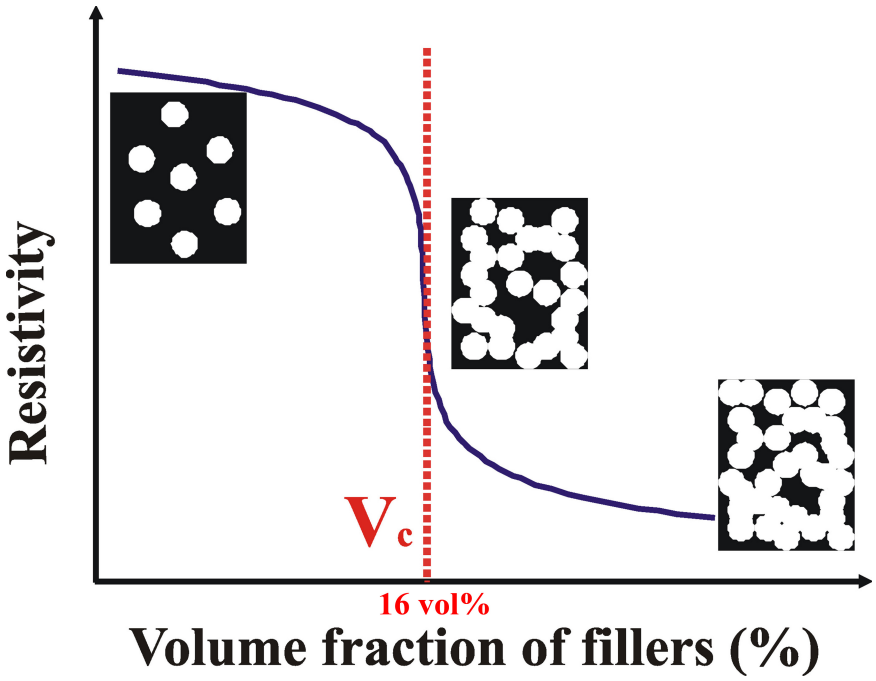

Figure 1.8 Dependence of the resistivity of ICAs on the volume fraction of electrically conductive fillers. For monosized spherical particles, the theoretical percolation threshold is about 16 vol%.

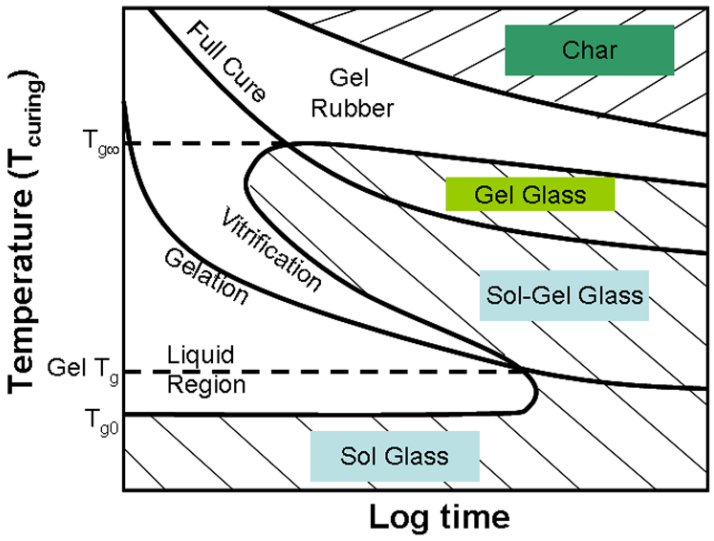

Figure 1.7 Time temperature transform (TTT) diagram [22].

Besides epoxies, silicones, cyanate esters, polyimide, and polyurethanes have also been employed in ICA formulations. The choice of an adhesive matrix and its formulation is critical to the properties of ICAs. In practice, many options exist for the adhesive matrix. The general properties of polymer matrices used in ICAs are compared in Table 1.3 [11]. Note that the chemical structure of any polymer matrix can be tailored readily to produce desired properties and to meet requirements for a specific application. An ideal matrix for ICAs should have the following properties: long shelf life (good room-temperature latency), fast cure, relatively high T_g, low moisture absorption, and good adhesion [6].

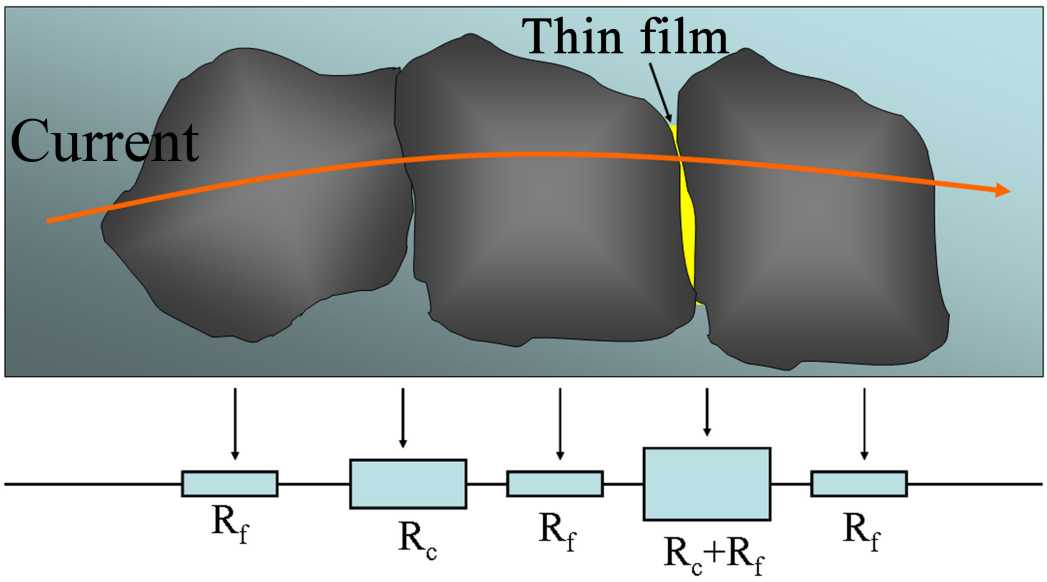

Figure 1.9 Electrical resistances of ICAs. The resistance of an ICA is the sum of filler resistance (R_f), constriction resistance (R_c), and tunneling resistance (R_t).

In an ICA, the particles could be separated by a thin layer of polymer, oxide or lubricants for most commercial silver flakes. The thickness of the interface can vary from 10 to 100 Å, depending on the physiochemical properties of the polymer matrix, filler, filler concentration, and the conditions of composite preparation [57-58, 60]. Particularly, the filler-polymer interaction energies play a key role in the formation of thin polymer interlayers in interparticle contact regions. For example, if the filler-filler interaction energy is lower than that of polymer matrix, each of the electrically conductive filler will be covered with a thin polymer layer. If the filler-filler interaction energy is larger than that of filler-polymer interaction energy, the aggregation of fillers is thermodynamically favored [58].

During the curing process, these interlayers may be squeezed from the interparticle region due to the internal stress caused by cure shrinkage [58]; oxide layers

may be broken or reduced; the thin layer of lubricants could be removed. In such cases, the direct contact of conductive fillers may occur. There is no clear conclusion regarding whether there is direct contact between conductive fillers or if there is a thin layer in between them [61]. It is possible that both situations co-exist within ICAs. The conductivity of an ICA is determined by the composite composition (such as filler loading), the surface properties of conductive fillers (the presence of a thin layer of lubricants or oxide film), physicochemcial properties of polymer matrix (cure shrinkage and the interaction between the polymer matrix and conductive fillers), interlayer thickness, temperature, processing conditions of ICAs, etc. [58]. In order to achieve conductivity, the volume fraction of conductive fillers in an ICA must be equal to or higher than the critical volume fraction. Similar to solders, ICAs provide the dual functions of electrical connection and mechanical bonding in an interconnection joint. In ICA joints, the polymer resin provides mechanical stability and the conductive filler provides electrical conductivity. Filler loading levels which are too high cause mechanical integrity of adhesive joints to deteriorate. Therefore, the challenge in formulating ICAs is to maximize conductive filler content to achieve high electrical conductivity without adversely affecting the mechanical properties. In a typical ICA formulation, the volume fraction of conductive fillers is about 25–30% [62-63].

1.3.3 Methods to Improve Electrical Conductivity

Compared with metal solders, ICAs have lower electrical conductivity. There is an increasing need for ICAs with higher electrical conductivity in the electronic industry. Various approaches to improve the electrical conductivity of ICAs have been reported in recent years.

1.3.3.1 Increase of the Polymer Matrix Shrinkage

ICA pastes before curing usually have low conductivities. During curing, the epoxy resin shrinks and the conductive fillers within the polymer matrix experience a compressive force. The compressive force brings the conductive fillers closer together and contributes to the improved electrical conductivity of ICAs after curing [64]. Formulations with higher crosslinking density have higher cure shrinkage and lower resistivity. For example, by adding 2 wt% and 10 wt% of trifunctional epoxy into the ICA formulation, the resistivity of ICAs decreases from 3.0×10^{-3} to 1.2×10^{-3} and 0.58 $\times10^{-3}\ \Omega$ cm, respectively [65].

1.3.3.2 Incorporation of Short-chain Diacids and Reducing Agents

As previously mentioned, a lubricant layer is typically present on the surface of commercially available silver flakes. This thin layer of lubricants plays an important role in the dispersion of silver flakes in epoxy resins, the viscosity, and the performance of the cured ICAs [51-52, 66-67]. After cure, the configuration of the contacts between conductive fillers is likely metal-lubricant (possibly epoxy)-metal, instead of direct metal-metal contacts. The length and surface orientation of these lubricant molecules affect the electron tunneling/hopping between silver flakes. In situ replacement of long-chain acids (such as stearic acid) with short-chain diacids (such as malonic acid) improve the electron tunneling/hopping between silver flakes leading to a decreased in resistivity, from ~7.3×10^{-4} to ~$4.7\times10^{-4}\ \Omega$ cm [68]. Li et al. also demonstrated that electrical resistivity of ICAs can be decreased from ~7.3×10^{-4} to $6.0\times10^{-5}\ \Omega$ cm by introduction of aldehydes into the formulations [69]. The improved electrical conductivity was attributed to the removal of silver oxide and the replacement of long-chain acids (stearic acid) with

short-chain acids on the surface of silver flakes. Both effects reduce the length of the tunneling/hopping gap and may enable direct metallic contacts, improving the electrical conductivity of the ICA.

1.3.3.3 Incorporation of One-dimensional Conductive Fillers

High-aspect-ratio conductive fillers enable conductive networks to form within a polymer matrix at a much lower filler loading than that of spherical particles. Low filler loadings enable the preparation of highly conductive ICAs without degradation of ICA mechanical properties and processibility. Wu et al. reported that the resistivity of ICAs filled with 56 wt% silver nanowires (30 nm in diameter and a length up to 1.5 μm) was $1.2 \times 10^{-4}\ \Omega$ cm, which was significantly lower than that of ICAs filled with 1 μm and 100 nm silver particles [70-72]. Several possible reasons for the improved electrical conductivity were proposed, including larger contact area, fewer contact points, more stable contact and enhanced tunneling between these particles due to the presence of a small amount of silver nanoparticles. Moreover, ICAs filled with silver nanowires have a better shear strength on an alumina plate (17.6 MPa) than that of ICAs filled with micron-sized silver particles (17.3 MPa). Similar results were reported by Tao et al [72]. Chen et al. demonstrated that the resistivity of ICAs could be improved by adding diluents containing silver nanoparticles and silver nanowires [73]. Besides silver nanowires, carbon nanotubes (CNTs) have also been added to ICA formulations to improve electrical conductivity. Table 1.4 shows the effect of adding multi-walled CNTs (MWCNTs) on the electrical resistivity of silver-filled ICAs with different silver contents [74] . The addition of MWCNTs into the formulation improves the electrical conductivity dramatically for ICAs whose filler loading is below percolation threshold. One dimensional fillers like

CNTs, improve the contact between conductive fillers and facilitate the formation of 3-D conductive networks. This improved contact between conductive fillers is especially significant prior to reaching the percolation threshold. However, no significant improvement of electrical conductivity is observed when the silver filler loadings reach percolation threshold. Oh et al. investigated the effect of adding single-walled CNTs (SWCNTs) with different surface properties on the electrical resistivity of a commercial silver paste filled with 80 wt% silver powders [35]. It was found that the addition of raw SWCNTs into the silver paste did not improve the electrical conductivity. The addition of an optimized amount (1.5 wt%) of acid-treated SWCNTs can decrease the electrical resistivity significantly. This decrease in resistivity was the result of increased dispersion and p-doping effects. However, the resistivity increased with the addition of more acid-treated SWCNTs. With the addition of silver-plated SWCNTs, the resistivity of the commercial silver-filled ICA was decreased by 83% [35].

Table 1.4 Electrical properties of the CNTs/Ag/epoxy composites with different compositions [74].

Silver (wt%)	45	52	57	66.5	72
Bulk resistivity of ICAs, ρ_1 (Ω·cm)	$>>10^8$	6.91×10^6	1.04×10^6	1.01×10^4	1.5×10^{-3}
Bulk resistivity of ICAs with the addition of CNTs, ρ_2 (Ω·cm)	4.8×10^3	3.82×10^1	2.4×10^{-2}	6.47×10^{-3}	1.43×10^{-3}
CNTs (wt%)	1.35	1.0	0.4	0.27	0.24
ρ_1/ρ_2	----	$\approx10^5$	$\approx10^8$	$\approx10^6$	1.05

1.3.3.4 Low Temperature Transient Liquid Phase Sintering

Liquid phase sintering is a special type of sintering where the liquid phase coexists with the solid particles and the solid phase is soluble in the liquid phase [75]. In transient liquid phase sintering, liquid exists only for a short period of time and then forms an alloy and solidifies. Transient liquid phase sintering materials enable the assembly process at a low temperature, minimizing stress level while withstanding high-temperature joint stability [76]. To exploit the advantages of both solder and conductive adhesives, transient liquid phase fillers have been incorporated into ICA formulations i.e. transient liquid phase sintered conductive adhesives [46-48, 76]. The filler used is a mixture of a high-melting-point metal powder (such as copper) and a low-melting-point alloy powder (such as Sn–Pb or Sn–In). The low-melting-point alloy filler melts during the curing process. The liquid phase forms an alloy with the high melting point particles. The electrical conduction is established through in-situ formed metallurgical connections between these two types of powders in a polymer binder and between the powders and the metal surfaces (Figure 1.10). The polymer binder with an acid functional ingredient fluxes both the metal powders and the metal surfaces to be joined. The fluxing process facilitates the transient liquid sintering between the conductive fillers and between the conductive fillers and the metal surface to be joined. Sintering enables the formation of stable metallic network within the interpenetrating polymer network. Metallurgical bonds between the metallic network within the polymer matrix and the metal surfaces enable good electrical contact, leading to low joint resistance. The polymer binder serves to form mechanical connections and can be tailored to meet the requirements for specific applications. The metallic and polymer networks provide robust electrical and mechanical interconnection. Compared with standard conductive adhesives, transient

liquid phase sintered conductive adhesives exhibit bulk and interfacial resistances comparable to solders and have substantially improved impact strength. Electrical characteristics of transient liquid phase sintered conductive adhesives remain consistent after reliability tests. Lu et al. developed an ICA filled with silver flakes and low-melting-point alloy fillers [45]. It was found that the ICA showed much lower bulk resistance than the commercial ICA and the control ICA filled with only the silver flakes. Moreover, the ICA filled with silver flakes and low-melting-point alloy fillers showed much lower initial contact resistance (0.15 Ω) than the ICA with only the silver flakes (~8.90 Ω) [45]. Due to the metallurgical interface between the ICA and the Ni substrate, the contact resistance of the ICA on Ni surfaces remained stable during 85 ^{o}C/85% RH (relative humidity) aging for 1000 h. Kim et al. investigated ICAs composed of fusible Sn-In alloy particles and two type of resins [49]. Resin **A** barely wetted copper surfaces while Resin **B** with reduction capability could flux the metal surfaces and allowed the solder to wet on the copper. Consequently, Resin **B** with reduction capability was effective at achieving good metallurgical interconnection between the fillers and metallization, producing a low electrical resistance.

The transient liquid phase sintered conductive adhesives provide the advantages of both conventional soldering technology and conductive adhesives. This hybrid approach produces strong electrical and mechanical interconnections that are resistant to humidity and temperature cycling. One critical limitation of this technology is that the numbers of combinations of low melting and high melting fillers are limited. Only certain combinations of metallic fillers, which are mutually soluble, exist enabling the formation of metallurgical interconnections by transient liquid phase sintering [5].

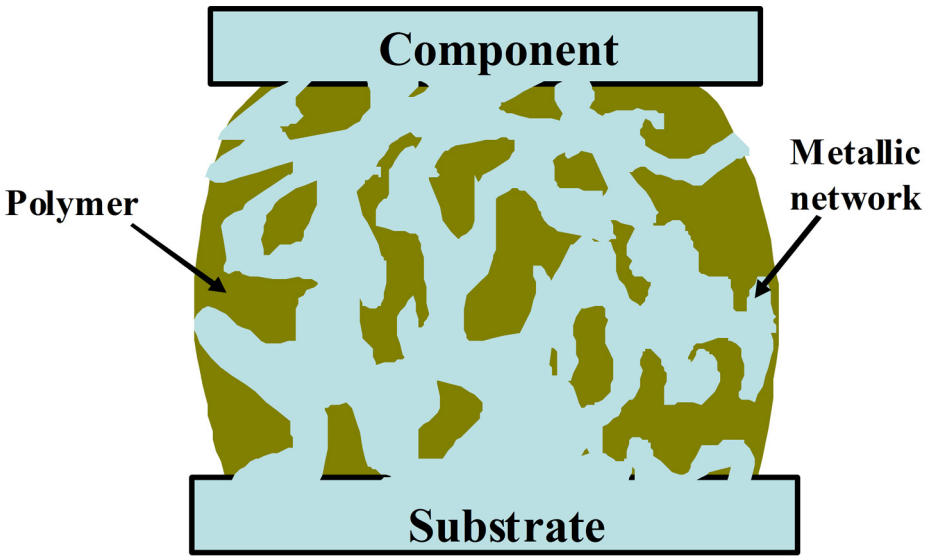

Figure 1.10 A joint formed by transient liquid phase sintered conductive adhesives.

1.3.3.5 Low Temperature Sintering of Silver Nanoparticles

Low temperature sintering of silver nanoparticles has been developed as a promising technique for a variety of electronic applications including device interconnect [77-84], metal-metal bonding process [85], production of conductive tracks [86-91] and electrodes by inkjet printing of silver inks for semiconductor devices [92]. Electrical resistivity of silver films close to that of bulk silver (1.6×10^{-6} Ω cm) has been achieved by sintering of silver nanoparticles in silver conductive inks at low temperatures (<200 ^{o}C) [90, 93-95]. Recently, silver nanoparticles are proposed to be used as conductive fillers for ICAs in an attempt to improve the electrical conductivity. The addition of silver nanoparticles increased the number of contact points between conductive fillers. Although the incorporation of silver nanoparticles decreases the resistivity near the percolation threshold [96], the addition of silver nanoparticles into micro-sized silver

flakes usually increase the resistivity dramatically if no sintering occurs [77, 83, 96-98]. The increase in resistivity is the result of the increased contact resistance. Through SEM studies, Ye et al. observed that addition of silver nanoparticles into a polymer matrix with micron-sized conductive fillers decreases the chance of direct contact among micron-sized fillers and the contact area between nano- and micron- sized particles is smaller than that between micron-sized particles [97]. In addition, the number of contact points significantly increase. As a result, contact resistance of ICAs filled with nano- and micron-sized particles increases as the percentage of silver nanoparticles increases. However, some research has shown that the electrical conductivity of ICAs can be improved by the addition of silver nanoparticles [77-78, 80, 83-84].

Jiang et al. investigated the effect of silver nanoparticles functionalized by different surfactants (S1, S2, S3, S4, and S5) on the electrical properties of ICAs filled with silver flakes and silver nanoparticles (Table 1.5) [83]. It was found that the chain length of the surfactants, the debonding temperature and the molecular behaviour are important parameters to initiate sintering of silver nanoparticles in the polymer matrix. These properties of the surfactant dictate the electrical conductivity of the ICA. By using appropriate diacids to functionalize silver nanoparticles, the resistivity of ICAs filled with silver flakes and silver nanoparticles (molar ratio of silver flakes to nanoparticles is equal to 6:4) was as low as 5×10^{-6} Ω cm when cured at 150 ^{o}C for 90 min [84]. Morphological studies showed that the decreased resistivity was the result of sintering of silver nanoparticles within the polymer matrix. Das et al. developed silver-based nano- and micro-filled conductive adhesives for z-axis interconnections [80]. It was found that with increasing curing temperature, the resistivity of the silver-filled paste decreased due to

sintering of the metal particles. The conductive adhesive cured at 190 ^{o}C for 2 h showed a resistivity of 2×10^{-5} Ω cm [80].

Table 1.5 The effect of different surfactant-treated silver nanoparticles on the resistivity of ICAs [83].

Fillers	Filler loading	Resistivity (Ω cm)
Untreated silver nanoparticles	60 wt%**	5.4×10^{-2}
S1-treated silver nanoparticles	70 wt%	5.4×10^{4}
S2-treated silver nanoparticles	70 wt%	2.4×10^{5}
S3-treated silver nanoparticles	70 wt%	2.4×10^{-4}
S4-treated silver nanoparticles	70 wt%	6.3×10^{-4}
S5-treated silver nanoparticles	70 wt%	4.3×10^{-4}

*The molar ratio of silver nanoparticles and surfactants was set as 1:1. The ICAs were cured at 150 ^{o}C for 90 min.

**The untreated particles were unable to be loaded with 70 wt%, due to high viscosity of the mixture.

1.3.4 Adhesion Strength of ICAs

One of the major functions of ICAs is to mechanically attach components onto a substrate during assembly. The adhesion strength of bonded interfaces between components and substrates should be able to withstand impact, thermal shocks, thermal cycling and vibration tests as specified for different applications. One critical reliability issue of ICAs is their lower adhesion strength compared to solder. The adhesion strength of ICAs used to bond different surfaces is dependent on the ability to wet the surfaces and the nature of the bonding mechanism. To achieve maximum adhesion, the adhesive must completely wet the surface to maximizing surface coverage and minimizing voids at the interface.

1.3.4.1 Adhesion Mechanisms

There are two types of adhesion mechanisms, chemical bonding and physical bonding, which contribute to the overall adhesion strength of ICAs on a surface [99]. Chemical bonding involves the formation of covalent, hydrogen, ionic or metallurgical bonds to join components to the substrates. Surface modification with coupling agents has emerged as an effective method to enhance adhesion. Coupling agents typically are organofunctional compounds based on silicon (Si), titanium (Ti), or zirconium (Zr). Figure 1.11 shows some typical coupling agents. A coupling agent consists of two parts and acts as intermediary to ‘‘couple’’ the substrate and polymer. For example, the methoxy or ethoxy groups in silane coupling agents can be hydrolyzed to form silanol groups. The silanol groups can react with the hydroxyl groups present on the surface of substrates through a condensation mechanism. The other functional groups, such as epoxide and amine groups, can react with epoxy resins or curing agents to form strong covalent bonds during the curing process. Physical bonding involves mechanical interlocking or physical adsorption between the polymer and the surface of substrate. In cases where the molecules of the polymer are highly compatible with the molecules of the substrate, they interact to form an inter-diffusion layer. In mechanical interlocking, polymer and substrate interact on a more macroscopic level, where the polymer flows into the crevices and the pores of substrate surface to establish adhesion [99]. Therefore, a polymer is expected to have better adhesion on a rougher surface because there is more surface area and ‘‘anchors’’ to allow for interlocking between the polymer and the substrate. Moreover, the rough adherence surface may enable a better stress transfer from the adherend to the adhesive [100]. High adhesion strength is a critical parameter in fine pitch interconnections that are especially fragile to shocks encountered during assembly,

handling and lifetime. Many efforts have been dedicated to improve the adhesion strength to enhance the reliability of fine pitch joints. Since electrical function is needed for ICA interconnects, ICAs are typically used to bond metal surface finishes. In the following section, we focus on the adhesion improvement of ICAs on metal surface finishes.

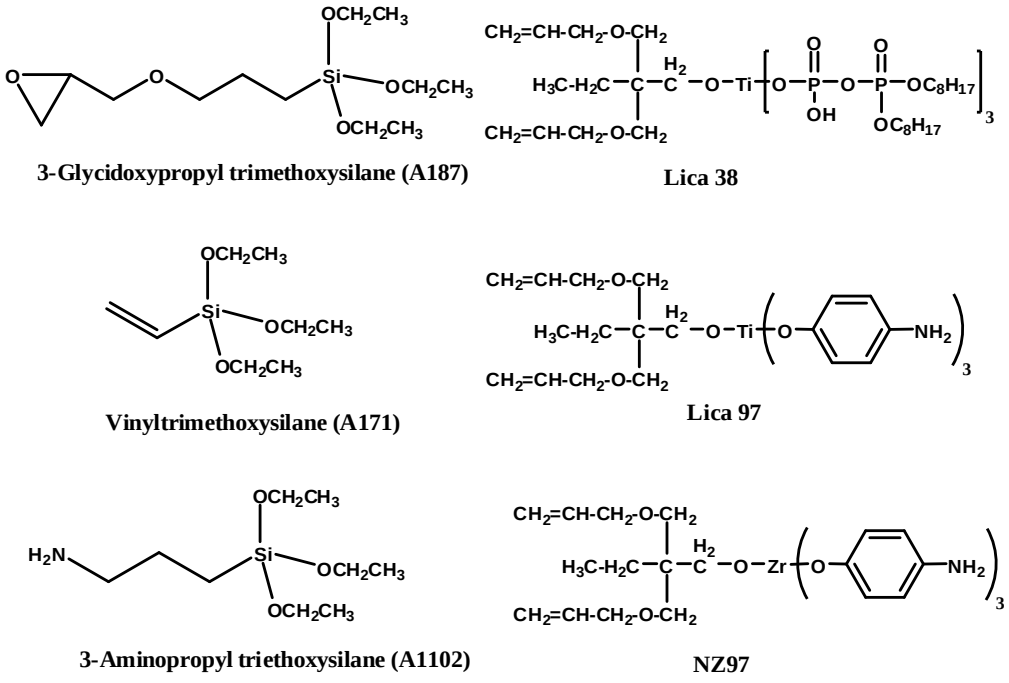

Figure 1.11 Structures of coupling agents based on silicon, titanium and zirconium.

1.3.4.2 Adhesion Improvements

Liong et al. investigated the adhesion strength of thermoplastic polyarylene ether derivative (PAE-2E)-based ICAs on the surfaces of Sn/Pb, Sn, Cu and Ni/Au [101]. It was observed that the surface roughness and die shear strength were strongly correlated indicating that adhesion of PAE-2E-based ICAs may be dominated by mechanical interlocking. Adhesions on these surfaces have been improved by incorporation of

coupling agents or epoxy blending. With incorporation of a coupling agent, adhesion strength on Ni/Au was approximately 2.75 times the adhesion strength without the coupling agent as a result of chemical interaction at the interface. Figure 1.12 shows the effect of the combined use of epoxy blending and coupling agents on the adhesion strength of PAE-2 based ICAs on Ni/Au and Sn/Pb surfaces before and after 85 ^{o}C/85% RH aging [102]. The combined use of epoxy blending and coupling agents was effective at increasing the adhesion strength of PAE-2 based ICAs on both Ni/Au and Sn/Pb surfaces before aging. After 85 ^{o}C/85% RH aging for 168 h, the adhesion strength of PAE-2 based ICAs with the incorporation of both epoxy and coupling agents on a Sn/Pb surface did not change significantly, while the control sample showed a large decrease in adhesion. However, the adhesion strengths on Ni/Au were reduced significantly to less than 50% after 85 ^{o}C/85% RH aging for 168 h. Factors responsible for these results may involve the hydrophilicity, surface roughness, and interaction between coupling agents (or polymer matrix) and metal surfaces.

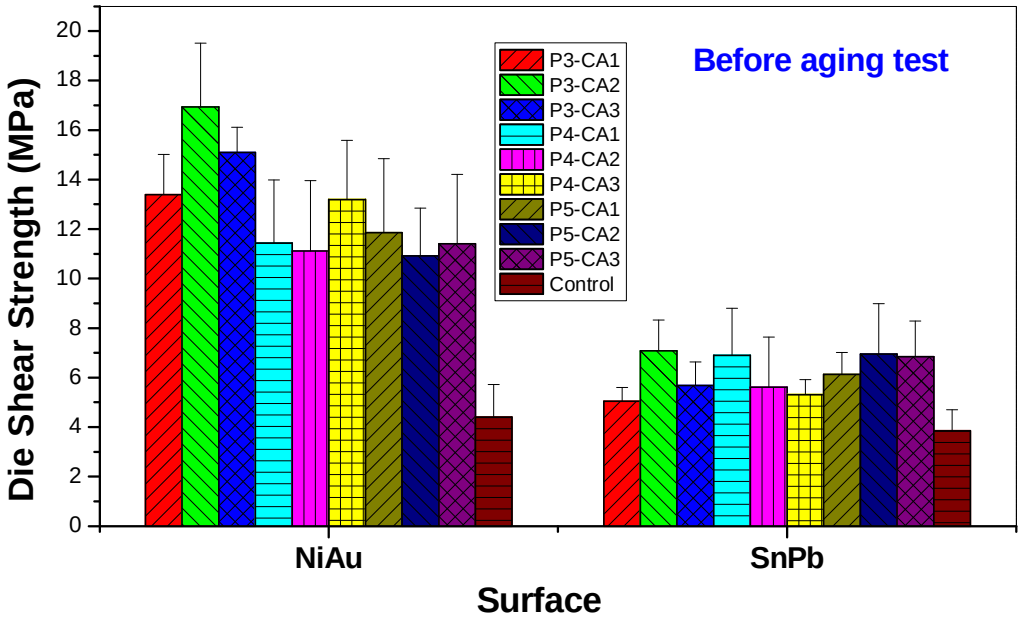

(a)

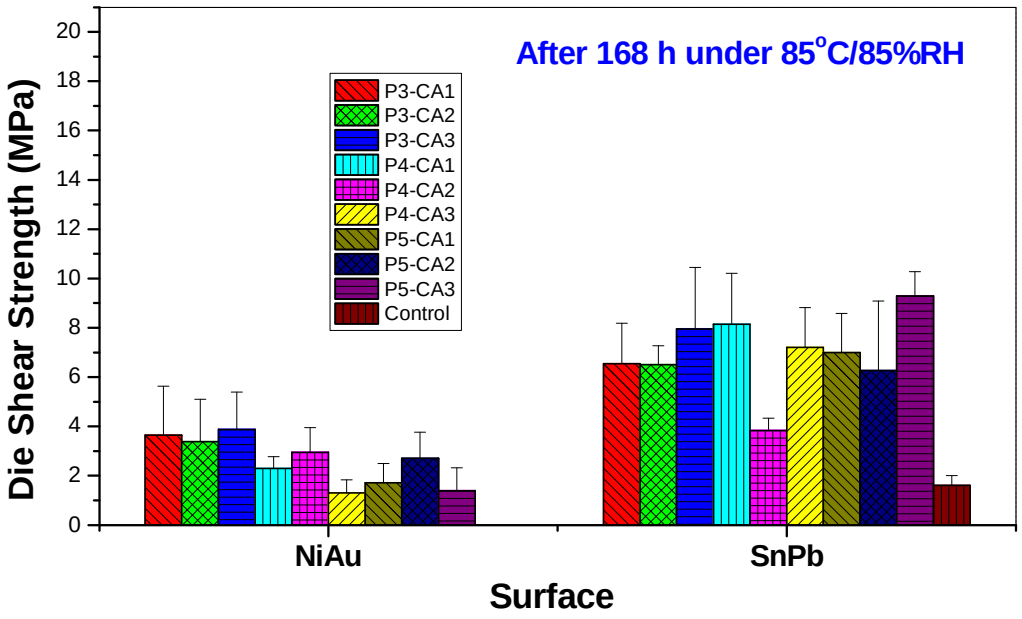

(b)

Figure 1.12 Adhesion strength of PAE-2 based ICAs on Ni/Au and Sn/Pb; (a) before aging and (b) after 85 °C/85% RH aging for 168 h. The ratios of epoxy to PAE-2 for P3, P4 and P5 are 1:3, 1:4 and 1:5, respectively. Two amino (CA1 and CA2) and one epoxy (CA3) terminated coupling agents were used as adhesion promoter [102].

Selection of functional groups (i.e. coupling agents) plays a key role in the determination of the adhesion strength since different functional groups have a different affinity to a metal surface. Table 1.6 summarizes the functional groups that may have strong affinities to different metals. To improve the adhesion strength of PAE-2 based ICAs on the surface of Ni/Au at elevated temperatures and relative humidities, thiol compounds, which can form self-assembled monolayers (SAMs) on metal surfaces, have been studied by Moon et al [103]. It was found that pretreatment of Ni/Au surface by

SAM molecules was more effective at enhancing the adhesion strength than the premixing of SAM molecules with the resin of PAE-2 polymer both before and after aging. Among the SAM molecules studied, SAM molecules containing both thiol and carboxylate groups were the most effective at maintaining the adhesion strength of PAE-2 polymer as well as PAE-2 filled with silver flakes after aging. Note that the pretreatment of the metal bond by SAM molecules with carboxylate group did not adversely affect the contact resistance stability during aging. Yi et al. studied the die shear strength of flexible ICAs, whose matrices were the blend of flexible and rigid epoxy resins, on glass, polyimide and gold substrates [104]. With the increase in the percentage of the flexible epoxy, the adhesion strength continuously decreases on glass and polyimide substrates. Comparing the adhesion strength of flexible ICAs on various substrates, the adhesion strength of flexible ICAs on Au was the lowest when using the same resin formulation. By treating Au substrate with a thiol compound, Zhang et al. showed that the adhesion strength of flexible ICAs on Au and Cu surfaces could be improved significantly [105-106]. The improved adhesion strength resulted from the capability of SAM molecules to strongly bind the metal surfaces and react with the epoxy resin. Compared with other coupling agents, there are two advantages of using thiol compounds for ICA interconnections. First, the formation of SAMs increases the number of molecules on the surface that can react with resins during curing, improving adhesion strength. Second, the available conjugated SAM molecules may be beneficial for electron transport at the interface.

Another way to enhance adhesion strength is to use ICAs filled with low-melting-point fillers, i.e. transient liquid phase sintered conductive adhesives. Transient liquid

phase sintered conductive adhesives have been developed as interconnect materials, enabling the metallurgical bonds to the metal pad and within the conductive fillers (Figure 1.10). The joints formed exhibit substantially improved impact strength [46-48].

Table 1.6 Functional groups for different surface finishes* [4-5, 107]

	Formula	Surface finish
	Compound	Au, Ag, Cu, Ni, Sn, Zn, Pt, Ru
Acids	Thiols	Ag, Fe, Co, Ni, Al
Nitriles	R-C≡N	Au, Ag, Ni, Cu, Pt
Nitrogen-containing compounds	R-NH_2, R_2-NH, R_3N, and others (such as azoles)	Cu, Au
Cyanates	R-N=C=O	Pt, Pd, Rh, Ru
Silanols	R-Si-OH	SiO_2, Al_2O_3, quartz, glass, mica, ZnSe, GeO_2
Phosphorus compounds	R_3P	Au, CdS, CdSe, CdTe
	R_3P=O	Co, CdS, CdSe, CdTe

*R denotes alkyl or aromatic groups.

1.4 Opportunities and Challenges of ICA Technology

Low temperature processibility and ability to form flexible interconnects are two key features of ICAs that enable ICAs to be widely used in emerging fields with huge markets, such as printed and flexible electronics and solar cell applications. In recent years, intense efforts have been devoted to the fabrication and formulation of flexible electronic materials (substrate, interconnect etc.) to address the dramatically increasing need for high performance, highly compact and portable devices. The flexible materials offer significant advantages of low profile, light weight, improved form factor and high-density electronic packaging, attractive for the current and emerging applications in microelectronics [108-109]. In particular, flexible interconnects allows for highly

integrated systems on flexible substrate materials to be light-weight, thin, bendable and potentially stretchable enabling the development of more compact end-products [109]. Flexible highly conductive interconnect materials with a low-temperature processing allow the assembly of electronic devices on the flexible, low cost, temperature-sensitive organic substrates, thus promising for emerging applications.

One major challenge of ICA properties is lower conductivity, compared with tin-lead solder. The lower conductivity of ICAs results from the physical contact of electrically conductive fillers, rather than metallurgical bonds. Therefore, fundamental understanding of the interface between electrically conductive fillers and engineering the interface are crucial to improve the electrical conductivity of ICAs. Moreover, high cost of silver flakes used as conductive fillers in ICAs further restricts the wide applications of ICAs. So far, research into low-cost ICAs has been a limited success.

1.5 Research Objective/Methodology

In recognition of the importance and challenges of ICA technology, the objectives of the dissertation are:

- to understand the interface between conductive fillers;
- to understand the role of surface chemistry and the thermal behavior of nanosized conductive fillers in the electrical conductivity of ICAs;
- to engineering the interface between conductive fillers to develop highly conductive ICAs;
- and to prevent the corrosion of copper and develop highly reliable, highly conductive, low cost ICAs.

It is well known that organic molecules (such as surface residues or lubricant) present on the surface of conductive fillers plays a key role in the electrical conductivity of ICAs. The presence of organic molecules facilitates the dispersion of conductive fillers in the polymer matrix while these organic molecules may inhibit the direct metal-metal contacts. Obviously, the presence of organic molecules on the surface of conductive fillers increases the contact resistance of ICAs. To improve the conductivity of ICAs, it is important to reduce and even eliminate the contact resistance between conductive fillers. Low temperature sintering technology is introduced to reduce and eliminate the contact resistance by forming metallurgical joints between conductive fillers. The first goal is to investigate the effect of surface chemistry of nanosized conductive fillers on the sintering and determine at what temperature that sintering can significantly contribute to the improved conductivity of ICAs. Through this study, it is learned that lower content and lower decomposition temperatures of surface residues are key factors to achieve low temperature sintering. Along with the optimization of nanoparticle synthesis, the study of the decomposition of lubricants on the surface of silver flakes is further conducted to reduce the sintering duration required to achieve high conductivity of ICAs, since long time sintering (1 h) is not preferred for industrial applications. So the second goal is to reduce the sintering duration and make the sintering (or curing) compatible with industrial reflow process. Although a very high conductivity has been achieved by sintering between the incoroporated silver nanoparticles and silver flakes, many challenges remain to be resolved such as high cost of the incorporated silver nanoparticles and efficient dispersion of silver nanoparticles. So the third objective is to solve these problems associated with the incorporated silver nanoparticles and develop

flexible highly conductive ICAs. As known, silver is very expensive while copper is much cheaper. However, copper is easily oxidized, resulting in the degradation of electrical properties of ICAs filled with copper particles. The final research objective in the dissertation is to replace expensive silver flakes with lower cost silver-coated copper flakes. The research mainly focuses on preventing the corrosion of silver-coated copper flakes to develop highly reliable, highly conductive and low cost ICAs.

1.6 Organization of the Dissertation

The dissertation is organized into the following chapters:

Chapter 2 introduces sintering technology (the driving forces, mechanisms and challenges) and investigates the effect of surface chemistry of silver nanoparticles and their thermal behavior on the electrical properties of ICAs.

Chapter 3 describes the fast preparation of printable highly conductive adhesives by the decomposition of silver carboxylates on the surface of silver flakes and sintering of silver nanoparticles. Silver nanoparticle synthesis is further optimized based on the results in Chapter 2. Chapter 3 also investigates the thermal behaviors of silver flakes and silver nanoparticles, the effects of sintering (curing) durations and temperatures on the electrical properties of ICAs, and the morphology of ICAs induced by sintering. The rheological properties of ICA pastes are also discussed and optimized for non contact printing.

Chapter 4 introduces a novel approach to prepare flexible highly conductive adhesives at a low temperature (150 ^{o}C) and solves many problems associated with the incorporation of silver nanoparticles as described in chapters 2 and 3. This chapter studies the epoxy compositions and the surface properties of silver flakes and explains the

conductivity enhanced mechanism. In addition, a coupling agent is used to improve the adhesion strength of flexible highly conductive adhesives on a gold surface.

Chapter 5 describes the preparation of highly reliable, highly conductive and low cost ICAs by the replacement of expensive silver flakes used in chapters 2-4 with low cost silver-coated copper flakes. This chapter describes the research progresses on low cost ICAs, the production of silver-coated copper flakes, and copper corrosion and its prevention using corrosion inhibitors. Followed are the characterization of silver-coated copper flakes and surface modification. Then this chapter studies the electrical properties of low cost ICAs and the contact resistance stability of the ICAs on a nickel/gold surface during the reliability tests (85 ^{o}C/85% RH and triple reflow).

Chapter 6 investigates the development of highly conductive, highly reliable and low cost ICAs by using an amine curing agent for in situ protection of silver-coated copper flakes. This chapter characterizes an epoxy resin cured with anhydride or amine curing agent by FT-IR. This chapter also compares the electrical resistivity betwen ICAs cured with an anhydride and ICA cured with an amine and their electrical resistivity stability during reliability tests. The reasons why ICAs cured with the amine have lower resistivity and better reliability than ICAs cured with the anhydride are discussed.

Chapter 7 summarizes the important research findings in chapters 1-6 and proposes future work.

CHAPTER 2

EFFECT OF THE SURFACE CHEMISTRY OF SILVER NANOPARTICLES ON THE ELECTRICAL RESISTIVITY OF ICAS

This chapter introduces sintering technology to reduce the contact resistance between conductive fillers and thus develop highly conductive adhesives. First, the driving force for sintering, sintering mechanisms and challenges of sintering within a polymer matrix are discussed. Followed by this understanding, silver nanoparticles with desired properties for sintering were synthesized by combustion chemical vapor condensation. Finally, the effect of surface chemistry of silver nanoparticles and their thermal behavior on the electrical properties of ICAs are investigated.

2.1 Introduction

The overall resistance of an ICA is the sum of the resistance of conductive fillers and the contact resistance between conductive fillers. The resistance of an ICA mainly results from the contact resistance between conductive fillers. Reducing the number of contact points between conductive fillers is an effective way to decrease the contact resistance. Two approaches have been reported to reduce the resistivity of ICAs. The first approach is to incorporate silver nanowires into the formulations [70-72]. High-aspect-ratio silver nanowires can reduce the percolation threshold effectively. However, the contact between conductive fillers is physical contact and as a result, the minimal resistivity of such ICAs reported in the literature is about 1.2×10^{-4} Ω cm [70]. The second approach is to incorporate silver nanoparticles into formulations and achieve

metallurgical joints between silver nanoparticles and silver flakes [80, 83-84], i.e. through sintering technology. It has been reported that ICA resistivity much lower than 10^{-4} Ω cm can be achieved by using sintering technology [80, 83-84]. "Sintering is a method for making objects from powder, by heating the material in a sintering furnace below its melting point (solid state sintering) until its particles adhere to each other [110]". Sintering of silver nanoparticles has been developed as a promising technique for a variety of electronic applications such as device interconnect [77-84], metal-metal bonding process [85] and production of conductive tracks [86-91]. Compared with solder technology, there are two advantages of using sintering of silver nanoparticles to achieve highly conductive ICA joints [81]. For solder technology, the solder interconnect has to operate at temperatures lower than their melting points. If high operating temperatures are needed, solders with high melting temperatures have to be used, which in turn requires high process temperatures. However, the sintered ICA joint can be formed at a temperature far below the melting point of silver (961.8 ^{o}C) and enable the joint to be operated at temperatures at or higher than their process temperature. Second, silver has higher electrical and thermal conductivities than solder.

2.1.1 The Driving Force for Sintering

The thermodynamic driving force for sintering is the reduction in interfacial energy. The differences in bulk pressure, vacancy concentration and vapor pressure, due to the difference in surface curvature of the particles, induce the mass transport [111]. These three parallel phenomena occur simultaneously and independently.

2.1.1.1 Bulk Pressure Difference

According to Young-Laplace equation, which relates the pressure difference to the shape of the surface, the pressure difference between the sphere surface and the neck surface:

$$\Delta P = P_0 - P_1 = \gamma_s(K_0 - K_1) = \gamma_s[\frac{1}{r} + \frac{1}{r} - (-\frac{1}{r_c} + \frac{1}{x})]$$

Here, we assume that K is the average curvature of the interface, while γ is the surface tension and r_0, r and x are the principal radii of curvature (Figure 2.1). The curvature of a concave surface and a convex surface are assumed to be negative and positive, respectively.

For r>> x>> r_c, $\Delta P = \frac{\gamma_s}{r_c}$

2.1.1.2 Vapor Pressure Difference

According to Kelvin equation, which relates the equilibrium vapor pressure of a liquid to the curvature of the liquid−vapor interface, the pressure difference between different surfaces:

$$RT \ln \frac{p}{p_0} = \gamma V_m (\frac{1}{r_1} + \frac{1}{r_2})$$

where p is the actual vapor pressure, p_0 is the saturated vapor pressure, γ is the surface tension, V_m is the molar volume, R is the universal gas constant, r_1 and r_2 are the principal radii of curvature, and T is temperature.

We assume K is the average curvature of the interface, r_1 and r_2 are the principal radii of curvature, then

$K = \frac{1}{r_1} + \frac{1}{r_2}$, for two sphere with same radius R, $K = \frac{2}{r} = \frac{1}{r_c}$ ($r = r_1 = r_2$) and r_c is the radius of the curvature

Then,

$$\ln\frac{p}{p_0}=\frac{2\gamma V_m}{RTr}=\frac{\gamma V_m}{RTr_c} \text{ (eqn. 1)}$$

In case of $\Delta p/p_0 << 1$, the following equation exists,

$$\ln\frac{p}{p_0}=\frac{\Delta p}{p_0} \quad (\Delta p = p - p_0)$$

Then, eqn. 1 becomes

$$\frac{\Delta p}{p_0}=\frac{\gamma V_m}{RTr_c}$$

Therefore, the difference of vapor pressure between the sphere surface and the neck surface is

$$\Delta p = p_0\frac{\gamma V_m}{RTr_c} \text{ or } p = p_0(1+\frac{\gamma V_m}{RTr_c})$$

Since we assume that the curvature of a convex (concave) surface is positive (negative), Δp becomes negative (positive). Therefore, the vapor pressure over a concave surface is lower than that over a convex surface. Equilibrium vapor pressure depends on droplet size. If $p_0 < p$, then liquid evaporates from the droplets. If $p_0 > p$, then the gas condenses onto the droplets increasing their volumes.

2.1.1.3 Vacancy Concentration Difference

It is assumed that the area of lower vapor pressure possesses a lower concentration of vapor molecules. Conversely, the surface of lower concentration of vapor molecules has a higher vacancy concentration [112]. If the vacancy concentration is C_0, corresponding to pressure P_0, then the vacancy concentration difference is

$\Delta C = C_0\frac{\gamma V_m}{RTr_c}$ [112].

2.1.2 Mechanisms for Sintering in the Two-sphere Model

When two particles come to contact, a small neck with high curvature forms. The difference in surface curvature between the neck surface and the particle surfaces results in the differences in bulk pressure, vapor pressure and vacancy concentration. These differences provide the driving force for mass transport to the neck during sintering. The mass transport contributes to the neck growth and to densification. Figure 2.2 illustrates the six alternative paths for mass transport during sintering [113]. The six transport mechanisms have the same driving force—the reduction in the total interfacial energy, however, with different diffusive paths, sources and sinks, as shown in Table 2.1 [113]. The dominant sintering mechanism depends on the material system, the particle size, the sintering temperature and time, and the pressure if applied [114].

All these transport mechanisms lead to the neck growth, but only some of them contribute to densification, i.e. grain boundary diffusion, lattice diffusion from grain boundary to neck surface and viscous flow. Viscous flow is typically not applicable to description of sintering process of a powder compact of crystalline particles unless extremely high stresses are applied [115]. Therefore, grain boundary diffusion is the source of mass transport for densification in a powder compact of crystalline particles.

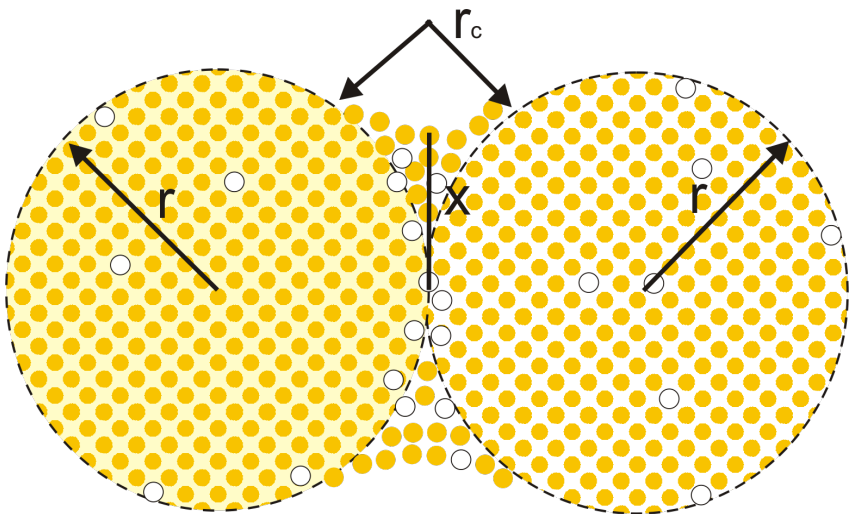

(a)

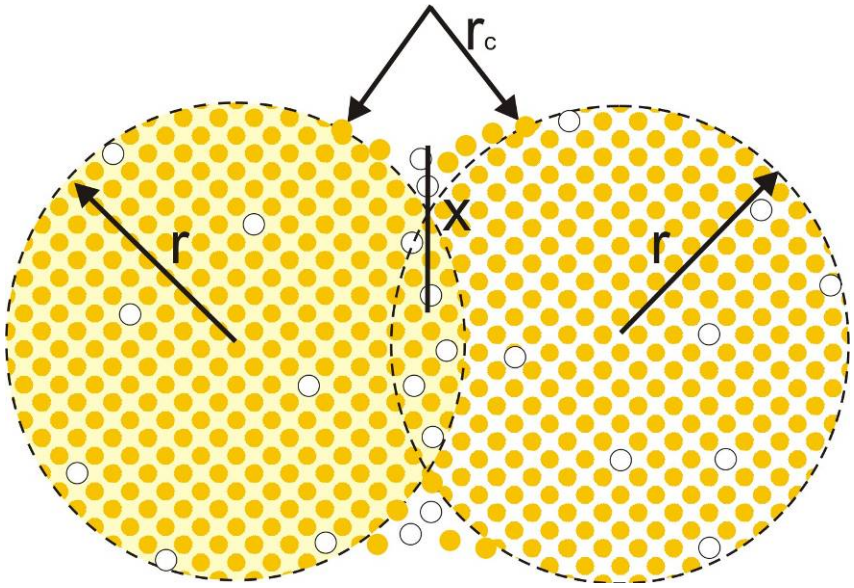

(b)

Figure 2.1 Two-sphere model for initial stage sintering (a) without shrinkage and (b) with shrinkage.

When two particles with different crystalline orientation come to contact, the grain boundary forms. Due to its atomic structure, vacancies move along the grain boundary readily while a net flow of material is in exactly the opposite direction. The

accumulation of vacancies along a grain boundary to form a disk of open volume which collapses by the attraction of the adjacent grains results in the densification or shrinkage [116].

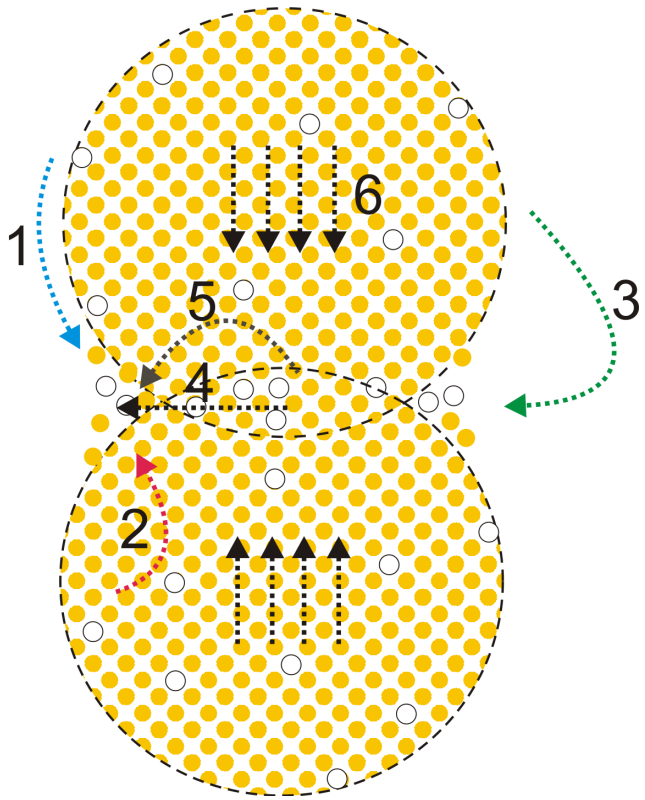

Figure 2.2 Mass transport mechanisms during sintering. 1. surface diffusion, 2. lattice (bulk or volume) diffusion from grain boundary to the neck surface, 3. grain boundary diffusion, 4. lattice diffusion from surface to neck, 5. evaporation-condensation, 6. viscous flow [113].

Table 2.1 Mass transport mechanisms during sintering [113]

Mechanism	Transport path	Source	Sink	Densification
1	Surface diffusion from particle surface to neck	Surface	Neck	No
2	Lattice diffusion from particle surface to neck	Surface	Neck	No
3	Evaporation-condensation	Surface	Neck	No
4	Grain boundary diffusion grain boundary to neck	Grain boundary	Neck	Yes
5	Lattice diffusion from grain boundary to neck	Grain boundary	Neck	Yes
6	Viscous flow	Bulk grain	Neck	Yes

In the two-sphere model, the equation that relates the neck radius (x), the particle radius (r), sintering time (t) and temperature (T) can be expressed as a general form during the initial stages of sintering:

$$(\frac{x}{r})^n = Fr^{m-n}t \quad \text{(eqn. 2)}$$

Theoretically, the mechanism of sintering can be determined by comparing the observed rate of neck growth with rates calculated based on one of the above mechanisms, or using Herring's scaling laws. The unambiguous determination of sintering mechanism is, however, usually complicated by the several simultaneous and independent mass transports [117].

Table 2.2 Values for the variables in eqn. 2 [75].

No.	Transport path	n	m	F	Neck growth	Shrinkage	Scale exponent (α)
1	Surface diffusion from particle surface to neck	7	3	$\frac{56D_s\delta_s\gamma_sV_m}{RT}$	$x^7=\frac{56D_s\delta_s\gamma_sV_mr^3t}{RT}$		4
2	Lattice diffusion from particle surface to neck	5	2	$\frac{20D_l\gamma_sV_m}{RT}$	$x^5=\frac{20D_l\gamma_sV_mr^2t}{RT}$		3
3	Evaporation-condensation	3	1	$\sqrt{\frac{18}{\pi}}\frac{p_\infty 20\gamma_sV_m}{d^2}(\frac{M}{RT})^{3/2}$	$x^3=\sqrt{\frac{18}{\pi}}\frac{p_\infty 20\gamma_sV_ma^2}{d^2}(\frac{M}{RT})^{3/2}rt$		2
4	Grain boundary diffusion grain boundary to neck	6	2	$\frac{48D_b\delta_b\gamma_sV_m}{RT}$	$x^6=\frac{48D_b\delta_b\gamma_sV_mr^2t}{RT}$	$\frac{\Delta l}{l}=(\frac{3D_b\delta_b\gamma_sV_m}{4RTr^4})^{\frac{1}{3}}$	4
5	Lattice diffusion from grain boundary to neck	4	1	$\frac{16D_l\gamma_sV_m}{RT}$	$x^4=\frac{16D_l\gamma_sV_mr}{RT}t$	$\frac{\Delta l}{l}=(\frac{D_l\gamma_sV_m}{RTr^3})^{\frac{1}{2}}t^{\frac{1}{2}}$	3
6	Viscous flow	2	1	$\frac{4\gamma_s}{\eta}$	$x^2=\frac{4\gamma_srt}{\eta}$	$\frac{\Delta l}{l}=\frac{3\gamma_st}{8\eta r}$	1

Symbols: x =neck radius, γ_s = surface energy, D_s = diffusion coefficient for surface diffusion δ_s = thickness for surface, V_m = atomic volume, R =gas constant, T =temperature, r =particle radius, t =sintering time, D_l = diffusion coefficient for lattice diffusion from particle surface to neck, p_∞ = vapor pressure, M = molecular weight, $d=\frac{M}{V_m}$ = theoretical density, D_b = diffusion coefficient for grain boundary diffusion, δ_b =thickness for grain boundary, D_l = diffusion coefficient for from grain boundary to neck, η =viscosity.

With an assumption of no grain growth, Ashby constructed a sintering diagram, based on the various sintering mechanisms, to identify the dominant sintering mechanism at a given temperature, particle size and neck size and to show the rate of sintering that resulted from all the mechanisms acting together [113]. Note the assumption may not be justified in real sintering. To experimentally determine a sintering mechanism, two requirements need to be met: (a) data are in agreement with the absolute values of calculated rates with Herring's scaling law and (b) the correct temperature dependence for the proposed mechanism [117]. Besides this, the distance between two spheres (i. e with or without shrinkage) could be used to differentiate the mechanisms of surface diffusion from particle surface to neck or evaporation-condensation from viscous flow, volume diffusion from grain boundary to neck or grain boundary diffusion.

It is generally believed that at low temperatures the dominant sintering mechanism is surface diffusion as surface diffusion requires low activation energies and has the easiest mass transport path. The much lower activation energy of grain boundary diffusion than lattice diffusion also makes grain boundary diffusion prevail in the initial stages of sintering [93].

2.1.3 Challenges for Low Temperature Sintering of Silver Nanoparticles in a Polymer Matrix

Sintering is dependent on many factors such as organic molecules on the nanoparticle surfaces, particle size, pressure, atmospheric gas, temperature and sintering duration [118]. In particular, the removal of organic molecules (or silver oxide) from the surface of silver nanoparticles plays an important role in low temperature sintering onsets, extent of densification and final grain sizes [81]. Although sintering can occur at

room temperature [90, 95], typically sintering temperature above 200 ^{o}C is required to achieve desirable electrical and mechanical properties [119-120], which is not compatible with most polymeric substrates [77, 86, 88]. The challenge of low temperature sintering (<200 ^{o}C) of silver nanoparticles synthesized by wet-chemical methods lies in the fact that various excellent stabilizers cannot be debonded/decomposed or take a long time to debond/decompose at low temperatures since the removal of organic molecules is a prerequisite for sintering to occur [121-123].

Although electrical resistivity of silver films close to that of bulk silver (1.6×10^{-6} Ω cm) has been achieved by sintering of silver nanoparticles in conductive silver inks at low temperatures (<200 ^{o}C) [90, 93], very limited researches on the preparation of polymer composites with very low resistivity (<10^{-4} Ω cm) by sintering of silver nanoparticles at low temperatures have been found in the literature. Instead, addition of silver nanoparticles into silver flakes-filled ICAs results in a dramatic increase in the bulk resistivity of the ICAs [96-97]. This increase in resistivity is related to number of contact points and reduced contact area between conductive fillers. A possible reason for the high resistivity is the difficult debonding or decomposition of organic molecules (or silver oxide) at the curing tempeature (<200 ^{o}C). Furthermore, the sintering of silver nanoparticles in polymer composites hindered by high volume fraction (typically 70-80 vol%) of highly cross-linked polymer matrices may also explain the high resistivity observed.

Since the decomposition of surface residues on silver nanoparticles plays a key role in the thermal sintering of silver nanoparticles, silver nanoparticles in the present study were synthesized by the combustion chemical vapor condensation (CCVC) method

as it offers many significant advantages over the most widely used wet-chemical methods for the synthesis of silver nanoparticles for highly conductive ICAs, including low decomposition temperatures of surface residues, low content of surface residues and increased production rates (up to 0.1-1 kg/h) [124]. Silver nanoparticles with the first two characteristics will promise a low sintering temperature and thus allow the formation of the metallurgical joints between the conductive fillers within a polymer matrix to reduce the contact resistance effectively (Figure 2.3). This would result in an ICA with very low resistivity at a low temperature. In order to identify the critical temperature at which the sintering of silver nanoparticles will lead to significantly improved electrical conductivity, thermal behavior of silver nanoparticles was investigated and used as a guideline for the preparation of the ICAs with very low resistivity.

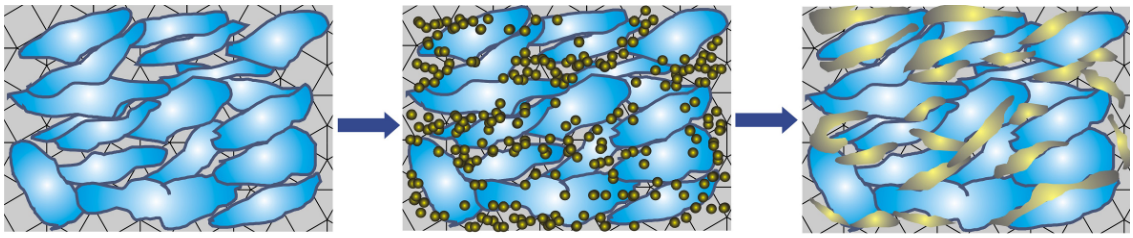

Figure 2.3 Schematic representation of ICAs. (a) an ICA filled with silver flakes; (b) an ICA filled with both silver flakes and nanoparticles; (c) an ICA filled with sintered particles among flakes [77].

2.2 Experimental

2.2.1 Materials

The epoxy resin and hardener used were diglycidyl ether of bisphenol F (DGEBF, Shell Chemical Co.), and hexahydro-4-methylphthalic anhydride (MHHPA, Lindau Chemicals), respectively. Catalyst was 1-cyanoethyl-2-ethyl-4-methylimidazole (2E4MZCN, Shikoku Chemicals Corp.) Molecular structures of these chemicals were shown in Figure 1.3. Silver flakes were donated by Ferro Corp. Typically, surface lubricants such as stearic acid were present on the silver flake to improve the rheological properties and prevent the agglomeration of silver flakes. Silver nanopartilces were synthesized by a CCVC method and donated by nGimat. All chemicals were used as received.

2.2.2 Synthesis of Silver Nanoparticles by CCVC

Figure 2.4 shows the combustion chemical vapor deposition (CCVD) process [125]. Precursors such as silver nitrate or silver carboxylate (in our case silver salt of fatty acid) were dissolved in a solvent (alcohol), which typically also acts as the combustible fuel [124, 126]. The solution was atomized to form submicron droplets, which were then mixed with oxidizing gas (O_2) and ignited to generate a flame spray. Combustion of the solvents provides heat to decompose the precursors and yield metal and oxide vapors that consist of gaseous atoms, ions, and molecular-oxide species. And these vapor species condense to form atomic clusters that may coalesce to form nanoparticles (Figure 2.4) [126-128].

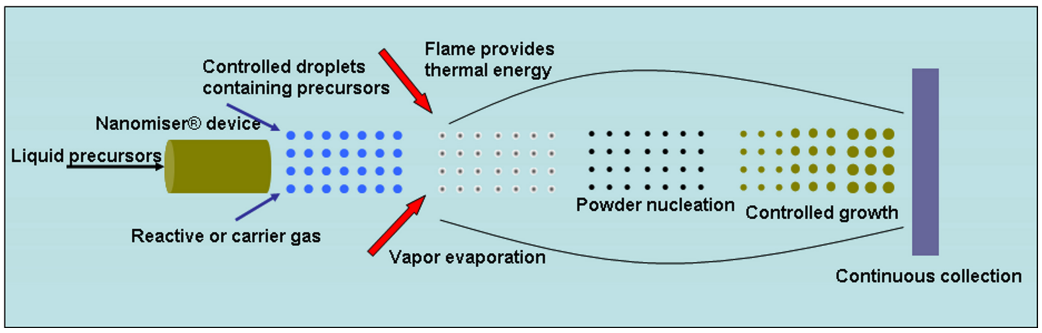

Figure 2.4 Combustion chemical vapor deposition (CCVD) process [125].

Two silver nanoparticles (nanoAg **A** and nanoAg **B**) were synthesized by CCVC using the same starting precursor (silver salt of fatty acid), but under different synthetic conditions. NanoAg **A** was synthesized under a reducing atmosphere and thus carbonaceous surface coating on silver nanoparticles formed. NanoAg **B** was made under an oxidizing atmosphere and the surface composition was mainly silver oxide. Additionally, during nanoparticles synthesis, a limited amount of the starting precursor may not be completely pyrolyzed and thus could be present in the nanoparticles.

2.2.3 Preparation of ICAs

A 4:6 molar ratio of silver nanoparticles to silver flakes (totally 80 wt%) were incorporated into the mixture of DGEBF and HMPA with a molar ratio of 1:0.85. The mixture was sonicated for more than 1 hour to disperse the conductive fillers. The catalyst was added into the formulations and the mixture was subsequently sonicated for another 0.5 hour. Following sonication, the formulated pastes were thermally cured at temperatures of 150 and 180 ^{o}C to prepare ICAs.

2.2.4 Characterization

The resistivity of ICAs was calculated from bulk resistance of a specimen with specific dimensions. Two strips of a Kapton tape (Dupont) were applied onto a pre-cleaned glass slide. The formulated paste was printed on the glass slide. After thermal cure, bulk resistance (R) of ICA strips was measured by a Keithley 2000 multimeter. The width and length of the specimen were measured by digital caliber (VWR). The thickness of the specimen was measured by Heidenhain (thickness measuring equipment, ND 281B, Germany). Bulk resistivity, ρ, was calculated using Equation (1):

$$\rho = \frac{t \times w}{l} \times R$$

where l, w, t are the length, width and thickness of the sample, respectively.

Weight losses of silver nanoparticles during heating in air were studied using a thermogravimetric analyzer (TGA) from TA Instruments, model 2050. The heating rate was 10 ^{o}C/min.

The morphology of silver nanoparticles and ICAs was studied by field emission scanning electron microscopy (SEM, Hitachi S-800 or LEO 1530).

X-ray diffraction analyses of silver nanoparticles were recorded at a scanning rate of 0.02 ^{o}/s in the 2θ range of 30-80^{o} using X-ray powder diffractometer (Philips PW 1800, PANalytical Almelo, The Netherlands) with a Cu-Kα radiation (λ=1.54 Å).

Raman spectra of silver nanoparticles were obtained by using a LabRAM ARAMIS Raman confocal microscope (HORIBA Jobin Yvon) equipped with a 532 nm diode pumped solid state (DPSS) laser. Si wafer was used as a substrate for Raman measurements.

X-ray photoelectron spectroscopy (XPS) experiments were performed on silver nanoparticles using a Thermo Scientific K-Alpha XPS with Al K_α source. The typical detection depth is about 5 nm.

2.3 Results and Discussion

2.3.1 Thermal Behavior of Silver Nanoparticles

Figure 2.5 shows TGA results of silver nanoparticles. NanoAg **A** shows a continuous weight loss starting at about 125 ^{o}C. The decomposition of surface residues was unfinished even up to 400 ^{o}C. This is indicative of the coating of nanoAg **A** by carbonaceous substances formed under reducing conditions. The small loss (0.61%) leading up to 200 ^{o}C indicates a relatively small amount of silver oxide on nanoAg **A**. NanoAg **B** shows two distinct characteristic weight losses. The first weight loss at 100 ^{o}C is due to moisture desorption from the surface of nanoAg **B** because silver oxide on nanoAg **B** has a much stronger affinity for moisture than hydrophobic carbonaceous substances on nanoAg **A**. The second significant weight loss at 205 ^{o}C (Figure 2.5, inset) is attributed to the decomposition of silver oxide and possibly a very small amount of organic surface residues formed during the synthesis. It seems that the decomposition of surface residues is almost finished at 220 ^{o}C.

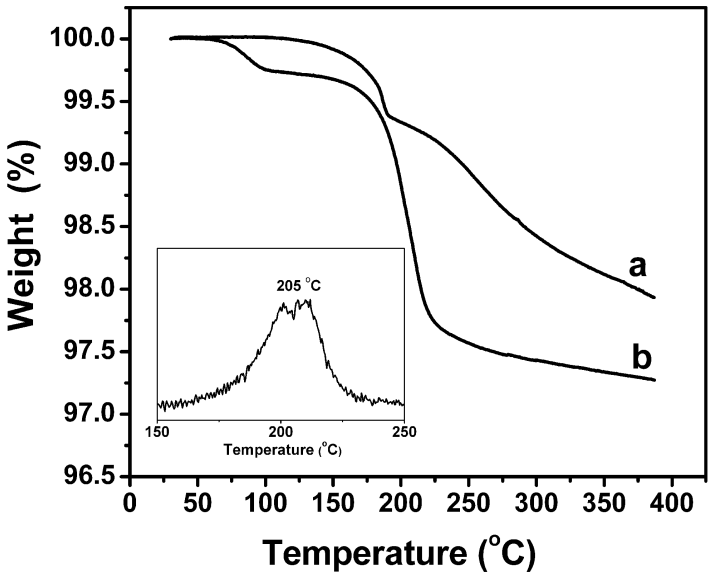

Figure 2.5 TGA results of nanoAg **A** and nanoAg **B**. Inset is the first derivative of the curve b in the temperature range of 150-250 ^{o}C.

The weight losses for nanoAg **A** and nanoAg **B** at 400 ^{o}C are 2.06% and 2.73%, respectively. The silver nanoparticles, in comparision with silver nanoparticles synthesized by wet-chemical methods (the content of surface residues, i. e. stabilizers, are typically higher than 10 wt%) [121-123], have much lower content of surface residues. For wet-chemical methods, stabilizers are used to prevent the agglomeration of silver nanoparticles and for the control of the size, shape, size distribution and solubility [129-130], including long-chain carboxylates [121], polyvinylpyrrolidone [96, 131], polyacrylamide [130], etc. Removal of these stabilizers from silver nanoparticles will cause severe agglomeration. Moreover, compared with nanoAg **B**, silver nanoparticles by wet-chemical methods show higher decomposition temperture of surface residues, typically >250 ^{o}C [96, 122, 129, 131] . Nguyen et al. reported nitrocellulose-stabilized

silver nanoparticles as low conversion temperature precursors for inkjet printed electronics [123]. Although the degradation of nitrocellulose starts at 135 ^{o}C, the process is slow and is not complete until 260 ^{o}C in the TGA experiments when heated at 10 ^{o}C/min [123]. NanoAg **B** with low content and a low decomposition temperature (starting at 160 ^{o}C and almost finished at 220 ^{o}C) of surface residues will be promising for thermal sintering at a low temperature.

Surface-enhanced Raman Spectroscopy (SERS) was used to study the surface residues on the silver nanoparticles. Figures 2.6 and 2.7 show SERS of both nanoAg **A** and nanoAg **B**. These two Raman spectra show similar features, which indicates that part of the precursor may not be fully pyrolyzed during the CCVC syntheses. However, the intensity of the band at 2936 cm^{-1} due to the stretching of C-H in Figure 2.6 is much stronger than that in Figure 2.7, indicating there is much more hydrocarbon on nanoAg **A** than that on nanoAg **B**. The peak at 1783 cm^{-1} assigned to C=O stretching in Figure 2.7 is related to the oxidation product during the CCVC synthesis under oxidizing conditions, which is absent in Figure 2.6. The most intense SERS peak at 1609 cm^{-1} assigned to aromatic C=C stretching was ascribed to the direct surface-ring π orbital interaction while the peaks at 862 and 820 cm^{-1} are assigned to the benzene ring modes.[25, 26] The peaks at 711 and 1394 cm^{-1} in Figure 2.6 (or 1387 cm^{-1} in Figure 2.7) are assigned to the deformation and the symmetric stretching mode of the -COO^{-} group, respectively. Additionally, weak peaks centered at 488 cm^{-1} in Figures 2.6 and 2.7 indicate the presence of silver oxide in both silver nanoparticles [132].

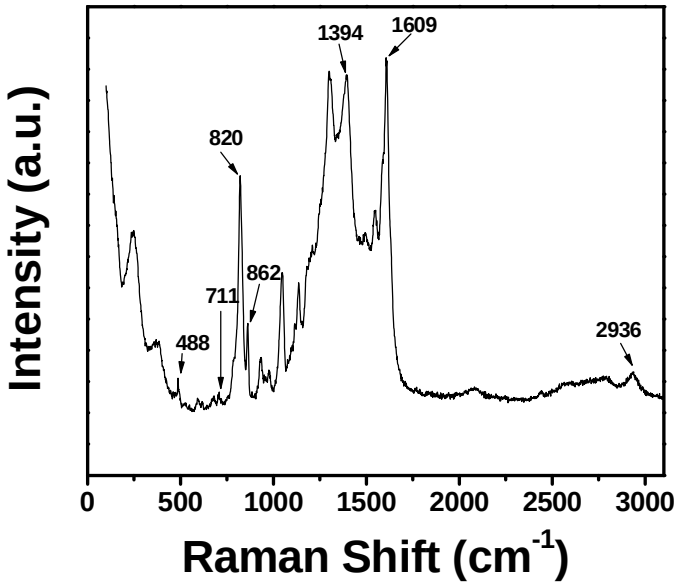

Figure 2.6 SERS of nanoAg **A**.

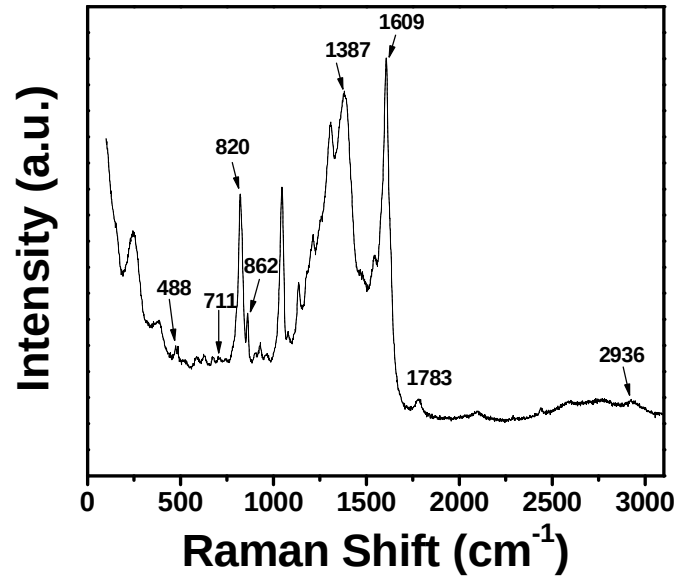

Figure 2.7 SERS of nanoAg **B**.

XPS spectra of nanoAg **A** and nanoAg **B** are shown in Figure 2.8. The peaks apparent in the two spectra include the Ag core-level peaks, the O1s and the C1s peaks.

Table 3.1 summarizes the atomic ratios of O/Ag of both nanoparticles before and after the isothermal treatments. It is found that nanoAg **B** has a higher O/Ag ratio than nanoAg **A**. After being treated at 150 ^{o}C for 1 h, nanoAg **A** shows a much higher increase in O/Ag ratio than nanoAg **B**. The increase of O/Ag ratios for both nanoparticles could be related to the oxidation of organic surface residues. Figure 2.9 shows the high resolution C1s XP spectra of silver nanoparticles before and after the isothermal treatments. NanoAg **A** shows two distinct peaks at 284.6 and 287.1 eV, which could be assigned to the carbon present on the hydrocarbon and carbonyl groups present on the surface residues, respectively [133]. After being treated at 150 ^{o}C for 1 h, two distinct peaks at 284.8 and 289.1 eV and a shoulder peak at 286.8 eV are clearly observed. The peaks at 286.8 and 289.1 eV could be assigned to the carbon present on the ketone/aldehyde and carboxylate (or possibly carbonate), respectively [133-135]. These results indicated that hydrocarbons present on the surface of nanoAg **A** have been oxidized during the thermal treatment at 150 ^{o}C. NanoAg **B** shows an asymmetric peak at 284.9 eV and a shoulder peak at 286.8 eV. The peak present at 286.6 eV could be assigned to the carbon present on the ketone/aldehyde. This is consistent with the Raman result, as C=O stretching is observed at 1783 cm^{-1}. After being treated at 150 ^{o}C for 1 h, nanoAg **B** shows a broadening peak at 284.9 eV and the peak at 289.1 eV almost disappears, which may indicate that carboxylate could have decomposed. After being treated at 180 ^{o}C for 1 h, nanoAg **A** shows an increase in O/Ag ratio while nanoAg **B** shows a decrease in O/Ag ratio. Combined the decreased in O/Ag ratio with the TGA results (Figures 2.5 and 2.15), it can be concluded that silver carboxlate and/or silver oxide on the surface of nanoAg **B** have been decomposed during the thermal treatment at 180 ^{o}C.

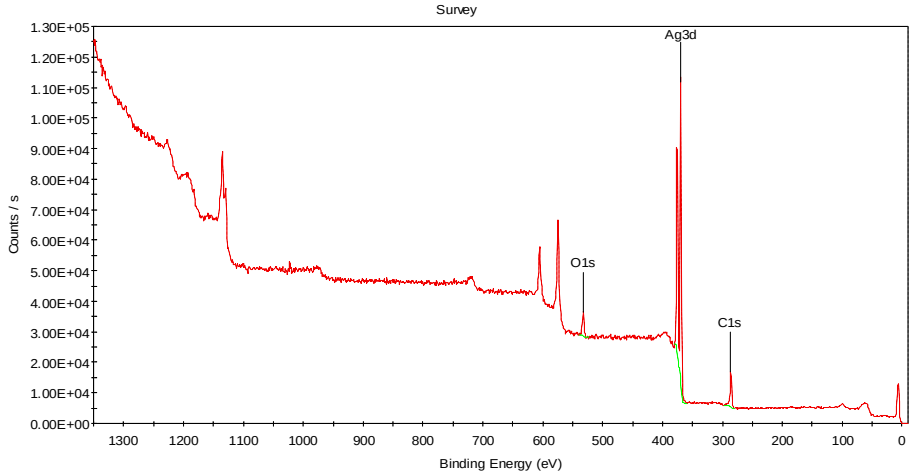

(a)

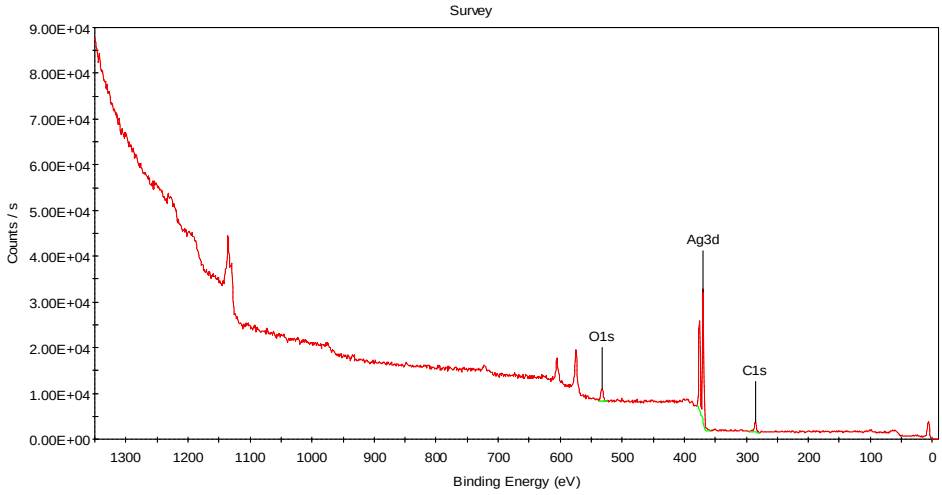

(b)

Figure 2.8 XPS survey spectra of (a) nanoAg **A** and (b) nanoAg **B**.

Table 3.1 Oxygen-to-silver atomic ratios.

	NanoAg **A** **(**O/Ag**)**	NanoAg **B** **(**O/Ag**)**
As received	0.45	0.70
150 ^{o}C	1.2	0.79
180 ^{o}C	0.49	0.40

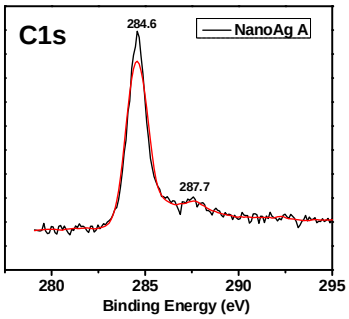

(a)

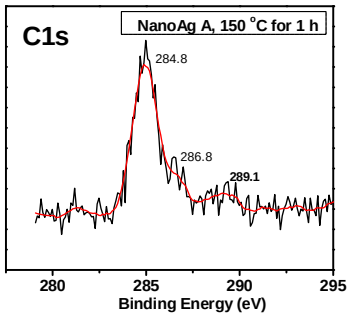

(b)

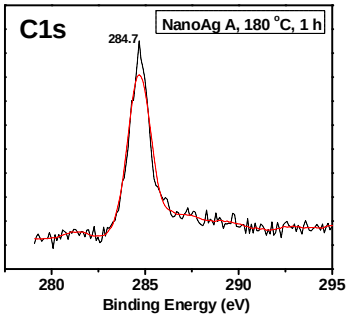

(c)

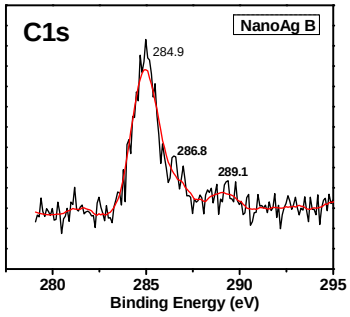

(d)

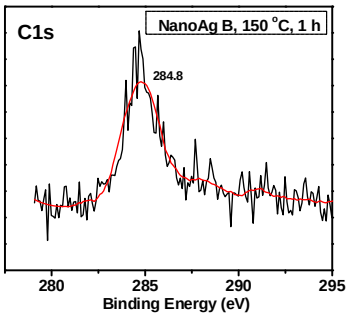
C1s
NanoAg B, 150 °C, 1 h
284.8
280
285
290
295
Binding Energy (eV)

(e)

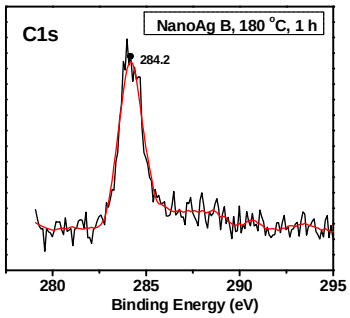
C1s
NanoAg B, 180 °C, 1 h
284.2
280
285
290
295
Binding Energy (eV)

(f)

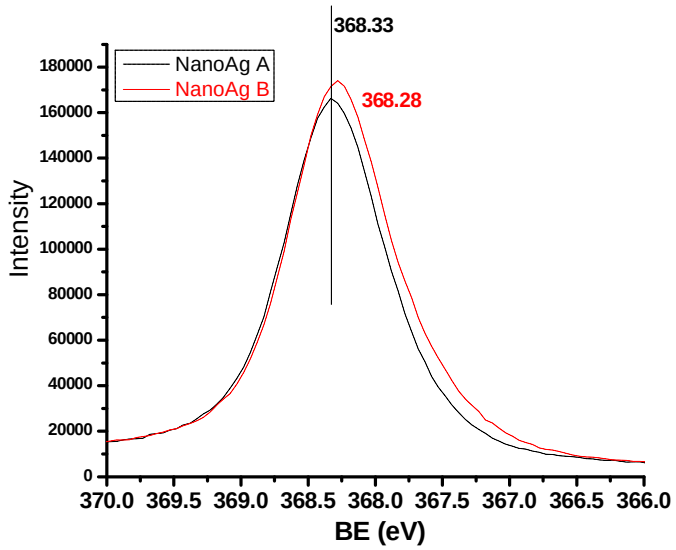
368.33
NanoAg A
NanoAg B
368.28
180000
160000
140000
120000
100000
80000
60000
40000
20000
0
Intensity
370.0
369.5
369.0
368.5
368.0
367.5
367.0
366.5
366.0
BE (eV)

(g)

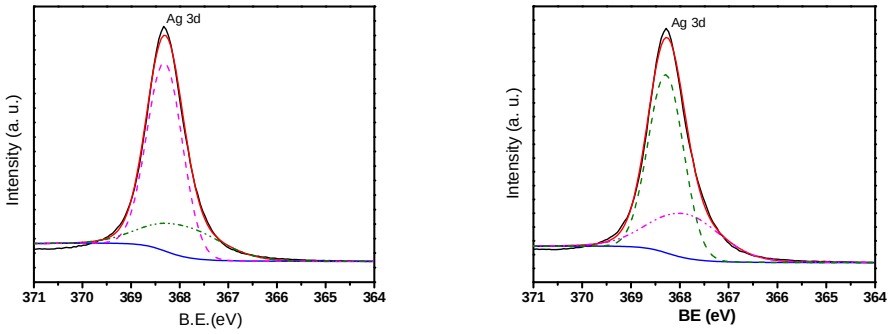

(h) (i)

Figure 2.9 High resolution C1s XP spectra of (a) nanoAg **A**, (b) nanoAg **A** treated at 150 ^{o}C for 1 h, (c) nanoAg **A** treated at 180 ^{o}C for 1 h, (d) nanoAg **B**, (e) nanoAg **B** treated at 150 ^{o}C for 1 h, (f) nanoAg **B** treated at 180 ^{o}C for 1 h. High resolution Ag 3d XP spectra of nanoAg **A** and nanoAg **B** (g). Peak fitting of the Ag 3d spectra of nanoAg **A** (h) and nanoAg **B** (i).

Figure 2.9(g) shows Ag 3d XP spectra of nanoAg **A** and nanoAg **B**. Compared with nanoAg **A**, NanoAg **B** shows a negative shift of 0.05 eV and a broader Ag 3d peak. It has been reported that silver shows a negative shift as the amount of silver oxide on silver surface increases. The negative shift of Ag 3d in silver oxides is determined by factors other than electronegativity differences such as crystal, field potential, work function and relaxation energy [135]. Deconvolution of the the asymmetric Ag 3d XP spectra of nanoAg **A** and nanoAg **B** further confirms nanoAg **B** contains a larger amount of silver oxide than nanoAg **A** (Figures 2.9(h) and (i)).

2.3.2 Sintering of Silver Nanoparticles

In order to observe distinct sintering of silver nanoparticles, nanoAg **A** and nanoAg **B** were annealed at 220 ^{o}C for 0.5 hour. After annealing, the necks formed between silver nanoparticles as a result of minimization of surface energy by atomic diffusion (Figure 2.10). However, the increase in the particle size and the width of necks of nanoAg **B** are much larger than those of nanoAg **A**. It has been proposed that surface diffusion is dominated at the initial stage of sintering, followed by grain boundary diffusion and lattice diffusion as the temperature increases, since activation energy of surface diffusion is lower than that of grain boundary and lattice diffusion [93]. Crystal structures of the nanoparticles before (at room temperature) and after sintering at 220 ^{o}C for 0.5 hour were investigated by XRD (Figure 2.11). Before sintering, the particles show slightly broadened peaks, due to smaller particle sizes compared with the annealed particles. By using the Scherrer's equation (Equation (2)), the crystallite size of the nanoparticles was calculated [79].

$$t = \frac{K\lambda}{\beta \cos\theta} \qquad (2)$$

where t is the crystallite size, K is a shape factor with a typical value of 0.9, λ is the X-ray wavelength, θ is the diffraction angle and β is the full width at half maximum intensity (FWHM) in radians. Figure 2.12 shows the crystallite size of nanoAg **A** and nanoAg **B** before (as received) and after annealing. After annealing, the crystallite sizes of both nanoparticles increase, and the increase in size of nanoAg **B** is much larger than that of nanoAg **A**. Thus, during the sintering process, not only particle size increases but also the crystal grains in the particle grow. The growth of silver nanoparticles along with

the formation of the necks between conductive fillers will considerably reduce contact resistance, and larger necks will result in lower resistivity.

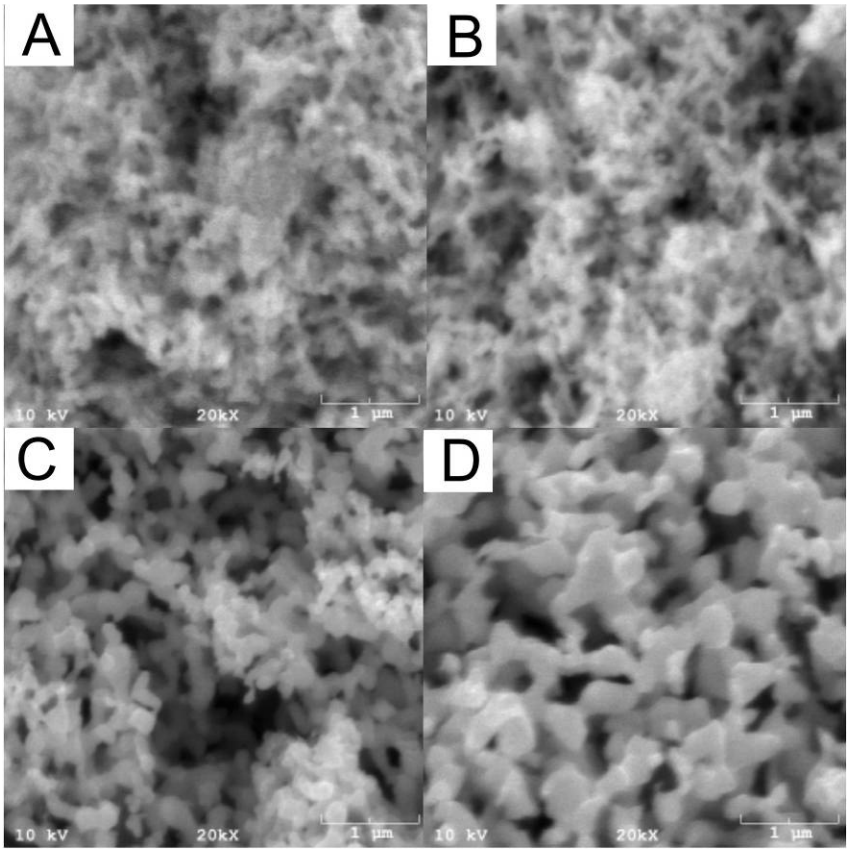

Figure 2.10 Comparison of the morphologies of (a) nanoAg **A** at room temperature, (b) nanoAg **B** at room temperature, (c) nanoAg **A** after annealing at 220 ^{o}C for 0.5 hour and (d) nanoAg **B** after annealing at 220 ^{o}C for 0.5 hour.

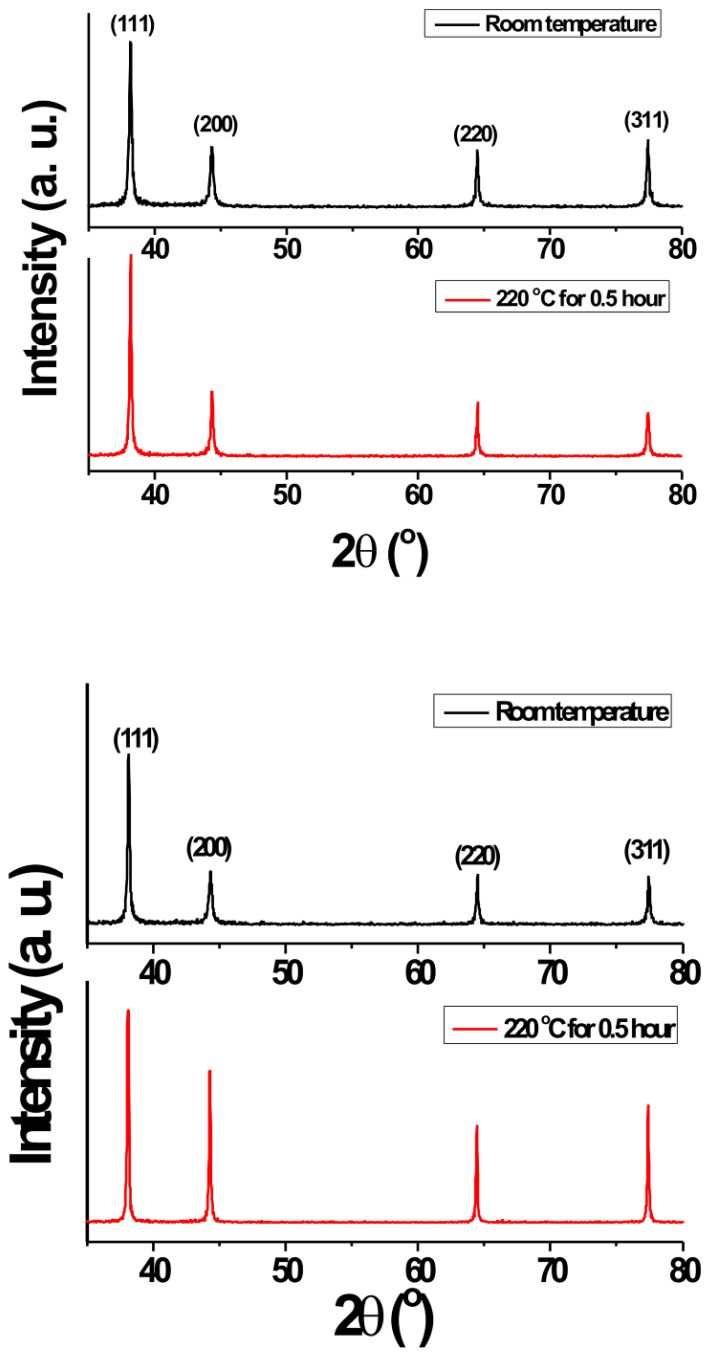

Figure 2.11 XRD of (a) nanoAg **A** and (b) nanoAg **B** before (at room temperature) and after annealing at 220 ^{o}C for 0.5 hour.

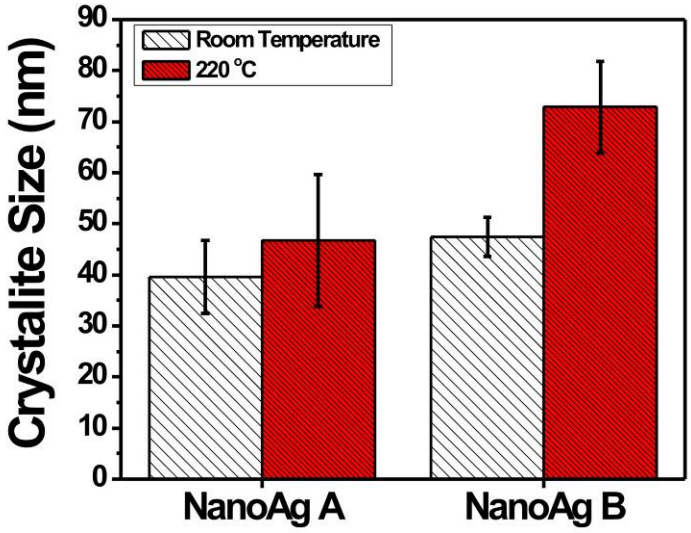

Figure 2.12 Crystallite sizes of silver nanoparticles before (at room temperature) and after annealing at 220 ^{o}C for 0.5 hour.

2.3.3 Electrical Properties of ICAs

Figure 2.13 shows bulk resistivity of ICAs filled with micron-sized silver flakes and the silver nanoparticles. When cured at 150 ^{o}C for 1 hour, bulk resistivities of ICAs filled with nanoAg **A** and silver flakes, and those with nanoAg **B** and silver flakes are 8.43×10^{-4} and 2.44×10^{-2} Ω cm, respectively, which are higher than that of typical micron-sized silver flake filled ICAs (~10^{-4} Ω cm). Figures 2.14 and 2.15 show that the weight losses of nanoAg **A** and nanoAg **B** are 0.73% and 1.11% (0.28% from moisture desorption) after heating at 150 ^{o}C for 1 hour, 0.87% and 2.62% (0.28% from moisture desorption) after heating at 180 ^{o}C for 1 hour, respectively. Comparing with the weight losses of nanoAg **A** (0.87%) and nanoAg **B** (2.62%) after heating at 180 ^{o}C for 1 hour in Figure 2.15, it can be concluded that, after curing at 150 ^{o}C for 1 hour, a relatively large

amount of silver oxide is still present on nanoAg **B** while silver oxide on nanoAg **A** is almost completely decomposed, although carbonaceous substances are still present on nanoAg **A**. Our previous studies indicate that silver oxide on silver flakes will cause a significant increase in the resistivity of the ICAs filled with silver flakes [69]. Thus the relatively higher electrical resistivity of ICAs filled with nanoAg **B** and silver flakes than that of those filled with nanoAg **A** and silver flakes could be from a relatively large amount of silver oxide on nanoAg **B**. By SEM studies, Ye et al. observed that addition of silver nanoparticles into a polymer matrix with micron-sized conductive fillers decreases the chance of direct contact among micron-sized fillers and the contact area between nano- and micron- sized particles is smaller than that between micron-sized particles [97]. In addition, the number of contact points will significantly increase. As a result, the resistivity of the ICAs with nano- and micron-sized particles increases as the percentage of silver nanoparticles increases.

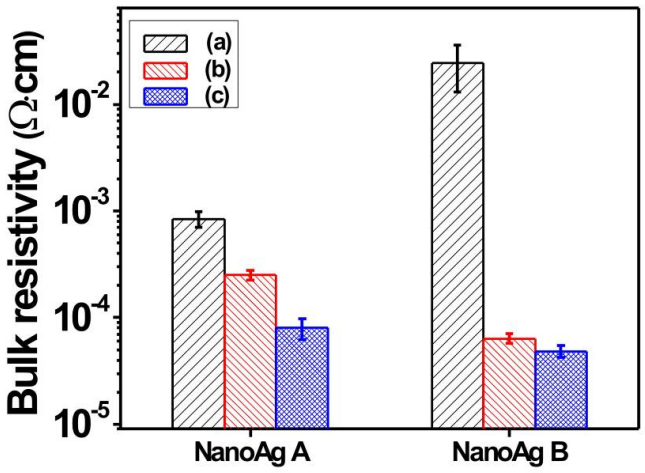

Figure 2.13 Bulk resistivity of ICAs filled with nanoAg **A** and silver flakes, and those with nanoAg **B** and silver flakes (a) cured at 150 ^{o}C, (b) annealed at 180 ^{o}C after curing, and (c) cured at 180 ^{o}C.

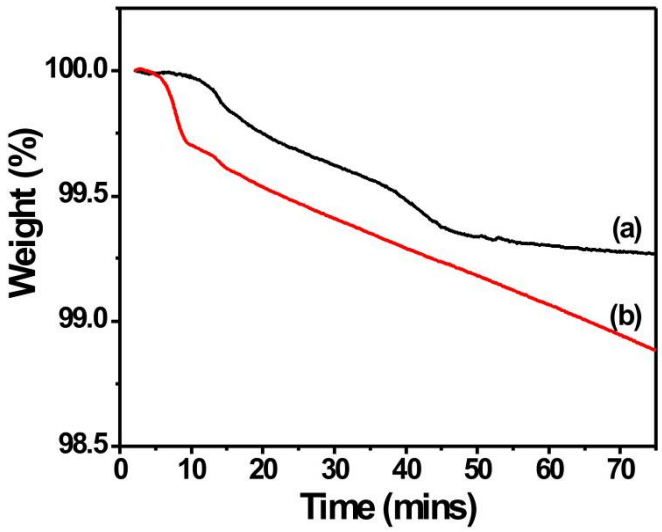

Figure 2.14 Weight losses of (a) nanoAg **A** and (b) nanoAg **B** isothermally heated at 150 ^{o}C for 1 hour.

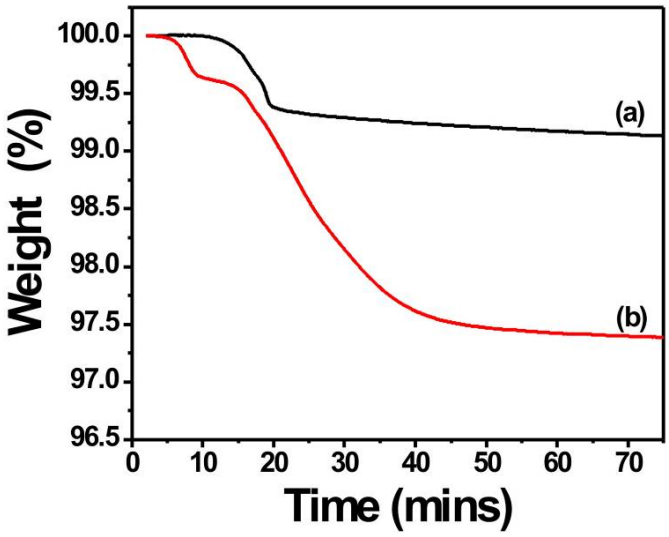

Figure 2.15 Weight losses of (a) nanoAg **A** and (b) nanoAg **B** isothermally heated at 180 ^{o}C for 1 hour.

After the samples were annealed at 180 ^{o}C for 1 hour, lower resistivities of both ICAs compared with those cured at 150 ^{o}C were obtained as a result of further sintering of silver nanoparticles. The resistivity of the annealed ICAs filled with nanoAg **A** and silver flakes is several times lower than that of the ICAs cured at 150 ^{o}C; the resistivity of ICAs filled with nanoAg **B** and silver flakes decreases more distinctly—three orders of magnitude lower than that before annealing. Comparing with the weight losses of nanoAg **A** (2.06% at 400 ^{o}C) and nanoAg **B** (2.73% at 400 ^{o}C) in Figure 2.5, it can be concluded that surface residues on nanoAg **B** have been almost completely decomposed while surface residues on nanoAg **A** have been partially decomposed after annealing at 180 ^{o}C for 1 hour. The nearly complete removal of the surface residues on nanoAg **B** at 180 ^{o}C contributes significantly to the growth of silver nanoparticles and thicker necks, compared with partial decomposition of the surface residues on nanoAg **A**. Moreover, the weight loss difference for nanoAg **B** between heating at 150 and 180 ^{o}C for 1 hour is much larger than that for nanoAg **A**. As a result, a dramatic decrease in bulk resistivity of ICAs filled with nanoAg **B** was observed after annealing at 180 ^{o}C for 1 hour, while the resistivity reduction of ICAs filled with nanoAg **A** was less significant. Figure 2.16 shows cross-sections of ICAs filled with silver flakes and nanoAg **B** cured at 150 ^{o}C for 1 hour, annealed at 180 ^{o}C for 1 hour and cured at 180 ^{o}C for 1 hour. When ICAs were cured at 150 ^{o}C (Figure 2.16 (a)), spherical silver nanoparticles were observed in the polymer matrix. When the samples were annealed at 180 ^{o}C or cured at 180 ^{o}C for 1 hour (Figures 2.16 (b) and (c)), the morphologies of the ICAs have been significantly changed and spherical silver nanoparticles have become an agglomerated mass, indicating sintering occurred between silver nanoparticles, and between silver nanoparticles and

silver flakes. More distinct sintering can be seen in Figure 2.16 (d) as some of the nanoparticles grow up into facets with loss of the spherical shape. The sintering of the conductive fillers allows the formation of the metallurgical joints between silver nanoparticles, silver nanoparticles and silver flakes, and thus 3-D conductive networks form within the polymer matrix. Consequently, sintering of nanoAg **B** within the polymer matrix at 180 ^{o}C will effectively reduce the contact resistance and thus ICAs with very low resistivity were achieved at 180 ^{o}C. In addition, even lower resistivity (4.8×10^{-5} Ω cm) is achieved for ICAs cured at 180 ^{o}C than that of the annealed one as curing of ICAs at 180 ^{o}C bypasses the low temperature regime and thus is more desirable for the particle growth and the neck formation between silver nanoparticles, and between silver nanoparticles and silver flakes.

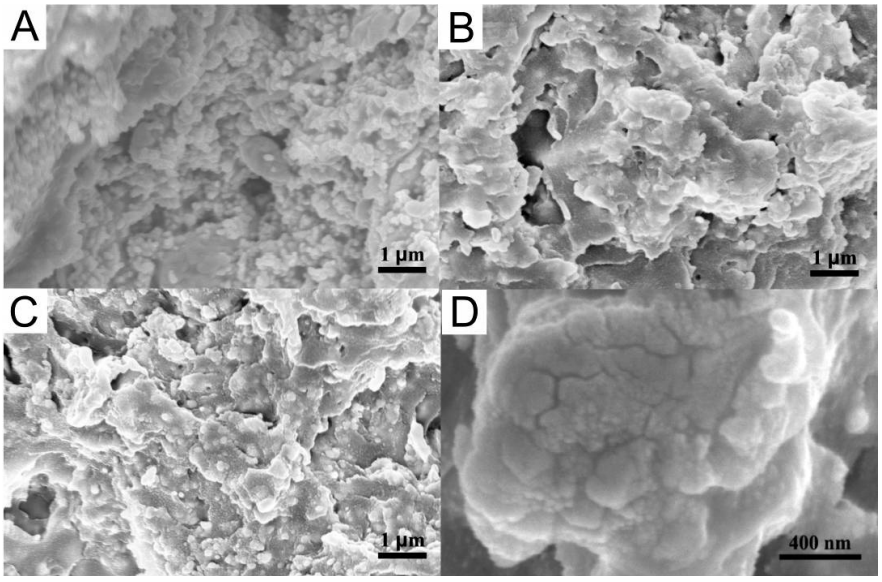

Figure 2.16 SEM images of cross-section of ICAs (a) cured at 150 ^{o}C, (b) cured at 150 ^{o}C and then annealed at 180 ^{o}C, (c) cured at 180 ^{o}C and (d) cured at 180 ^{o}C at a larger magnification.

2.4 Conclusions

Thermal behavior of silver nanoparticles has been studied by TGA, SERS, SEM, XPS and XRD to select silver nanoparticles suitable for the preparation of ICAs with very low resistivity at low temperatures. By the comparative studies of thermal behavior of silver nanoparticles, the critical processing temperature that leads to very low resistivity of ICAs has been identified for different silver nanoparticles. It is found that the surface chemistry of silver nanoparticles plays a key role in low temperature sintering. Silver nanoparticles with complete decomposition of surface residues at a lower temperature are more desirable for the preparation of highly conductive ICAs at low temperatures. The formulated ICAs with very low resistivity (4.8×10^{-5} Ω cm) at a low temperature (180 ^{o}C) will enable the electrical interconnection between temperature-sensitive surface mounted devices and non-solderable or flexible low-cost organic substrates.

CHAPTER 3

FAST PREPARATION OF PRINTABLE HIGHLY CONDUCTIVE ICAS

Based on the experimental results obtained in chapter 2, chapter 3 describes the further optimization of silver nanoparticles for the fast preparation of printable highly conductive ICAs. In this chapter, thermal behavior of silver flakes and silver nanoparticles are first investigated to provide a guideline for the processing temperature leading to highly conductive ICAs. Then, the effects of sintering (curing) durations and temperatures on the electrical properties of ICAs are studied. Finally, the rheological properties of ICA pastes are discussed and optimized for non contact printing.

3.1 Introduction

The preparation of novel printable conductive adhesives or inks is essential to providing new solutions to the dramatically increasing need for low cost, high performance, electrically functional devices in printed electronics. Inkjet printing of conductive silver inks on a substrate followed by sintering of silver nanoparticles or thermal decomposition of metallo-organic precusors has been developed as a promising technique for a variety of electronic applications. These applications include the interconnection of circuitry on a printed circuit board and the fabrication of conductive tracks or electrodes for thin-film transistors (TFTs), light-emitting diodes, solar cells, sensors, and radio frequency identification (RFID) tags, etc. [92, 136-137]. However, current commercially available silver conductive ink technologies have unaffordable drawbacks. Silver conductive inks do not offer strong enough adhesion on many

substrates for use as an interconnect material or for mechanical reliability in flexible substrates [138-139]. After printing and subsequent sintering, the resulting silver films lack cohesion and tend to crack due to considerable shrinkage [139]. Moreover, sintering processes take ten minutes [140] or longer durations [77, 80, 83-84, 88, 141-142] limiting commercial applications. To address the drawbacks of silver inks, highly conductive ICAs with a combination of electrical, mechanical and adhesive functions are a promising solution for printed electronics. One of the main disadvantages of ICAs is the relatively high electrical resistivity (3.5×10^{-4} Ω cm), compared with eutectic Sn/Pb solders ($1.5\text{-}3\times10^{-5}$ Ω cm) [5, 143]. By incorporation of silver nanoparticles with nearly complete decomposition of surface residues at the curing temperature, highly conductive ICAs with electrical resistivity of 4.8×10^{-5} Ω cm have been prepared at 180 ^{o}C for 60 minutes in chapter 2 [77]. However, the trend towards mixed assembly technologies, having components attached with both solder and ICAs on the same board requires uniformity of the curing profile/solder reflow processes. To obtain maximum device level reliability and reduce the cost, ICAs are required to be cured in a short duration, and most preferably during the solder reflow process.

This chapter describes the preparation of printable, highly conductive ICAs by fast sintering of silver flakes and silver nanoparticles within a polymer matrix. The thermal behavior of silver flakes and silver nanoparticles has been studied by Thermogravimeteric Analysis (TGA), Surface-enhanced Raman Spectroscopy (SERS) and Scanning Electron Microscopy (SEM). This provides a guideline for the processing temperature for the preparation of highly conductive ICAs. At certain temperatures, the thermal decomposition of silver carboxylate on the surface of silver flakes forms highly

reactive silver nanoparticles. The formation of silver nanoparticles on the surface of the silver flakes as well as the thermal decomposition of residues on the surface of the incorporated silver nanoparticles occurs. Both the in-situ formed and the incorporated silver nanoparticles are highly reactive due to their high surface-to-volume ratios and minimal surface residues. The lack of surface residues facilitates the sintering among silver flakes, in-situ formed silver nanoparticles and the incorporated silver nanoparticles. The sintering process enables the formation of metallurgical joints between the conductive fillers, instead of physical contacts, within the polymer matrix. The formation of metallurgical joints effectively reduces and even eliminates the contact resistance among the conductive fillers, leading to highly conductive ICAs (Figure 3.1). The effects of sintering time and temperature on the electrical resistivity of the ICAs have been studied. In addition, the correlation between the rheological properties of ICA pastes and the non-contact printing process are discussed. Finally, the non-contact printing of conductive adhesive pastes on different substrates is demonstrated.

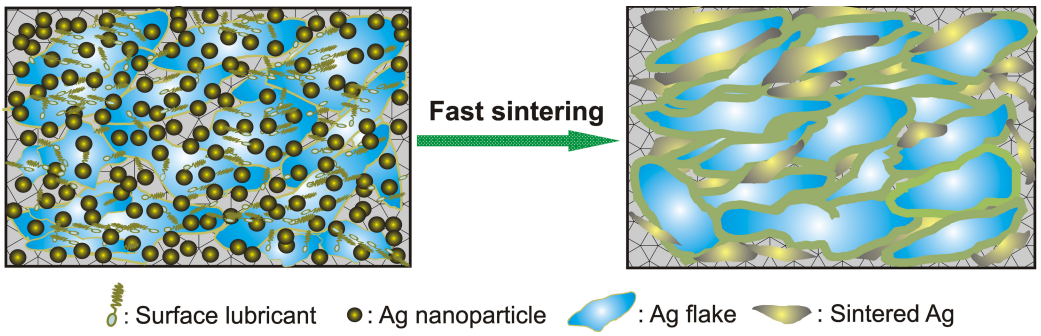

Figure 3.1 Schematic illustration of the sintering between silver nanoparticles and silver flakes within a polymer matrix.

3.2 Experimental

3.2.1 Preparation of ICAs

Silver nanoparticles used in the present study were synthesized by Combustion Chemical Vapor Condensation (CCVC) method. Silver flakes with a surface area of 0.57 m^2/g were donated by Ferro Corp. The wide size distribution of silver flakes in the range of several to about twenty microns was used to improve the packing density. Typically, surface lubricants such as stearic acid were present on the surface of silver flakes to improve the rheological properties and prevent the aggregation of silver flakes. Silver nanoparticles and silver flakes with an optimized ratio of 4:6 (totally 80 wt% of the mixture) were incorporated into the mixture of diglycidyl ether of bisphenol F (DGEBF, Shell Chemical Co.) and hexahydro-4-methylphthalic anhydride (HMPA, Lindau Chemicals). The weight ratio of DGEBF to HMPA is 1:0.85. The mixture was sonicated for one hour to disperse the conductive fillers within the epoxy resin. Following sonication, the catalyst, 1-cyanoethyl-2-ethyl-4-methylimidazole (2E4MZ-CN, Shikoku Chemicals Corp.), was added into the formulations and the resulting conductive adhesive paste was further sonicated for another 30 minutes. Two strips of a Kapton tape (Dupont) were applied onto a pre-cleaned glass slide. The formulated paste was printed on the glass slide and put into the oven with a preset temperature for curing. Reflow tests were conducted in a BTU oven (BTU International). The reflow oven has seven chambers and one cooling station. The temperatures for each chamber were set to 75, 110, 156, 198, 221, 255 and 175 ^oC, characteristic of a typical lead-free solder reflow profile.

3.2.2 Characterization

The electrical resistivity of ICAs was measured as according to the method described in chapter 2. Weight losses of the silver nanoparticles and flakes during heating in air were studied using TGA (TA Instruments, model 2050) at a heating rate of 20 ^{o}C/min. Raman spectra of the silver nanoparticles were obtained by using a LabRAM ARAMIS Raman confocal microscope (HORIBA Jobin Yvon) equipped with a 532 nm diode pumped solid state (DPSS) laser. Silicon wafer was used as a substrate for Raman measurements. The rheological properties of the ICA pastes were measured with cone-plate (2°) geometry at 23 ^{o}C by a stress-controlled rheometer from TA Instruments, model AR1000-N. Non-contact printing (or jetting) of the pastes was performed at room temperature by ASM Pacific Technology Ltd. using a jet dispenser with air pressure of 0.1-0.15 bar and jetting time of 5 ms. The nozzle size was 50 μm.

3.3 Results and Discussion

3.3.1 Thermal Decomposition of Silver Carboxylate on the Surface of Silver Flakes

Commercial silver flakes are generally produced from silver powders by a ball-milling process. To prevent the aggregation of silver powders, an organic lubricant, generally a fatty acid (such as stearic acid), is typically used during the production of silver flakes. After production, a thin layer of lubricant is present on the surface of silver flakes [51-52, 66-67]. The thin layer of lubricant affects the interaction of silver flake with other silver flakes and with the polymer system [66]. Consequently, this layer of surface lubricant affects the dispersion of silver flakes, the rheology of formulated pastes and the electrical conductivity of the resulting ICAs. Figure 3.2 shows Raman spectra of the lubricant on the surface of silver flakes without thermal treatment and after isothermal heating at 230, 250 and 260 ^{o}C for five minutes. While the very small shoulder peak at

1700 cm^{-1} indicates the presence of a trace amount of the fatty acid, the peaks at 1432 and 1591 cm^{-1} are assigned to the symmetric ($\nu_s(COO^-)$) and antisymmetric ($\nu_{as}(COO^-)$) stretching vibrations of the carboxylate group, respectively [144-146]. The presence of the strong bands due to the stretching vibrations of the carboxylate group and a very weak band due to the carbonyl stretching of a carboxylic acid indicates that most fatty acid molecules have been converted into carboxylate on the surface of silver flakes. It is well known that the binding of fatty acid to a silver surface will lead to the breaking of the O-H bond in the fatty acid and subsequent formation of a carboxylate species, which formed a bond between the oxygen in the carboxylate group and the silver surface (-COOAg) [51-52, 66-67]. Therefore, the thin layer of lubricant is a silver salt formed between fatty acid and silver, i.e. silver carboxylate, rather than a free fatty acid, which is consistent with previous studies [51-52, 66-67]. The peak at 933 cm^{-1} is due to C-COO^- stretching. The peaks at 2850 and 2924 cm^{-1} are assigned to the symmetric and asymmetric stretching vibrations of the methylene group. The methylene twisting, wagging and scissor appear at 1297, 1362 and 1474 cm^{-1}, respectively [144]. Figure 3.3 shows the TGA results of the silver flakes. A weight loss started at 150 ^oC and it continued up to 223 ^oC with a weight loss of 0.14%. This weight loss was followed by a weight increase of 0.01% until 234 ^oC. The weight increase is due to the oxidation of the lubricant on the silver flakes [52]. After 234 ^oC, further weight loss was observed and final weight loss at 450 ^oC was 0.23%. The weight loss (0.23%) results from the decomposition of the carboxylate. This amount of the surface lubricant corresponds to roughly a monolayer of stearate on the surface of silver flake [67]. This lubricant monolayer plays a key role in the sintering between silver flakes as it provides an energy

barrier for sintering. Substantial removal of the lubricant layer is a prerequisite for sintering to occur. After isothermal heating at 230, 250 and 260 ^{o}C for five minutes, the weight losses of the silver flakes are 0.16%, 0.17% and 0.18%, respectively. The corresponding SERS of the lubricant on the surface of silver flakes after thermal treatments are shown in Figure 3.2. The Raman intensities of the lubricant on the surface of the treated silver flakes were significantly reduced. With the thermal treatment at 230 ^{o}C, C-C stretching at 1062 cm^{-1}, -COO^{-} deformation at 695 cm^{-1} and Ag-O stretching (-COOAg) at 253 cm^{-1} became prominent, while the peak at 483 cm^{-1} disappeared indicating the decomposition of silver oxide [77, 132]. The presence of both the Ag-O stretching and the carboxylate species further indicates that the lubricant layer is silver carboxylate. A Raman peak at 1769 cm^{-1} assigned to C=O stretching appeared after thermal treatment, which further confirmed the oxidation of surface lubricants during the thermal treatment (Figure 3.2, inset). As the temperature was increased to 250 ^{o}C, the peaks at 2924, 2850 and 933 cm^{-1} disappeared and the peak at 253 cm^{-1} showed lower intensity and broadening. Meanwhile, the peak at 1769 cm^{-1} became more obvious indicating more surface lubricants being oxidized. A further increase in the temperature resulted in the nearly complete disappearance of all peaks except a small peak at 1062 cm^{-1}, indicating that most surface lubricants were decomposed. It is well-documented that the thermal decomposition of silver carboxylate leads to the formation of silver nanoparticles [94, 147-151]. The thermal decomposition products of silver carboxylate are related to the decomposition atmosphere, heating rate and temperature [150, 152]. Studies from Liu et al. reveal that the thermal decomposition product of silver behenate is CO_2 at 230 ^{o}C, and hydrogen and water at 260 ^{o}C, respectively, verified by combined

thermogravimetry-differential thermal analysis-mass spectrometry (TG-DTA-MS) analysis [151]. In the present study, the thermal decomposition was conducted in air, so the final products were metallic silver and gases (CO_2 and H_2O) [149, 151]. From the TGA and Raman results, it can be concluded that, during isothermal heating at the temperatures, the thin layer of lubricant—silver carboxylate—present on the surface of silver flakes has been substantially decomposed, facilitating the sintering between silver flakes.

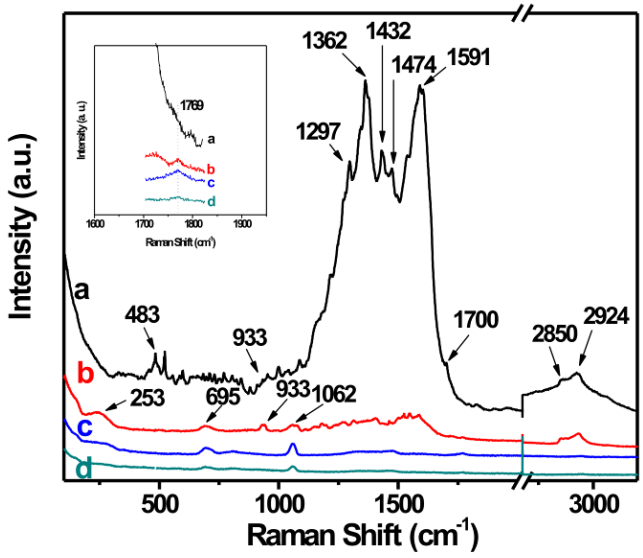

Figure 3.2 Raman spectra of the lubricants on the surface of silver flakes (a) without thermal treatment and after being isothermally heated at different temperatures for 5 min: (b) 230, (c) 250, and (d) 260 °C.

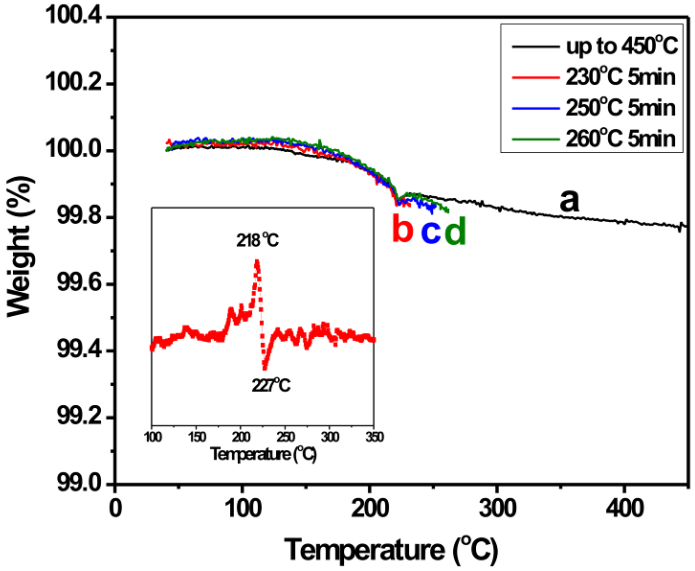

Figure 3.3 TGA of the silver flakes (a) without thermal treatment and after being isothermally heated at different temperatures for 5 min: (b) 230, (c) 250, and (d) 260 °C. Inset is the first derivative of TGA curve a in the temperature range of 100-350 °C. Significant weight loss and increase are at 218 and 227 °C, respectively.

Figure 3.4 shows the SEM images of the silver flakes untreated and after isothermal heating at 230, 250 and 260 ^{o}C for five minutes. As shown in Figure 3.4 (a), the silver flakes have a broad size distribution, which enables higher packing density improving conductivity at given filler loadings. There are some nano-sized silver bumps on the surface of untreated silver flakes, but the surface is relatively smooth (Figure 3.4 (a), inset). After the thermal treatments, the surface of silver flakes shows increased roughness. The increased surface roughness is the result of thermal decomposition of silver carboxylate on the surface of silver flakes, which forms highly reactive nano- or submicron-sized silver particles that sintered with the silver flakes (Figure 3.4 (b) and

inset). Note that sintering between adjacent nano-sized bumps on the surface of a silver flake is dependent on the decomposition of silver carboxylate since the activation energy of surface diffusion is lower than that of bulk diffusion. The lack of a surfactant on the surface of these particles means they have a high surface energy facilitating mass transport, even at temperatures well below the melting temperature of bulk silver (961.8 ^{o}C). Sintering of these nanoparticles is evident by the formation of "bridges" between silver flakes after isothermal treatment at 230 ^{o}C for five minutes. The higher thermal treatment temperature led to wider necks and rougher surfaces (Figure 3.4 (c) and inset). As the temperature increases to 260 ^{o}C, there was a transition to edge by edge sintering and no isolated flakes were observed at that temperature (Figure 3.4 (d) and inset). It should be emphasized that, during isothermal heating, the thermal decomposition of silver carboxylate to form in situ highly reactive silver nanoparticles is crucial for the sintering between silver flakes, including the sintering between nano-sized silver bumps on the surface of silver flakes. Without the thermal decomposition, sintering will not proceed. The formation of "bridge" or edge by edge sintering enables the formation of metallurgical joints among silver flakes which remarkably facilitates the electron transport among the silver flakes.

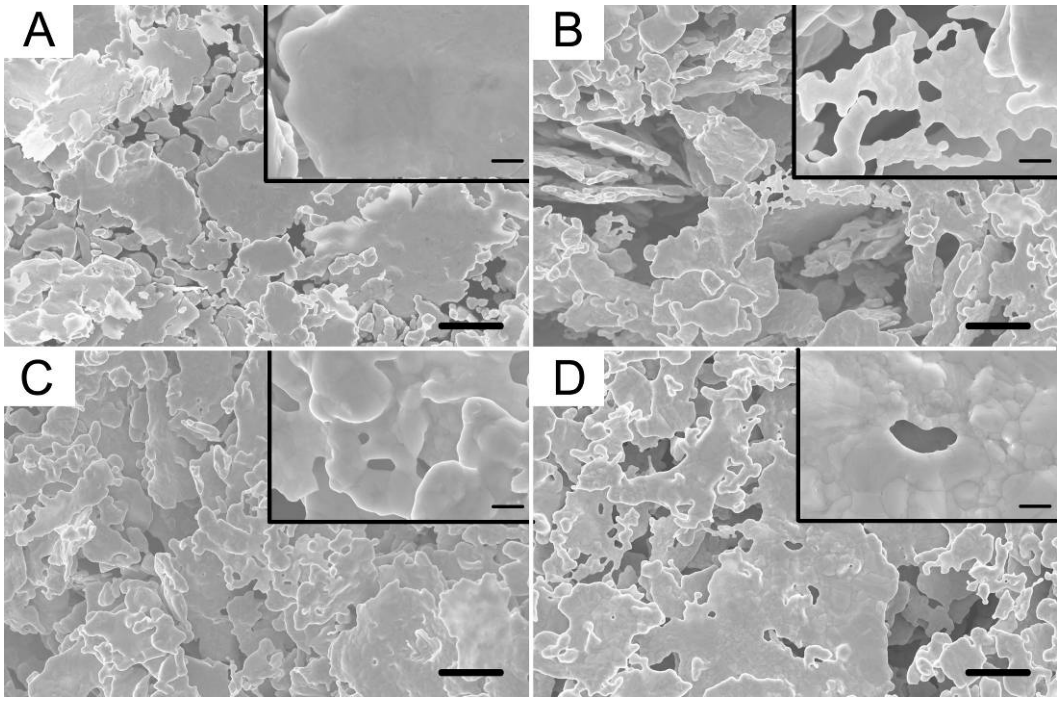

Figure 3.4 SEM images of the silver flakes (a) without thermal treatment and after being isothermally heated at different temperatures for 5 min: (b) 230, (c) 250, and (d) 260 °C. Scale bars are 4 μm and 400 nm (inset), respectively.

3.3.2 Thermal Behavior of Silver Nanoparticles

Nanoparticles tend to sinter or Ostwald ripen to reduce their total free energy [85, 93, 111]. As mentioned in chapter 2, during the synthesis of silver nanoparticles, a variety of stabilizers are utilized to control the size, size distribution and stability. These stabilizers provide an energy barrier to sintering. Sintering only occurs after the substantial removal of the stabilizers. However, the removal of the stabilizers typically requires a temperature higher than 250 ^{o}C and a relatively long time, due to a relatively large amount of surface residues on the particle surface (>10 wt%) in most cases [123, 131, 153], low mobility of surfactants and the tendency of surfactants to physically

adsorb. However, these surfactants are necessary to obtain a good dispersion and prevent aggregation of silver nanoparticles in the polymer matrix. To address these challenges, silver nanoparticles were synthesized by Combustion Chemical Vapor Condensation (CCVC). Silver nanoparticles synthesized by CCVC offer many significant advantages over those by wet chemical methods for the preparation of highly conductive ICAs. CCVC nanoparticles synthesis produces nanoparticles whose surface residues have minimal surface coverage and low decomposition temperatures. For example, silver nanoparticles synthesized by CCVC showed a 2.45% weight loss of surface residues at 450 ^{o}C; the decomposition of surface residues started at 160 ^{o}C and was almost finished at 220 ^{o}C [77]. Additionally, nanoparticles produced from CCVC methods have narrow size distribution and high production rates (up to 0.1-1 kg/h) [77, 124]. In chapter 2, it has been found that silver nanoparticles with lower decomposition temperatures of surface residues and lower content of surface residues are more desirable for low temperature sintering of silver nanoparticles and the preparation of highly conductive ICAs [77]. To facilitate the fast sintering, the experimental condition for CCVC nanoparticle synthesis was further optimized in the present study. Figure 3.5 shows the TGA results of the silver nanoparticles. The weight loss of the silver nanoparticles started at 150 ^{o}C and was nearly completed at 195 ^{o}C. The final weight loss at 450 ^{o}C was 0.49%. The present silver nanoparticles with lower decomposition temperatures of surface residues and lower content of surface residues will better facilitate the fast sintering between silver nanoparticles and the fast preparation of highly conductive ICAs. The significant weight loss observed at 191 ^{o}C may be attributed to the decomposition of silver oxide or possibly organic residues during the synthesis [77]. After isothermal heating at 230, 250 and 260

°C for five minutes, the weight losses of the silver nanoparticles were 0.40%, 0.42% and 0.42%, respectively. Comparing the net weight loss of the silver nanoparticles at 450 °C (0.49%), it can be concluded that the surface residues have almost been decomposed at these temperatures. The nearly complete decomposition of surface residues at these temperatures within five minutes facilitates the fast sintering of silver nanoparticles. The novel use of CCVC nanoparticles in ICAs allows for the fast preparation of highly conductive ICAs.

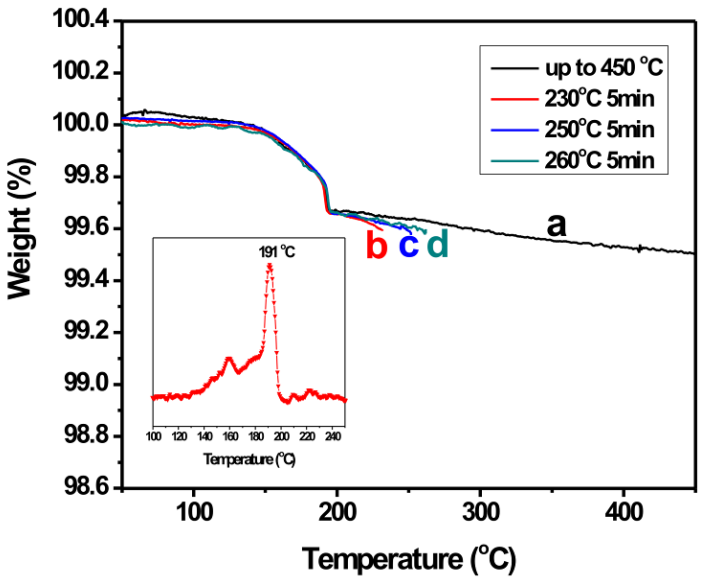

Figure 3.5 TGA of the silver nanoparticles synthesized by CCVC (a) without thermal treatment and after being isothermally heated at different temperatures for 5 min: (b) 230, (c) 250, and (d) 260 °C. Inset is the first derivative of curve a.

Figure 3.6 shows the SEM images of the silver nanoparticles without thermal treatment and after isothermal heating at 230, 250 and 260 °C for five minutes. Compared with the untreated silver nanoparticles (Figure 3.6 (a)), the size of the thermally treated

silver nanoparticles increased significantly. These nanoparticles formed a porous 3-D continuous network after isothermal heating at 230 °C for five minutes (Figure 3.6 (b)). The formation of necks among the silver nanoparticles was the result of surface diffusion driven by a reduction in surface energy. Surface diffusion dominates at the initial sintering stage since the activation energy of surface diffusion is lower than that of grain boundary and lattice diffusions [93]. As the temperature increases to 250 °C, the particle sizes increased further and the necks between them widen (Figure 3.6 (c)). Densification observed at 260 °C indicates the dominant grain boundary/lattice diffusions during the sintering process (Figure 3.6 (d)).

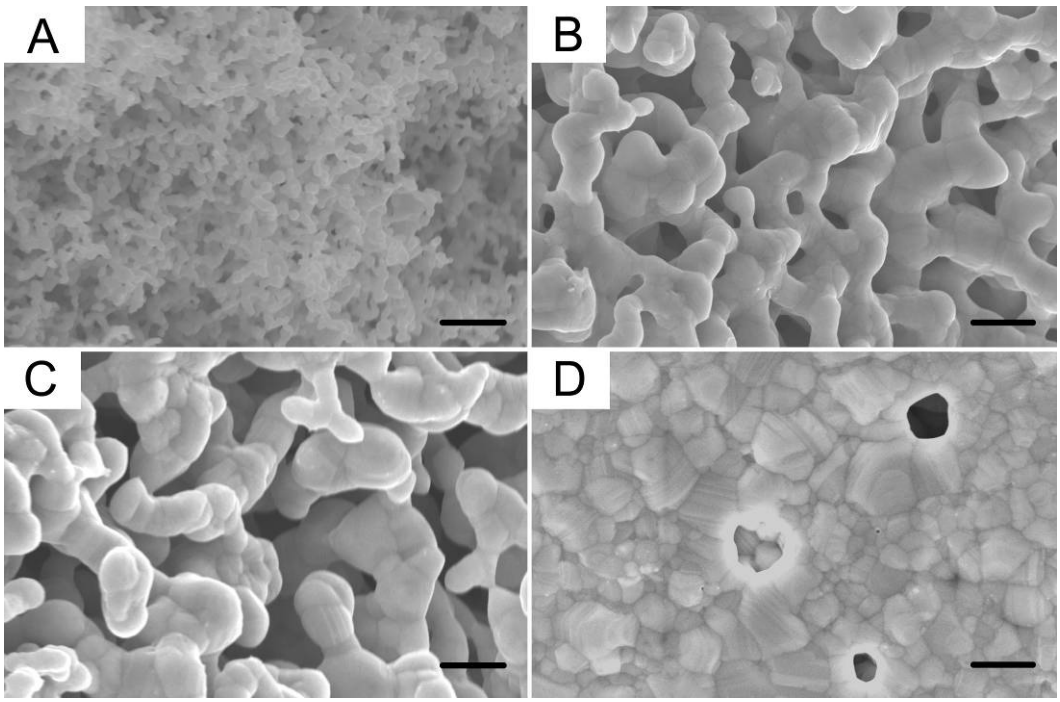

Figure 3.6 SEM images of the silver nanoparticles synthesized by CCVC (a) without thermal treatment and after being isothermally heated at different temperatures for 5 min: (b) 230, (c) 250, and (d) 260 °C. Scale bars are 400 nm.

3.3.3 Electrical Properties of ICAs

Although the electrical resistivity of silver films close to that of bulk silver (1.6×10^{-6} Ω cm) has been achieved by sintering of silver nanoparticles in silver inks, it remains a challenge to sinter silver nanoparticles within polymer matrices to achieve highly conductive ICAs. The incorporation of silver nanoparticles into a polymer matrix results in an ICA with a very high resistivity [96-97, 131], as a result of increased contact points and reduced contact area among conductive fillers [97]. The possible reasons are: 1) the difficult debonding or decomposition of organic molecules (or silver oxide) at curing temperatures; 2) the impediment of the sintering of silver nanoparticles by high volume fraction (typically 70-80 vol%) of highly cross-linked polymer matrices [77]. In the present study, the curing of the epoxy resin and the sintering among the conductive fillers occur simultaneously. Figure 3.7 shows the effect of curing (or sintering) time and temperature on the resistivity of ICAs. When cured at 230 and 250 ^{o}C for two minutes or at 260 ^{o}C for one minute, the ICAs show high resistivities. When the curing time is three minutes, the ICAs prepared at 230 ^{o}C show a lower resistivity (9.8×10^{-5} Ω cm) than those of conventional silver-filled ICAs at the same filler loading. As the temperature increases, ICAs with lower resistivities can be obtained. Increasing curing time to five minutes led to a further decrease in electrical resistivity for the samples cured at 260 ^{o}C. This improvement in conductivity was less pronounced for the samples cured at 230 and 250 ^{o}C. Extending the curing time to 10 minutes at 260 ^{o}C results in the ICAs with a resistivity of as low as about 6.0×10^{-6} Ω cm, close to the resistivity of bulk silver. In addition, ICAs cured using a typical lead-free solder reflow profiles show electrical resistivity of 6.3×10^{-5} Ω cm. The preparation of highly conductive ICAs during solder

reflow reduces the processing steps and cost enabling the natural integration into standard industrial electronic packaging processes.

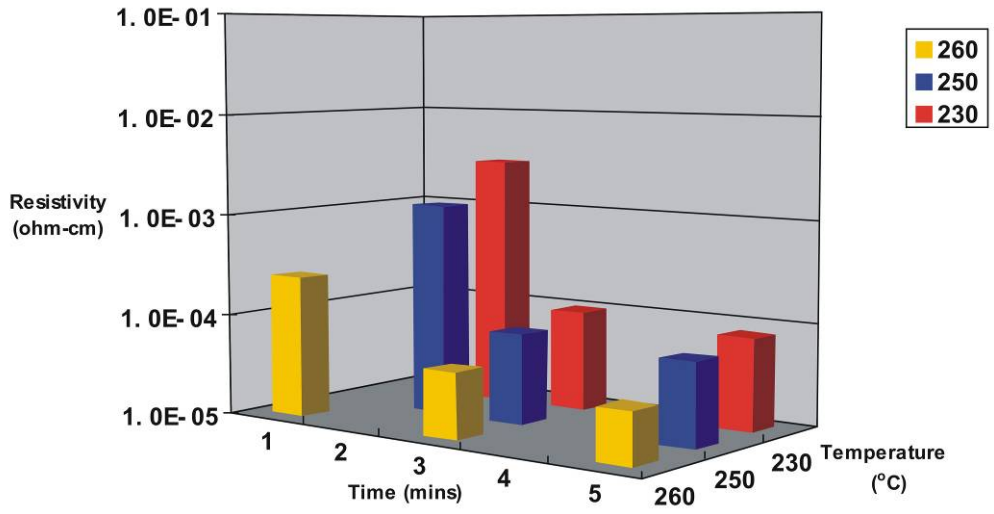

Figure 3.7 Effects of curing time and temperature on the resistivity of ICAs.

Figure 3.8 shows the cross-section of ICAs cured at 230, 250 and 260 ^{o}C for five minutes and 260 ^{o}C for ten minutes. At 230 ^{o}C, the particles within the polymer matrix were connected to one another and formed necks (Figure 3.8 (a)). At 250 ^{o}C, the neck size between the particles increased and rod-like structures formed (Figure 3.8 (b)). When increasing the temperature to 260 ^{o}C, the particles grew significantly and necking was more prominent (Figure 3.8 (c)). When curing was conducted at 260 ^{o}C for ten minutes, smoother facets with elongated particle structures formed (Figure 3.8 (d)). The necking exhibited during the sintering process reduces and even eliminates the contact resistance effectively among the conductive fillers and enable the formation of 3-D continuous conductive networks within the polymer matrix, leading to the highly conductive ICAs.

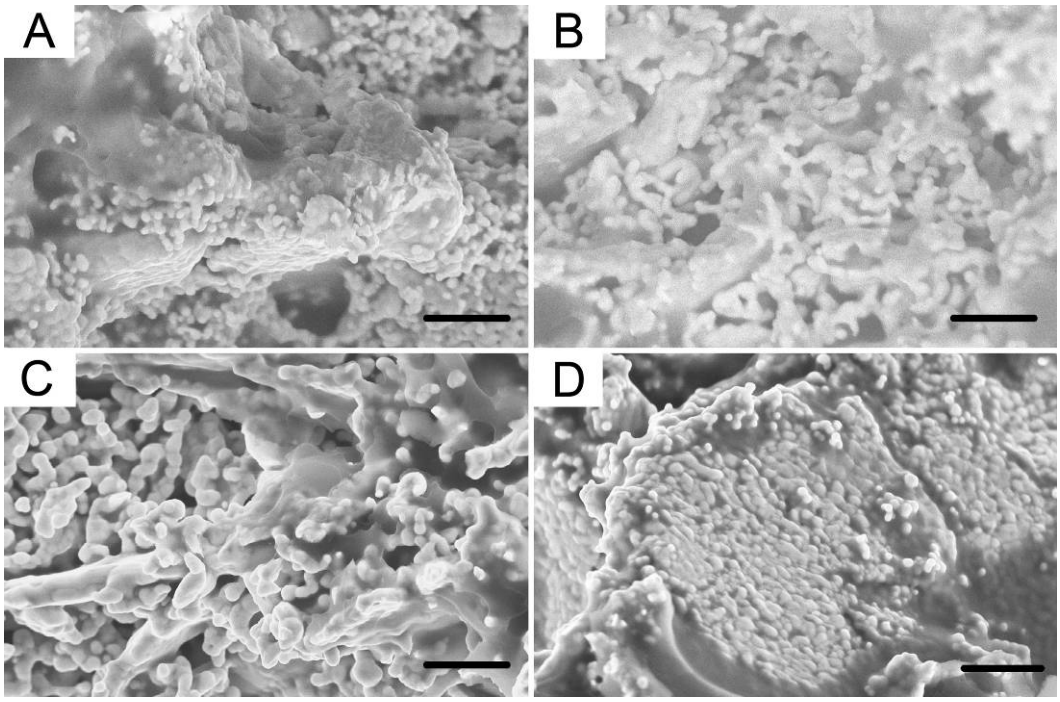

Figure 3.8 SEM images of the cross-section of ICAs cured at (a) 230 °C, 5 min; (b) 250 °C, 5 min; (c) 260 °C, 5 min; and (d) 260 °C, 10 min. Scale bars are 2 μm.

3.3.4 Rheological Properties of ICA Pastes

Non-contact printing is defined as the accurate dispensing of materials onto a selective location without physical contact in a controlled manner. The attractive features of non-contact printing technologies are cost-effectiveness, reduced waste of precious materials, the accurate dispensing of a small amount of materials onto a selective location, no special requirements for substrates (e.g., roughness, flexibility), and environmental friendliness [119-120, 154]. Despite these advantages many of the necessary processing conditions are still not fully understood. Most importantly, the effect of the rheological properties of the printed materials on the printing process is still undetermined. The viscosity of any printed composite materials strongly depends on the

filler loading, filler size, shape, and additives that are used to tune the rheological properties. Non-contact printing technologies require that the materials should readily flow and have the ability to recover its viscosity rapidly to retain the shape of the adhesive paste after printing [155]. With the incorporation of silver nanoparticles, the viscosity of the conductive adhesive paste (the mixture of conductive fillers, the epoxy resin, etc. before curing) increases dramatically at low shear rates. However, the addition of large amounts of solvent to reduce the viscosity would result in the sedimentation of silver flakes, which causes variations in the local silver concentration and may block the nozzle [138]. These requirements render non-contacting printing of highly viscous pastes challenging. Figure 3.9 shows the viscosity vs. shear rate of the ICA paste. The paste showed a typical shear thinning behavior. The viscosity of the paste at a shear rate of 2500 s^{-1} was 221 mPa·s, much higher than that of typical silver inks (<40 mPa·s). The shear thinning behavior of the paste is related to the tradeoff between break-down due to flow stresses and build-up due to in-flow collision and Brownian motion [156-157]. When no shear force is exerted on the paste, the particles aggregate due to attraction forces such as van der Waals force. Aggregation caused by these forces can promote the formation of spatial networks, which creates an internal structure. The internal structure is important to provide long-term dispersion stability [155]. Under shear, the weak forces within the paste are broken and the paste is dispensed easily. To gain insights into the structure and measure the viscoelasticity of the paste, oscillatory stress sweep of the paste was performed, as shown in Figure 10 (inset). Storage modulus (G') and loss modulus (G'') measured in the oscillatory test represent solid and liquid characteristics of the paste. At low shear stresses the paste shows a dominant solid-like behavior (G'>G'') and

as the applied stress increases, the paste gradually changes from solid-like (elastic) behavior to liquid-like (viscous) behavior. The point at which G'=G'' is a solid-fluid transition and an indicator for assessing the cohesiveness of the paste [158]. It has been found that if the applied shear stress at the point where G'=G'' was too low, splashing occurred during the printing. In the present study, the applied stress was 4.37 Pa when G'=G'', which was optimal for the non-contact printing.

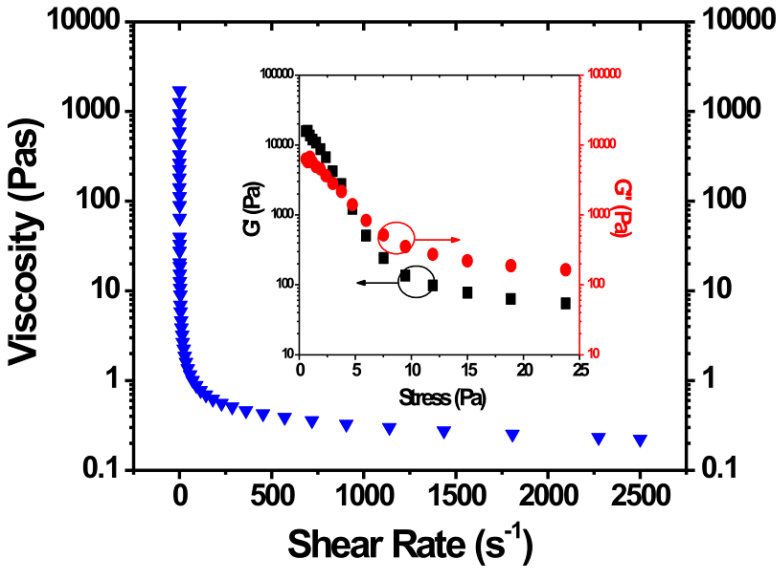

Figure 3.9 Viscosity as a function of shear rate for the paste filled with 80 wt % silver fillers. Inset is an oscillatory stress sweep test for the paste.

3.3.5 Non-contact Printing of ICA Pastes

Figure 3.10 shows the non-contact printing of the paste on the surfaces of glass (Figure 3.10 (A)) and a silver-plating lead frame (Figures 3.10 (B), (C) and (D)). Depending on the interaction between the paste and substrates, the paste can either totally wet the glass surface with a radius of about 220 μm and a height of about 14.5 μm, or

form a dot with a radius of 130 μm and a height of 49 μm on the silver-plating lead frame under optimized conditions. Following cure, due to the shrinkage of epoxy resins, the printed dots have a radius of 120 μm and a height of 28 μm. Generally, the Weber number (We), defined as the ratio of kinetic energy to the surface energy of a droplet (Equation (2)), provides a good estimate whether the droplet has sufficient kinetic energy to overcome the surface tension at the orifice and to create a free flying droplet [159]. There is a critical Weber number below which a free flying droplet cannot be created. For inviscid liquids (an ideal liquid that has no viscosity), the critical Weber number is about 12 (Equation (3)); for printed materials whose viscosities are not negligible, the critical Weber number can be much larger than 12 and is related to the viscosity through the Ohnesorge number (Oh) (Equations (4) and (5))

$$We = \frac{\rho D v^2}{\sigma} \qquad (2)$$

$$We_{critical} \approx 12 \ (\eta \approx 0) \ (3)$$

$$We_{critical} = 12 \times (1 + 1.07 Oh^{1.6}) \ (\eta > 0) \ (4)$$

$$Oh = \frac{\eta}{\sqrt{\rho D \sigma}} \qquad (5)$$

Where ρ is the density, ν is the velocity, D is the drop diameter before impact, σ is the surface tension, and η is the dynamic viscosity. Increasing the viscosity of the printed materials leads to an increase in Ohnesorge number and a dramatic increase in the critical

Weber number, making the creation of small droplets from viscous materials very difficult [159]. To the best of our knowledge, this is the first successful attempt to print highly viscous ICA pastes into dot arrays with such a small size on the substrate in the open literature. The non-contact printing of the highly viscous ICA pastes opens up new avenues for low-cost printed electronics. Increased understanding of the correlation between the rheological properties and the non-contact printing process is needed to optimize material and printing parameters to obtain ultra-high resolution non-contact printing technologies for low cost interconnects of the future.

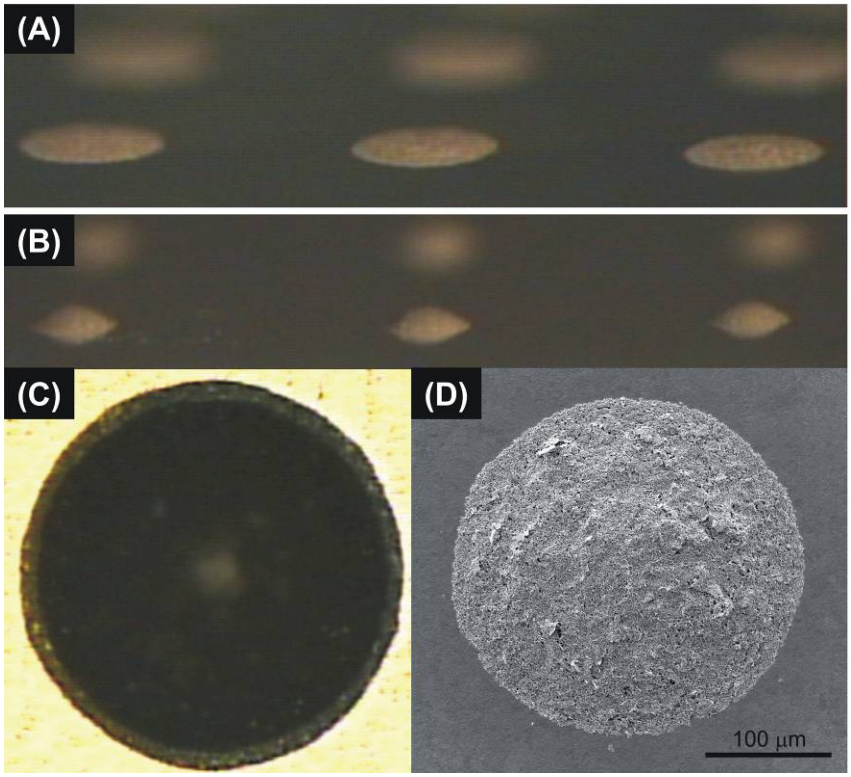

Figure 3.10 Noncontact printing of the ICA pastes with 80 wt % silver fillers on (A) a glass slide (side view, optical microscopy) with a radius of about 220 μm, (B) on an silver-plating lead frame with a radius of 130 μm (side view, optical microscopy), (C) on

an silver-plated lead frame with a dot size (top view, microscopy) before curing, and (D) on an silver-plated lead frame with a dot size (top view, SEM) after curing.

3.4 Conclusions

This chapter demonstrates the fast preparation of printable highly conductive ICAs using thermal decomposition of silver carboxylate on the surface of silver flakes and sintering between conductive fillers during the ICA curing process. The sintering between conductive fillers reduces and eliminates the contact resistance effectively, leading to ICAs with the electrical resistivities of 8.1×10^{-5}, 6.0×10^{-6} and 6.3×10^{-5} Ω cm when ICAs were prepared at 230 ^{o}C for five minutes, at 260 ^{o}C for ten minutes and using a typical lead-free solder reflow process, respectively. The highly viscous ICA pastes with optimized rheological properties can be non-contact printed into a micro-array of dots with a radius of 130 μm. The developed ICAs with superior electrical conductivity and fast processing along with non-contact printing technologies will considerably reduce the cost of interconnection in printed electronics enabling their wide scale industrial application.

CHAPTER 4

LOW TEMPERATURE APPROACH TO PREPARE FLEXIBLE HIGHLY CONDUCTIVE ADHESIVES

This chapter describes the preparation of flexible highly conductive adhesives at a low temperature (150 ^{o}C) by in situ reduction of silver carboxylates on the surface of silver flakes. The reduction of silver carboxylates forms highly reactive silver nanoparticles that lead to the sintering between silver flakes. This approach solves many problems associated with the incorporation of silver nanoparticles into the formulation, as described in chapters 2 and 3. In this chapter, epoxy compositions and the surface properties of silver flakes are first characterized. Then silver flakes are treated with epoxy resins and their surface morphologies and properties change induced by the treatment are characterized to explain the conductivity enhanced mechanism. In addition, a coupling agent is used to improve the adhesion strength of flexible highly ICAs on a gold surface.

4.1 Introduction

The preparation of novel flexible highly conductive interconnect materials at low temperatures (preferably 150 ^{o}C or below) is essential for the future of low-cost flexible electronics [4-5, 108, 160-162]. The popularity of flexible circuits and building electronic devices on flexible substrates requires the interconnect materials to be mechanically compliant and highly conductive [108, 163-165]. Low processing temperatures of the interconnect materials are also required to enable the wide use of low cost, flexible substrates such as paper and polyethylene terephthalate (PET). Flexible conductive

polydimethylsiloxane (PDMS) composites have been developed for various microelectronic applications, owing to the unique physical and chemical properties of PDMS. These properties include superior elasticity and flexibility, optical transparency, biocompatibility and stable physical and chemical properties over a wide range of temperatures from -50 ^{o}C to +200 ^{o}C [166]. Agar et al. reported that the resistivity of PDMS filled with 80 wt% bimodal distribution of micron-sized silver flakes is about 7×10^{-4} Ω cm [60]. Electrical resistivity of PDMS filled with 19 vol% silver particles showed a resistivity of about 10^{-2} Ω cm and the resistivity of the PDMS-based conductive composites exhibited no significant decreases as the filler loading increased [166]. Lutz and Cole reported the lowest resistivity of 2×10^{-4} Ω cm for PDMS filled with 80 wt% silver particles and the resistivity leveled off even increasing the filler loading [167]. However, a minimum resistivity of on the order of 10^{-5} Ω cm is required to avoid severe resistive losses [168]. Another limitation of flexible conductive PDMS composites lies in the poor adhesion on metal surfaces due to the low surface energy of PDMS. This further limits their wide application as a flexible interconnect material. Therefore, new flexible interconnect materials with low electrical resistivity, good adhesion and low processing temperature must be developed for flexible electronic applications.

The resistivity of a conductive polymer composite is determined by the composite composition (such as filler loading), the surface properties of conductive fillers (such as the presence of a thin layer of lubricant or oxide film), physicochemical properties of polymer matrix (such as cure shrinkage and the interaction between the polymer matrix and conductive fillers), interlayer thickness, temperature, processing conditions of conductive polymer composites, etc. [4, 58, 169]. The resistance of a conductive polymer

composite is the sum of filler resistances (R_f) and inter-particle contact resistances (R_c). The contact resistance is composed of constriction resistance and tunneling resistance [54, 56, 70, 97, 170-173]. Constriction resistance occurs as the current must squeeze through the small area of contact. Tunnel resistance is due to the intermediate layer between conductive fillers. In conductive polymer composites, conductive fillers may be separated by a thin layer of polymer, oxide or lubricant for most commercial silver flakes which have been extensively used for the preparation of ICAs [4, 58, 172]. The thickness of the interface can vary from 10 to 100 Å, depending on the physiochemical properties of the polymer matrix, filler, filler concentration, and the conditions of composite preparation [58]. Relatively low conductivity of conductive polymer composites such as conductive PDMS composites results from the physical contact, instead of metallurgical joints between conductive fillers [77-78, 84]. Reducing and eliminating the contact resistance between conductive fillers is crucial for the preparation of highly conductive polymer composites.

This chapter describes a novel approach to enable the formation of metallurgical joints between silver flakes within a flexible polymer matrix by simply incorporating a flexible epoxy with reduction capability—diglycidyl ether of polypropylene glycol (DGEPG), leading to flexible highly conductive ICAs. The approach involves i) *in situ* reduction of silver carboxylate present on the surface of silver flakes by DGEPG, a mild reducing agent, to form nano/submicron-sized silver particles both on the surface of and at the edge of silver flakes; ii) the *in situ* formed nano/submicron-sized silver particles, due to high surface area-to-volume ratios and lack of strong capping agents, are highly surface reactive, which results in the low temperature sintering between silver flakes

during curing. Sintering enables the formation of metallurgical joints and reduces the contact resistance among the conductive fillers effectively, leading to highly conductive ICAs.

4.2. Experimental

4.2.1 Materials

Epoxy resins used were diglycidyl ether of polypropylene glycol (DGEPG, D.E.R. 732, Dow Chemical, Figure 4.4) and diglycidyl ether of bisphenol F (DGEBF, EPON 862, Shell Chemical Co., Figure 4.4). DGEPG has a much lower viscosity (60-70 mPas) than DGEBF (2500-4500 mPas). The curing agent was hexahydro-4-methylphthalic anhydride (MHHPA) donated by Lindau Chemicals. Catalyst was 1-cyanoethyl-2-ethyl-4-methylimidazole (2E4MZ-CN, Shikoku Chemicals Corp.) Two silver flakes with different sizes and surface lubricants (Ag-FA and Ag-FB, Ferro Corp.) were used to improve the packing density and adjust the viscosity of the formulated pastes. All chemicals were used as received.

4.2.2 Reduction of Silver Carboxylate on the Surface of Silver Flakes

An epoxy resin (DGEBF or DGEPG) was mixed with silver flakes and then heated at 150 ^{o}C for 10 or 30 min. Silver flakes lost their luster and the surface appeared dull after being treated with DGEPG, while no significant change of surface appearance was observed for silver flakes treated with DGEBF. Acetone was added to the mixture and the resulting mixture was centrifuged. After removal of the superant, the silver flakes were re-dispersed in acetone. Five cycles of dispersing and centrifugation were used in an effort to remove the residual epoxy resin. Note that the lubricant on the surface of silver

flakes was hardly washed off by acetone during the process [174]. Finally, the silver flakes were dried in vacuum before the characterization.

4.2.3 Preparation of ICAs

Different ratios of DGEBF and DGEPG were mixed with 80 wt% silver flakes (Ag-FA and Ag-FB with a mass ratio of 1:1), MHHPA and the catalyst. Two strips of a Kapton tape (Dupont) were applied onto a pre-cleaned glass slide. The formulated pastes were printed on the glass slide. Then the pastes were thermally cured at 150 ^{o}C in air for 1 h. To show flexibility of the ICAs, the formulated pastes were printed on the surface of polyethylene terephthalate. After curing, the samples were bended conformally to the surface of cylinders with different radii to measure the resistivity change under bending condition.

4.2.4 Characterization

Mass spectrum of DGEBF was analyzed by fast atom bombardment–mass spectrometry (FAB-MS) using thioglycerol as a matrix. Mass spectrum of DGEPG was collected with the Voyager 4700 MALDI-TOF-TOF system (ABI) operated in reflector mode. Alpha-Cyano-4-hydroxycinnamic acid (CHCA) was used as a matrix for MALDI.

The resistivity of ICAs was measured according to the method described in chapter 2.

Weight losses of silver flakes during heating in air were studied using thermogravimetric analyzer (TGA, TA Instruments, model 2050). The heating rate was 20 ^{o}C/min.

Morphologies of the treated silver flakes and the ICAs were studied by field emission scanning electron microscopy (SEM, LEO 1530). Decomposition of the

lubricants on the surface of silver flakes was studied by differential scanning calorimetry (DSC, TA Instruments, Q100). The heating rate was 10 ^{o}C/min.

Raman spectra were obtained by using a LabRAM ARAMIS Raman confocal microscope (HORIBA Jobin Yvon) equipped with a 532 nm diode pumped solid state (DPSS) laser. Si wafer was used as a substrate for Raman measurements.

Gold surface was treated with 1 mM 4-mercaptobenzoic acid in alcohol for 24 h. Then the surface was rinsed with alcohol to remove non-adhering molecules and dried. Silicon dies (2 mm by 2 mm) were placed on the untreated or treated gold surface with ICAs that containing a uniform size of glass beads. These glass beads were used to control the thickness of ICA between silicon die and the substrate. For adhesion study, a die shear tester (Dage series 4000) was utilized, with a configuration as shown in Figure 4.1.

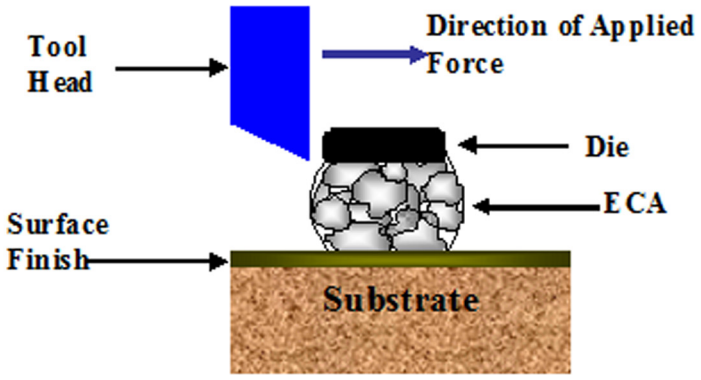

Figure 4.1 Schematic illustration of die shear test.

4.3 Results and Discussion

4.3.1 Characterization of DGEBF and DGEPG

EPON Resin 862 (Diglycidyl Ether of Bisphenol F, DGEBF) is a low viscosity, liquid epoxy resin manufactured from epichlorohydrin and bisphenol-F with NaOH at about 65 ^{o}C (Figure 4.2). The reaction of DGEBF with bisphenol F results in the formation of higher molecular weight resins, as shown in Figure 4.2. The excess amount of epichlorohydrin is required to limit the production of higher molecular weight products. Mass spectrum of EPON Resin 862 indicates that higher molecular weight products are present in the resin, which contains secondary –OH groups. D.E.R. 732 liquid epoxy resin is a reaction product of epichlorohydrin and polypropylene glycol. Mass spectrum of D.E.R. 732 indicates that D.E.R. 732 contains molecules with different units of propylene oxide and verifies the presence of primary –OH groups (Figure 4.3). The primary –OH groups may come from the incomplete reaction between epichlorohydrin and polypropylene glycol. Molecules present in the resins are shown in Figure 4.4.

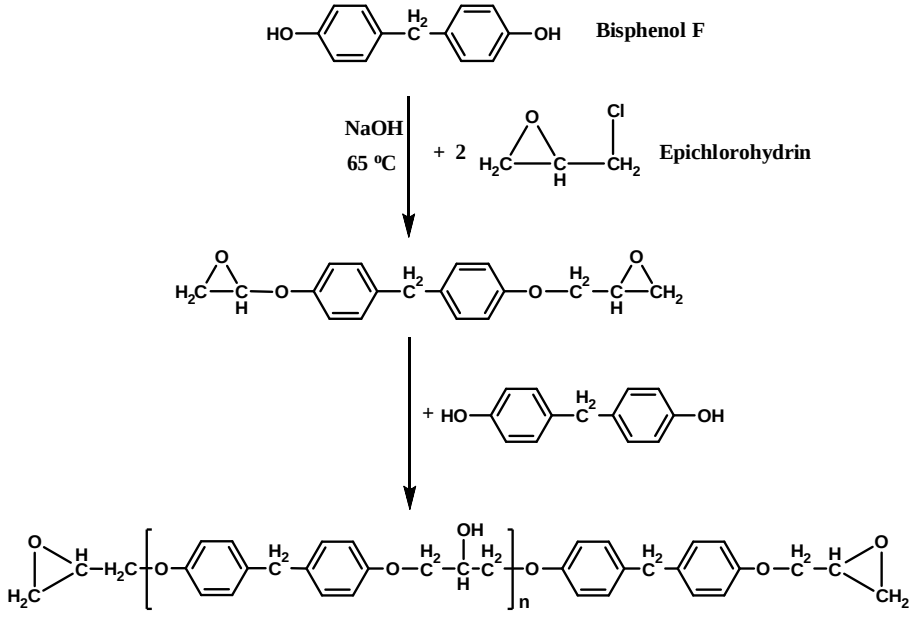

Figure 4.2 Synthesis of diglycidyl ether of bisphenol F.

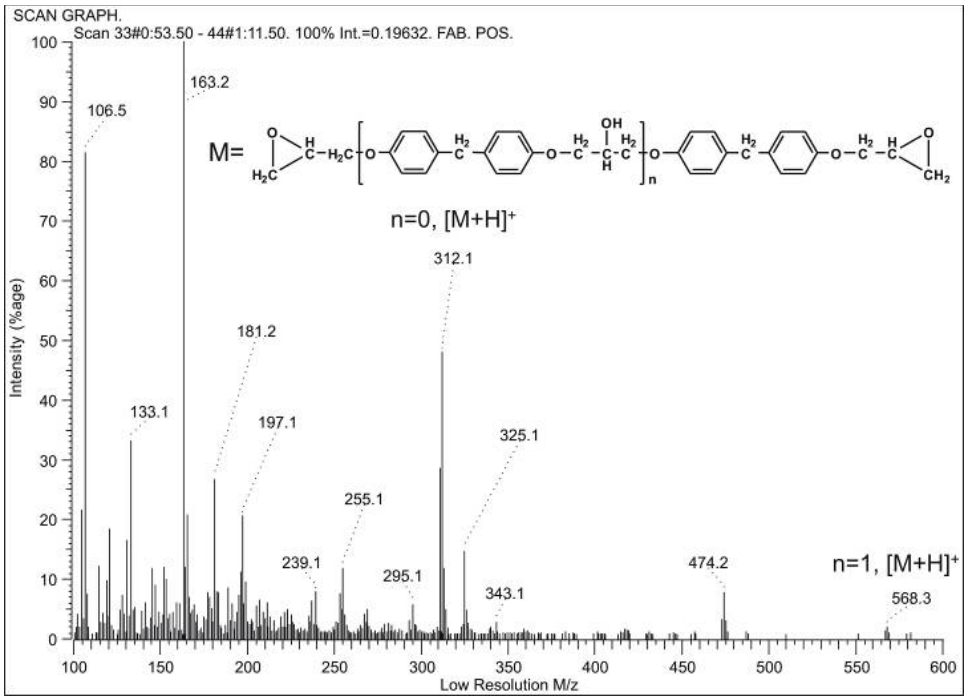

(a)

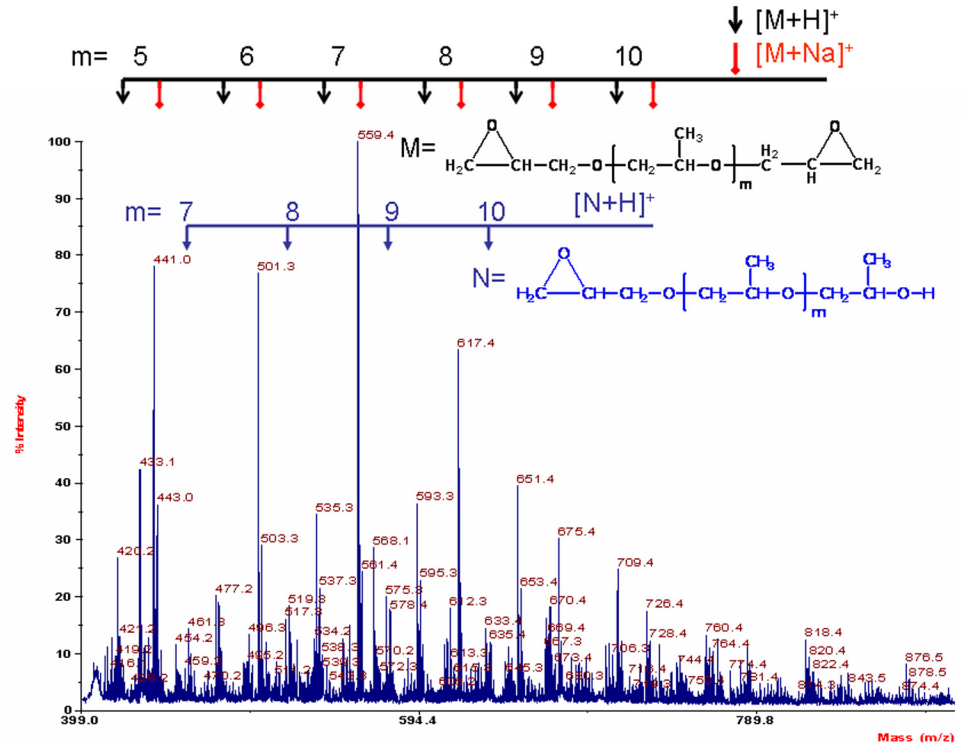

(b)

Figure 4.3 Mass spectra of (a) DGEBF and (b) DGEPG.

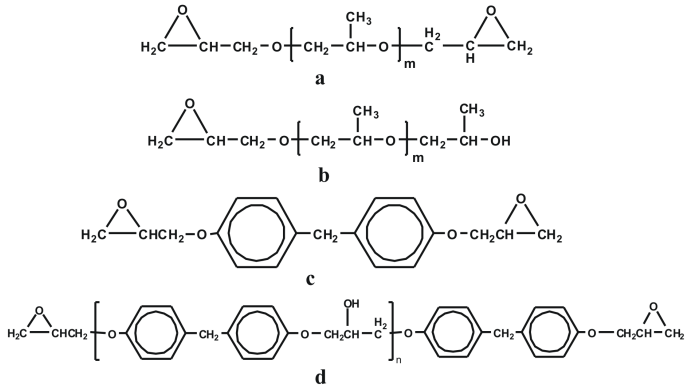

Figure 4.4 Molecular structures of DGEPG (a) mainly m=5, 6, 7, 8, 9 and 10 and (b) mainly m=7, 8, 9 and 10, and DGEBF (c) and (d) (n=1).

4.3.2 Characterization of Silver Flakes

Figure 4.5 shows SEM images of silver flakes in this study. Typically bimodal fillers are used to increase the packing density and thus higher conductivity at a given filler loading. It is well known that a thin layer of lubricant is present on the surface of commercial silver flakes to prevent the aggregation of silver flakes during production. This layer of lubricant affects the interaction of silver flake with other silver flakes and with the polymer system and thus affects the dispersion of silver flakes, the rheology of formulated pastes and the electrical conductivity of the resulting polymer composites [52, 66-67, 174]. Figure 4.6 shows Raman spectra of the lubricant on the surface of silver flakes. The presence of carboxylate groups on the surface of silver flakes was verified by the symmetric ($\nu_s(COO^-)$) stretching at 1432 cm^{-1} (or 1438 cm^{-1}) and asymmetric ($\nu_{as}(COO^-)$) stretching at 1591 cm^{-1} (or 1587 cm^{-1}) [66, 144-145]. These results are

consistent with previous studies that the lubricant layer is indeed silver carboxylate [52, 66-67, 174]. The distinct differences between the two spectra were i) the intensity of the peaks at 930 and 664 cm^{-1} in Figure 4.6 (a), assigned to the C-COO^- stretching and the deformation of -COO^- [145], was much stronger than that of the corresponding peaks in Figure 4.6 (b); ii) The SERS peaks of C-H stretching of the lubricant on Ag-FA were well resolved, compared with those of the lubricant on Ag-FB (Figure 4.6, inset); iii) the methylene twisting, wagging and scissor appeared at 1297, 1362 and 1474 cm^{-1} [144], respectively in Figure 4.6 (b). These distinct differences are related to the chain length of lubricants and their surface orientation and conformation [145]. Figure 4.7 shows TGA results of the silver flakes. Ag-FA and Ag-FB showed significant weight losses at 188 ^oC and 218 ^oC, respectively (Figure 4.7, inset). This clearly indicates the presence of lubricants on the surface of silver flakes. Weight losses of Ag-FA and Ag-FB at 450 ^oC were 0.09% and 0.23%, respectively. Both Ag-FA and Ag-FB showed endothermic peaks at 232 and 247 ^oC, respectively (Figure 4.8). Lu et al. found that silver flakes lubricated with fatty acids of a longer chain showed exothermic DSC peaks at higher temperatures [51]. These exothermic DSC peaks in air of lubricated silver flakes are due to the oxidation of the lubricant layer [51-52]. These results indicated that the lubricant on the surface of Ag-FB may have a longer chain than that on Ag-FA.

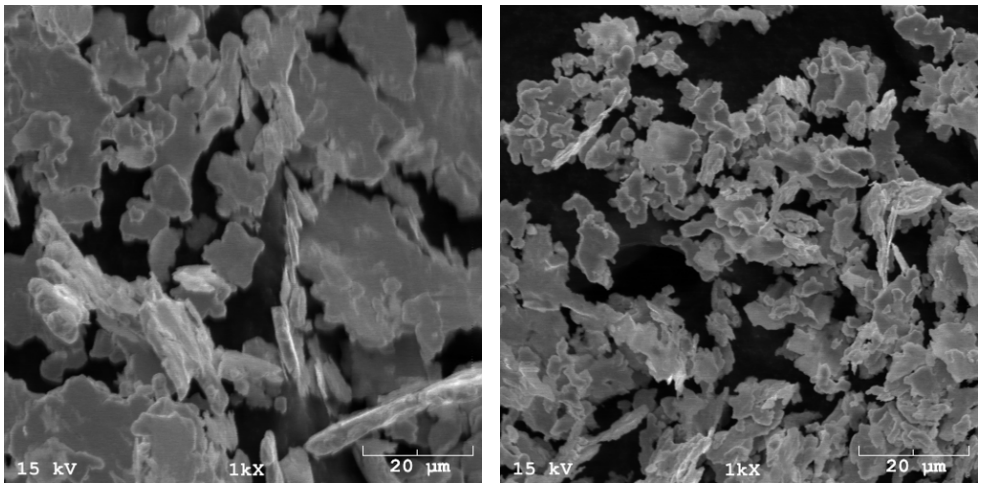

(a) (b)

Figure 4.5 Silver flakes (a) Ag-FA and (b) Ag-FB.

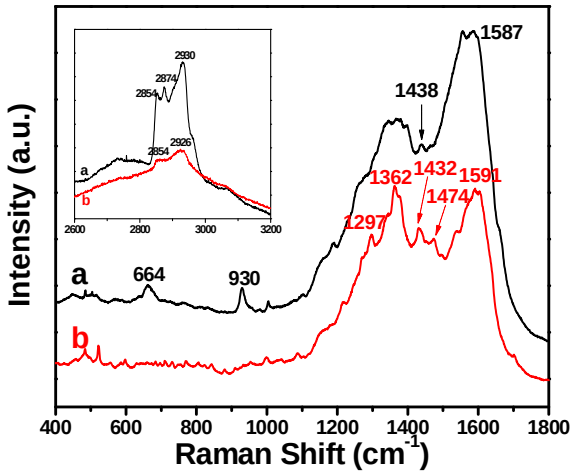

Figure 4.6 Raman spectra of the lubricant on the surface of (a) Ag-FA and (b) Ag-FB. Inset is the spectra in the range of 2800-3200 cm^{-1}.

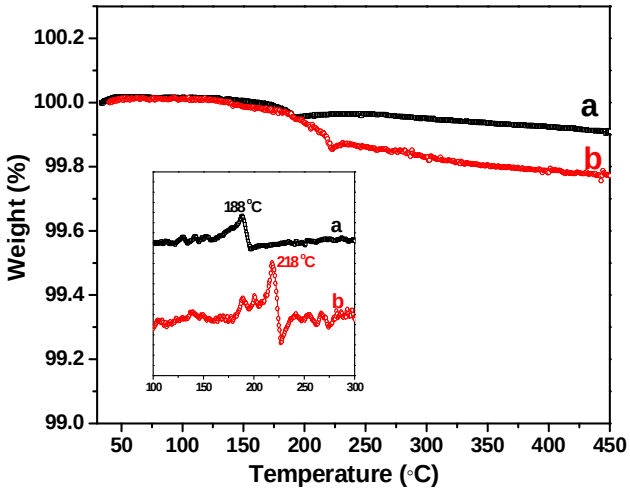

Figure 4.7 TGA of (a) Ag-FA and (b) Ag-FB. Inset is the first derivative of curve a and b in the temperature range of 100-300 ^{o}C.

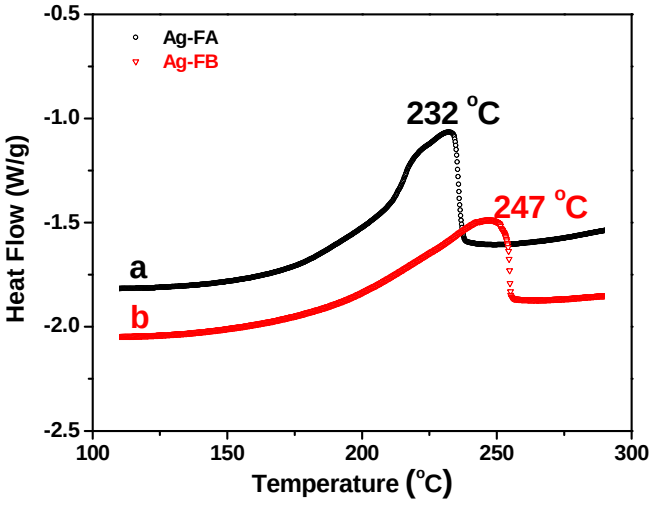

Figure 4.8 DSC of (a) Ag-FA and (b) Ag-FB.

4.3.3 Reduction of Silver Carboxylate on the Surface of Silver Flakes

To investigate the reduction of silver carboxylate and the formation of silver particles on the surface of silver flakes, Ag-FA and Ag-FB were treated with DGEBF and

DGEPG at the curing temperature (150 ^{o}C). Figures 4.9 and 4.10 show the surface morphology changes of silver flakes after isothermal treatment. When treated with DGEBF at 150 ^{o}C for 10 min, the surface of silver flakes remained relatively smooth (Figures 4.9 (a) and 4.10 (a)). Compared with silver flakes treated with DGEBF, silver flakes treated with DGEPG showed clearly the growth of silver nano/submicron-sized particles on their surfaces and at their edges (Figures 4.9 (c) and 4.10 (c)). As the time for treatment increased, silver flakes treated with DGEBF became rough (Figures 4.9 (b) and 4.10 (b)). The relatively rough surface was the result of the reduction of silver carboxylate and the formation of highly surface reactive silver nano/submicron-sized particles. These particles then sintered with the silver flakes. The growth of silver nano/submicron-sized particles was more prominent when silver flakes were treated with DGEPG for 30 min (Figures 4.9 (d) and 4.10 (d)). Moreover, neckings between silver flakes were observed. The neckings between silver flakes are indicative of effective sintering between silver flakes. This may result from the relatively stronger reduction capability of the primary –OH group in DGEPG than secondary –OH group in DGEBF at 150 ^{o}C.

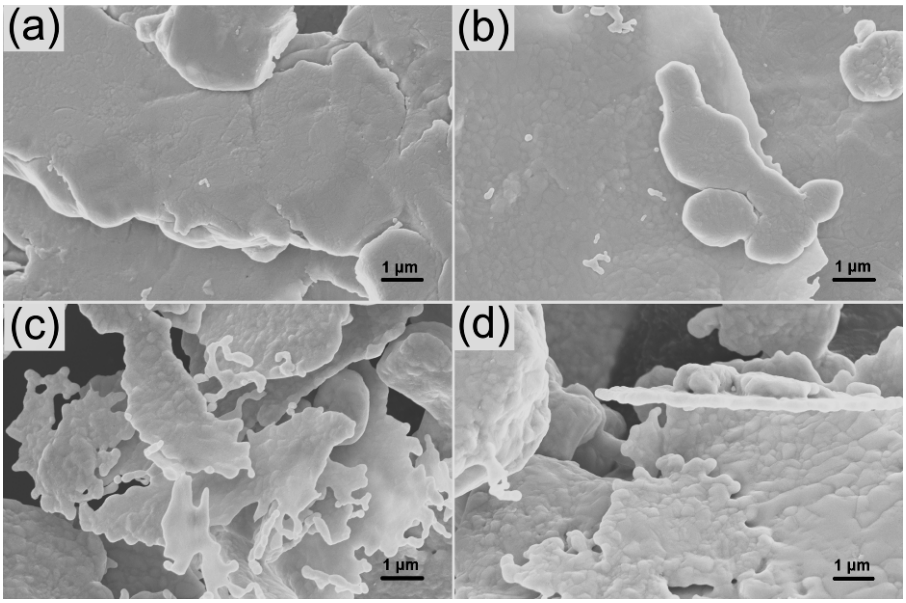

Figure 4.9 Ag-FA treated with DGEBF for (a) 10 min, (b) 30 min and with DGEPG for (c) 10 min, (d) 30 min at 150 ^{o}C

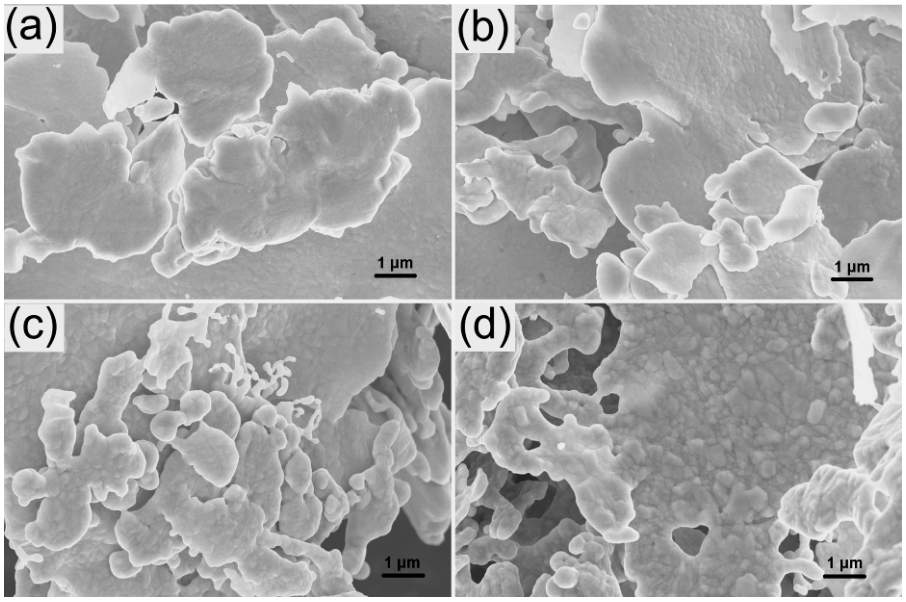

Figure 4.10 Ag-FB treated with DGEBF for (a) 10 min, (b) 30 min and with DGEPG for (c) 10 min, (d) 30 min at 150 ^{o}C.

Figure 4.11 shows DSC of silver flakes (Ag-FB) treated with DGEBF or DGEPG. Ag-FB shows clearly an exothermic peak and a mild broad peak at 276 ^{o}C after isothermal treatment with DGEBF for 10 and 30 min, respectively. The shift of the exothermic peak from 247 ^{o}C (Figure 4.7) to 276 ^{o}C may result from the physical absorption of DGEBF onto the surface of silver flakes that delays the oxidation of the lubricant. The physical absorption was verified by the peak at 915 cm^{-1} (Figure 4.12 (b)), the characteristic vibration of epoxy rings, in the Raman spectrum of silver flakes treated with DGEBF (Figure 4.12 (c)). After treatment with DGEPG, the exothermic DSC peak disappeared (Figure 4.11) and Raman peaks of the lubricant on the surface of silver flakes almost disappeared (Figures 4.12 (a) and (d)). Both DSC and Raman results indicated that silver carboxylate on the surface of silver flakes were reduced and removed. This was consistent with the lack of luster on the surface of DGEPG treated silver flakes. It is well-documented that organic molecules on the surface of silver particles play an important role in the sintering onsets, the extent of densification and final grain sizes [81]. These organic molecules provide an energy barrier to sintering. The particles sinter if the thermal energy is sufficient to overcome the activation energy provided by the organic molecules [149]. The nearly complete removal of the lubricant from the surface of silver flakes facilitated the sintering between silver flakes for DGEPG treated silver flakes and thus the electron transport.

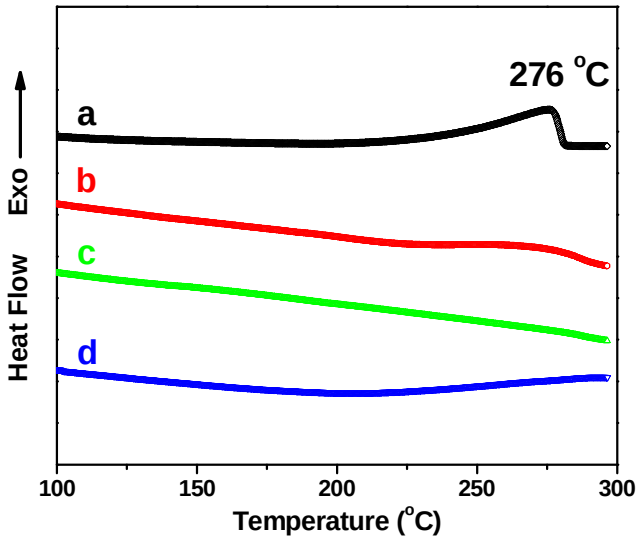

Figure 4.11 DSC of Ag-FB treated with DGEBF (a) 10 min, (b) 30 min and with DGEPG (c) 10 min, (d) 30 min at 150 °C.

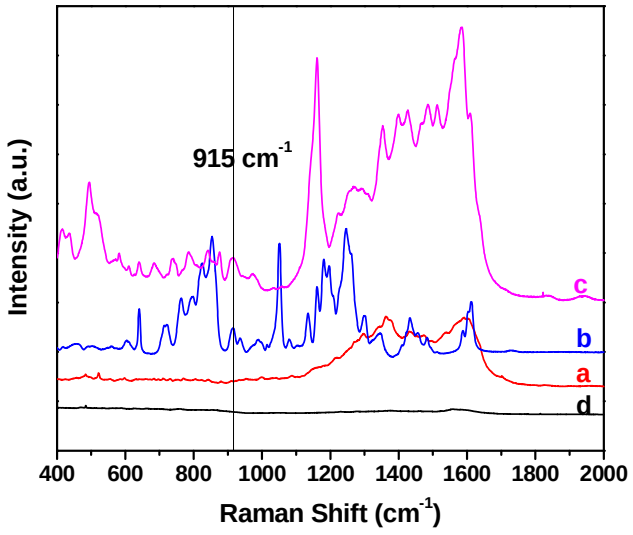

Figure 4.12 Raman spectra of (a) the lubricant on the surface of silver flakes (Ag-FB), (b) DGEBF, silver flakes treated with (c) DGEBF and (d) DGEPG at 150 °C.

4.3.4 Properties of Flexible Highly Conductive ICAs

Electrical conduction of an ICA is established through the cure shrinkage of the polymer matrix, which brings metal fillers into intimate contacts and forms 3-D conductive networks within the polymer matrix. Figure 4.13 shows bulk resistivity of the ICAs filled with 80 wt% silver flakes using different ratios of DGEBF and DGEPG as polymer matrices. DGEBF filled with 80 wt% silver flakes shows an averaged resistivity of 2.3×10^{-4} Ω cm, which is comparable to that of commercially available ICAs. The averaged resistivity decreased to 1.4×10^{-4} Ω cm and the lowest resistivity was 6.5×10^{-5} Ω cm for the ICAs with equal amounts of DGEBF and DGEPG. The ICAs showed a lower electrical resistivity (3.5×10^{-5} Ω cm) with an increased DGEPG content (70 wt% of the mixture of DGEBF and DGEPG). This could be due to the enhanced reduction of silver carboxylate and increased necking area between silver flakes. The resistivity of the DGEPG filled with 80 wt% silver flakes is 2.5×10^{-5} Ω cm, about one order of magnitude lower than that of the ICAs composed of DGEBF and 80 wt% silver flakes. Figure 4.14 shows the cross-sections of the ICAs. Without DGEPG, the surface of silver flakes within the polymer matrix was relatively smooth (Figure 4.14 (a)). There are lubricants (or possibly oxide) at the interface between silver flakes. The presence of the lubricants increases the tunneling resistance between silver flakes. With the incorporation of DGEPG, silver nano/submicron-sized particles formed both on the surface and at the edges of the silver flakes (Figure 4.14 (b)). As the content of DGEPG increased, larger particles and neckings between silver flakes formed (Figures 4.14 (c) and (d)). Therefore, two factors contribute to the significantly improved electrical conductivity of the ICAs with the incorporation of DGEPG. First, the growth of highly surface reactive silver

nano/submicron-sized particles facilitates the sintering between silver flakes. The sintering leads to the formation of metallurgical joints and reduces and eliminates the contact resistance effectively. Second, the removal of surface lubricant, as verified from Figure 4.12, enables direct metal-metal contacts between silver flakes, decreasing the contact resistance. The resistivity of flexible highly conductive ICAs with ratios of 70:30 and 50:50 of DGEPG to DGEBF increased by 43.9±8% and 66.3±24%, when the radius of curvature of the samples was changed from 30 mm to 14 mm, respectively.

Highly conductive ICAs have been prepared by low temperature sintering (<200 ^{o}C) of the incorporated silver nanoparticles [77, 83-84, 175]. The limitations of these approaches include i) low dispersion efficiency of untreated nanoparticles in the epoxy matrix. Surface functionalization with short-chain diacids can enhance the dispersion and prevent the oxidation as well as facilitate the sintering, but decrease the catalytic capability and tend to result in poor mechanical properties of the ICAs [83-84]; ii) the relatively high cost of silver nanoparticles. A large amount of silver nanoparticles used to improve the electrical conductivity increases the cost; iii) complicated and expensive processes such as surface functionalization [83-84], synthesis of multi-walled carbon nanotubes decorated with silver nanoparticles [175] and relatively long-period sonication [77, 83-84]. These complicated, time-consuming steps limit their industrial applications; iv) difficulties in printing pastes filled with nanomaterials. A high loading of nanomaterials increases the viscosity of the paste dramatically at low shear rates. The increased viscosity makes the paste difficult to flow and to be printed, especially for low cost jet dispensing technologies. Compared with these studies, the present study offers a much simpler, lower cost approach to achieve highly conductive ICAs.

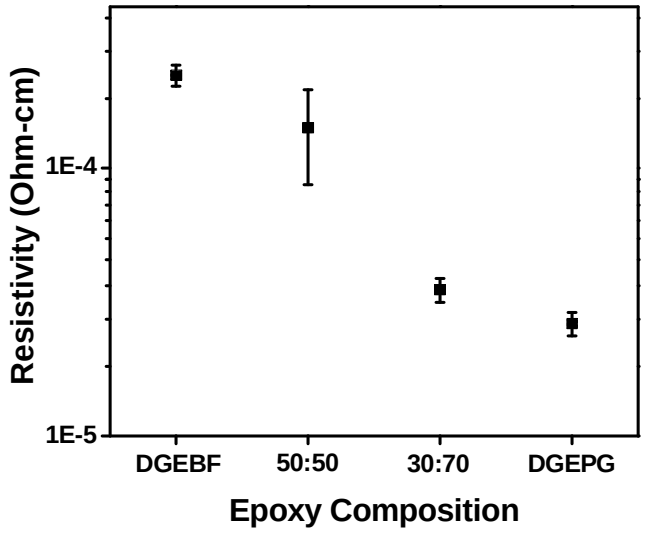

Figure 4.13 (a) Electrical resistivity of ICAs filled with 80 wt% silver flakes by using different polymer matrices including DGEBF (100%), a 50:50 mixture of DGEBF and DGEPG, a 30:70 mixture of DGEBF and DGEPG, and DGEPG (100%).

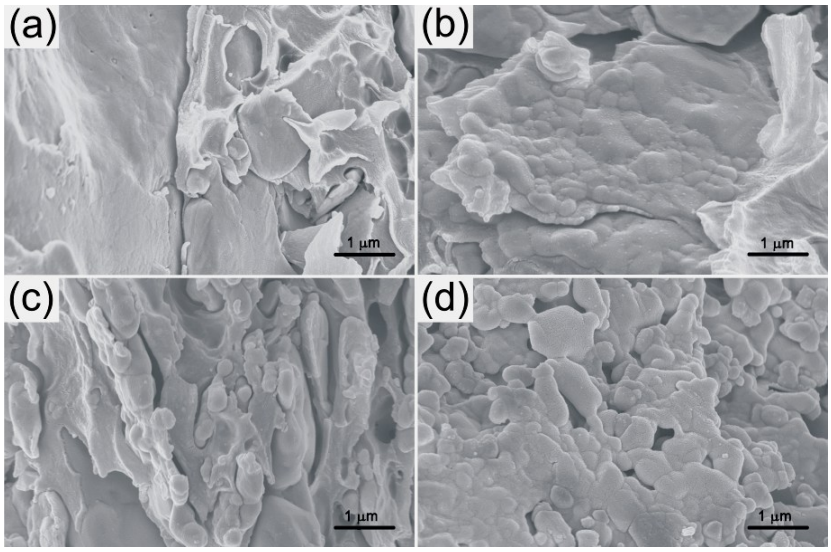

Figure 4.14 SEM images of cross-sections of ICAs filled with 80 wt% silver flakes by using different polymer matrices (a) DGEBF (100%); (b) 50:50 mixture of DGEBF and DGEPG, (c) 30:70 mixture of DGEBF and DGEPG, (d) DGEPG (100%).

4.3.5 Adhesion Improvements

Adhesion strength is an important factor to evaluate the performance of the joint. Flexible highly conductive adhesives (FHCA) with different ratios of flexible epoxy and rigid epoxy were formulated and the die shear strengths of the FHCA on glass, polyimide and gold substrate have been reported. Typically with the increase in the fraction of flexible epoxy, the adhesion strength continuously decreases. Comparing the adhesion strength of FHCAs on various substrates, the adhesion strength of FHCAs on Au was the lowest with the same resin formulation [104]. Depending on the surface properties of the substrate, coupling agents containing different functional groups such as thiol, carboxylic acid, amine and epoxide groups have been used to improve the adhesions strength. In order to enhance the adhesion strength of FHCAs on Ni/Au surface, 4-mercaptobenzoic acid was selected since thiol group has a strong affinity to Au surface while carboxylic acid can react with epoxy resins (Figure 4.15). Figure 4.16 shows the XPS of the gold surface treated with 4-mercaptobenzoic acid. The presence of S2s, S2p, C and O indicated that the surface has been modified with 4-mercaptobenzoic acid. Contact angle measurement further confirm the successful coating as the contact angle decrease from 60^{o} (untreated gold surface) to 40^{o} after the surface being treated with the molecules.

The adhesion strengths of FHCA on Au treated with 4-mercaptobenzoic acid were measured for the formulations with 50 wt% and 70 wt% flexible epoxy. As shown in Figure 4.17, flexible highly conductive adhesives with ratios of 70:30 and 50:50 of DGEPG to DGEBF exhibited die shear strengths of 9.8 and 14.7 MPa (1 MPa means 10.2 kg force per square centimeter, which also equals to about 10 atm) on a gold surface, respectively. The adhesion strength on the gold surface can be improved significantly by

surface modification with a coupling agent and increased to 14.2 and 32.9 MPa correspondingly [106]. These improvements are attributed to the capability of the coupling agent to form strong bonds with both the FHCAs and Au substrates. Simple device level tests indicated that interconnects based on the flexible highly conductive polymer composites are robust during the substrate rolling/bending, enabling the application of the flexible highly conductive ICAs in flexible electronics [106].

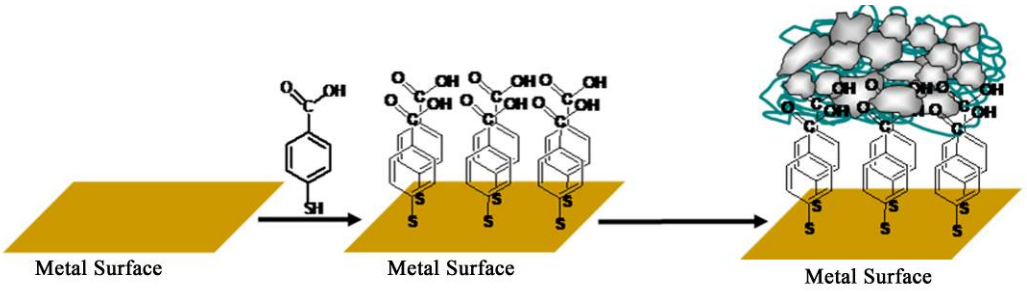

Figure 4.15 Schematic illustration of metal surface coated with a coupling agent for adhesion improvement.

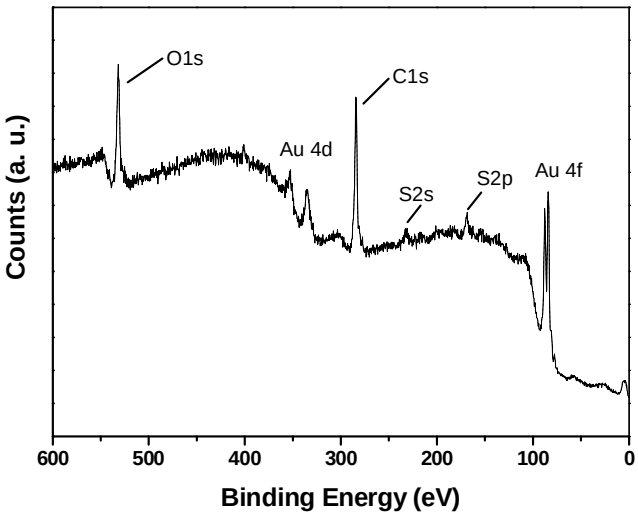

Figure 4.16 XPS of a gold surface treated with 4-mercaptobenzoic acid.

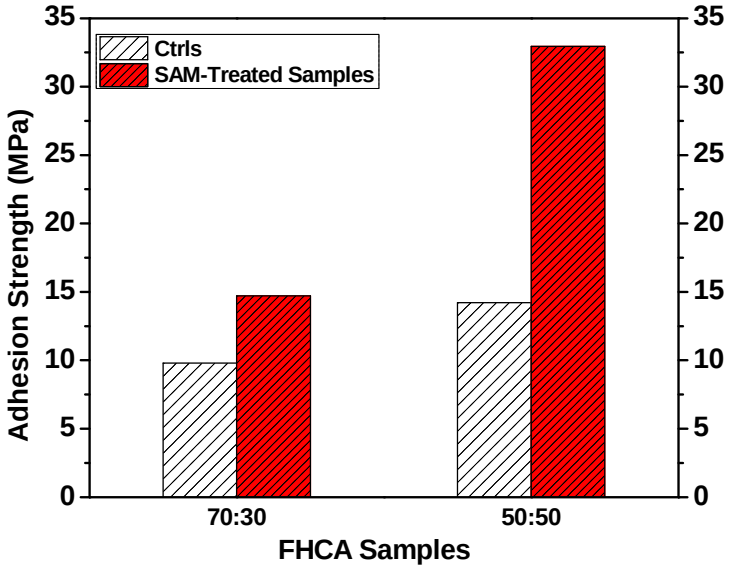

Figure 4.17 Adhesion strength of FECA on Ni/Au surfaces with and without the treatment.

4.4 Conclusions

Flexible highly conductive ICAs with electrical resistivity as low as 2.5×10^{-5} Ω cm were prepared at 150 ^{o}C by simply incorporating flexible epoxy (DGEPG) into the ICA formulations. DGEPG functioned as a mild reducing agent for the in situ reduction of silver carboxylate on the surface of silver flakes. The reduction of silver flakes by DGEPG removed the surface lubricant and allowed the metallurgical joints and direct metal-metal contacts between the conductive fillers. This reduced and eliminated the contact resistance effectively, enabling the preparation of flexible highly conductive ICAs at a low temperature. The approach developed offers many significant advantages such as

i) reduced materials cost;

ii) low processing temperature compatible with low cost, flexible substrates such as paper and PET;

iii) simple processing;

iv) low viscosity of the formulated pastes with DGEPG, allowing the paste to be used for low cost jet-dispensing technologies;

v) tunable mechanical properties;

vi) flexibility and high electrical conductivity.

Future printed electronics requires ICAs to be mechanically compliant to fit the non-planar forms, to have a high conductivity, to have strong adhesion on many substrates and to have low processing temperatures to be compatible with low cost, flexible substrates. The multi-functional ICAs developed in this study are attractive for current and emerging applications in flexible electronics.

CHAPTER 5

SURFACE MODIFICATION OF SILVER-COATED COPPER FLAKES FOR HIGHLY RELIABLE LOW COST ICAS

This chapter describes the replacement of expensive silver flakes used in chapters 2-4 with lower cost silver-coated copper flakes and the development of highly reliable, highly conductive, low cost ICAs. First, this chapter gives a literature review on low cost ICAs, describes the production of silver-coated copper flakes, and discusses copper corrosion and its prevention using corrosion inhibitors. The characterization of silver-coated copper flakes and surface modification are then conducted. Followed are the electrical properties of ICAs filled with silver-coated copper flakes. Finally, the contact resistance of the ICAs on nickel/gold surface during the reliability tests (85 ^{o}C/85% RH and reflow) is studied.

5.1 Introduction

5.1.1 Literature Review on Low Cost ICAs

One of the main hurdles for the wide use of current commercial silver-filled ICAs is the high cost of silver fillers (silver: $35/ounce in March 2011). Significant research has been devoted to the development of low cost ICAs. Copper (copper: $0.27/ounce in March 2011) could be a promising candidate for low cost electrically conductive fillers, due to its low resistivity, low cost and reduced electro-migration compared to silver [23, 176]. Other low-cost electrically conductive fillers have also been developed to replace silver for ICAs, including solder particles [46-47], a mixture of solder and copper [46-

47], copper alloys [43, 177-178], copper coated with a thin layer of low melting point metals, Pb-free metals (such as Sn, In, Bi, Sb, Zn and their alloys) [44], and silver-coated copper fillers [24-26, 178-179]. The challenge associated with ICAs filled with the low-cost conductive fillers lies in the oxidation and corrosion of the filler particles during curing and reliability tests. The formation of non-conductive oxides deteriorates the electrical properties of the ICAs limiting their applications in electronic packaging. Yim et al. developed ICAs filled with copper flakes and investigated the effect of silane coupling agents (SCAs) on the oxidation prevention of copper powder [23]. It was found that the oxidation of copper flakes occurred during the curing of copper-filled ICAs. With the incorporation of the SCA as corrosion inhibitor, the contact resistance of copper-filled ICAs dramatically reduced (about 0.3 Ω), compared with copper-filled ICAs without a corrosion inhibitor (about 100 MΩ). The improvement was attributed to the protection of copper flakes from oxidation by SCA during the curing at 150 ^{o}C. However, the developed ICAs showed a significant increase in bulk resistivity, from 1.28×10^{-3} to 3.00×10^{-3} Ω cm during 85 ^{o}C/85% RH aging for only 24 h. Copper readily oxidizes even at low temperatures and cannot form a self-protective layer to prevent further oxidation [180-181]. Recently, Ho et al. investigated the properties of ICAs filled with copper and copper alloyed with Ag, Ge, Mg and Zn in terms of electrical conductivity, thermal stability, and the effects of the trace alloy elements on the oxidation resistance of the metallic fillers [179]. The ICAs filled with these fillers showed similar electrical conductivity after curing. However, after exposure at 125 ^{o}C for 1000 h in air, the resistivity of ICAs filled with copper alloyed with silver and Mg increases from 2.38×10^{-4}

to 2.43×10^{-3} Ω cm and from 4.53×10^{-4} to 7.3×10^{-3} Ω cm, respectively. The resistivity of ICAs filled with other fillers (such as Ge and Zn) increased dramatically.

To enhance oxidation resistance of copper particles, the effect of coating copper particles with silver has been investigated [24-26, 178-179]. Lin et al. reported that a silver coating on copper flakes provided good oxidation resistance at temperatures lower than 175 ^{o}C [24]. However, the resistivity of ICAs filled with the silver-coated copper flakes increased from 1.6×10^{-3} Ω cm before the treatment of the fillers to 2.5×10^{-3} Ω cm after the heat treatment at 175 ^{o}C for two hours as a result of the formation of Cu_2O on the silver-coated copper flakes (38). The oxidation of silver-coated copper flakes may result from incomplete plating of the copper flakes with silver. Park et al. investigated the effect of SCAs and dispersing agents on the electrical conductivity and corrosion stability of silicone sealants filled with silver-coated copper powders [26]. With the most effective SCA, 3-aminopropyltriethoxysilane, silicone sealants filled with the silver-coated copper flakes showed a 30% increase in the resistivity after storage at 50 ^{o}C for 24 h. These results indicate oxidation of the silver-coated copper powders at high temperatures. Additionally, due to the difference in electrochemical potential between copper and silver, galvanic corrosion can occur in pits in the silver plating. Although silver-coated copper has been used with limited success, the coating of silver on copper particles greatly prevents the oxidation of copper particles.

5.1.2 Production of Silver-coated Copper Particles

In order to overcome copper oxidation/corrosion, the production of silver-coated copper particles (including sphereical particles, flakes and other forms) has been explored. Generally the coating of copper particles with silver can be achieved by either

electroplating or electroless plating. Takeshima et al. in US Patent No. 4,954,235 describes the electroplating of fine copper particles (0.1-10 μm) with silver [182]. Figure 5.1 shows schematic principle of the electroplating of copper particles with silver. A stationary circulating flow of a suspension of copper particles in the copper ion-containing electrolyte is specially designed in the bath to collide with the surface of the cathode, but not coming in contact with anode. When the particles come to contact with the surface of the cathode, electric charges of the cathode transfer to the particles (Figure 5.2 (a)) and then the charged particles leave the surface (Figure 5.2 (b)). Silver ions which are present in the vicinity of the charged particles electrostatically come in contact with the charged particles and deposit thereon (Figure 5.2 (b)). The flow of the copper particle suspension is repeatedly brought in collision with the cathode and the coating process proceeds continuously. If all the surface of the cathode is unceasingly hit by copper particles, then silver ions in the electrolyte may only deposit on the surface of copper particles without substantial deposition on the surface of the cathode. To meet this desired condition, optimization of the particle concentration and particle velocity is essential. The electroplating method is very difficult to uniformly electroplating of each and every copper particle with a size smaller than 10 μm with a high yield.

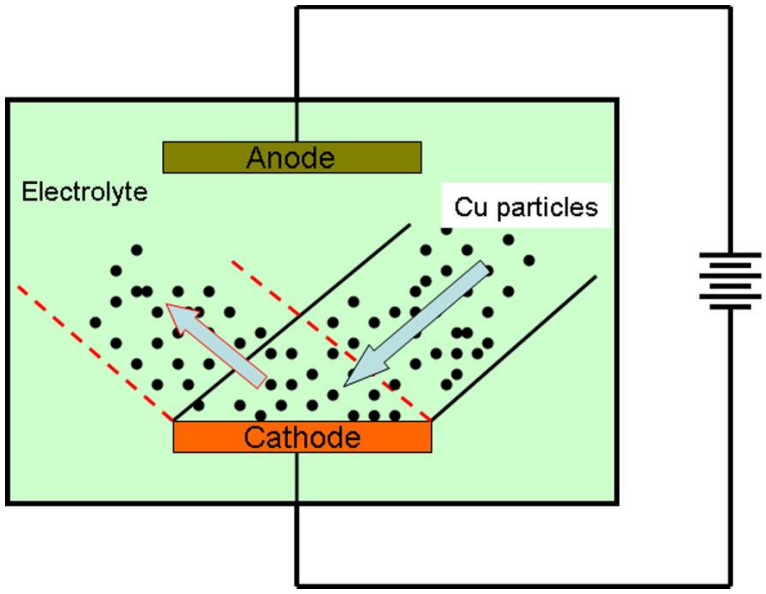

Figure 5.1 Schematic illustration of electroplating of copper particles with silver.

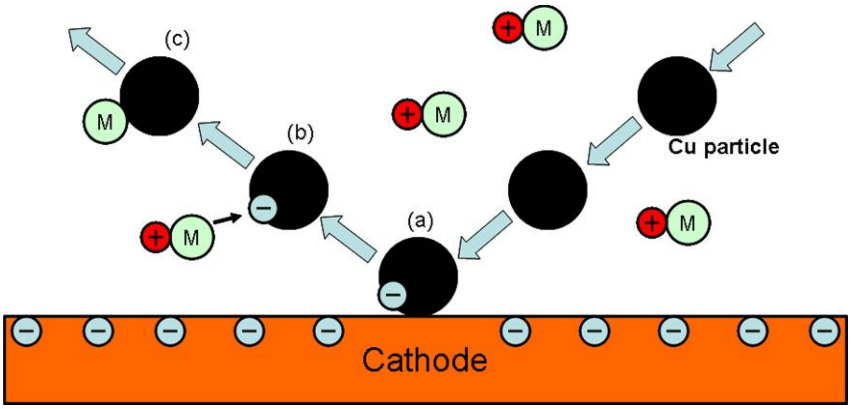

Figure 5.2 Schematic illustration of electroplating process of a single particle.

Electroless silver plating on copper particles has been found to be more efficient. According to US Patent 5,945,158, electroless silver plating on copper particles usually involves four steps [183]:

1. Removal of copper oxides and hydroxides by ammonia and ammonium sulfate to provide a clean surface for silver deposition (eqn. (1)-(3)).

$$Cu_2O + 2NH_4OH + (NH_4)_2SO_4 = [Cu(NH_3)_2]SO_4 + 3H_2O \quad (1)$$
$$CuO + 2NH_4OH + (NH_4)_2SO_4 = Cu(NH_3)_4SO_4 + 3H_2O \quad (2)$$
$$Cu(OH)_2 + 2NH_4OH + (NH_4)_2SO_4 = Cu(NH_3)_4SO_4 + 3H_2O \quad (3)$$

2. Once the copper surface is clean and activated, silver ion solution, which is freshly prepared by dissolution of silver nitrite in ammonium hydroxide (eqn. (4)-(6)) were added to the slurry of copper particles in the ammonium sulfate solution plus a reducing agent, i.e. sodium potassium tartrate. Sodium potassium tartrate functions as both a mild reducing agent of the silver ions and as a complexing agent for Cu^{2+} ion to suppress precipitation of copper hydroxides.

$$2AgNO_3 + 2NH_4OH = Ag_2O\downarrow + 2NH_4NO_3 + H_2O \quad (4)$$
$$Ag_2O + 4NH_4OH = 2[Ag(NH_3)_2]OH + 3H_2O \quad (5)$$
$$[Ag(NH_3)_2]OH + NH_4NO_3 = [Ag(NH_3)_2]NO_3 + NH_4OH \quad (6)$$

3. After the addition of the silver ion solutions and the reducing agent, the following displacement reaction takes place at the active copper surface (Eqn. (7)). A comparison of the standard reduction-oxidation potentials indicates the displacement reaction is favored [184].

$$Ag(NH_3)_2^+ + e = Ag\downarrow + 2NH_3 \qquad E^o = +0.373\ V$$

$$Cu + 4NH_3 - 2e = Cu(NH_3)_4^{2+} \qquad E^o = -0.05\ V$$

$$Cu + 2[Ag(NH_3)_2]NO_3 = [Cu(NH_3)_4]_2(NO_3)_2 + 2Ag \qquad \triangle E^o = +0.696\ V \qquad (7)$$

4. Subsequent reduction of the silver ion by sodium potassium tartrate, as proposed (eqn. (8) and (9)), leads to the growth of silver coating at room temperature.

$$2Ag(NH_3)_2^+ + 2OH^- = Ag_2O\downarrow + 4NH_3 + H_2O \qquad (8)$$

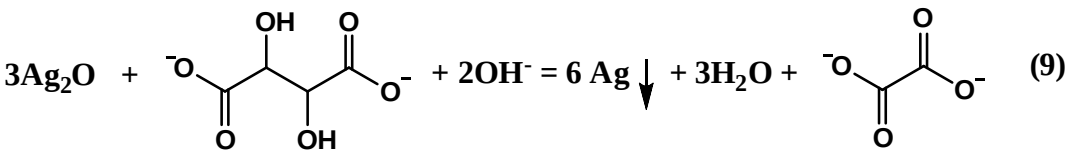

(9)

The resulting silver-coated copper particles are filtered and washed with deionized water at pH=7 and finally dried at 105 ^oC. Although the production of silver-coated copper flakes has improved significantly, integral silver coverage on copper particles with uniform thickness remains a challenge. Therefore, the prevention of oxidation and corrosion of the exposed copper on silver-coated copper flakes is crucial for the preparation of highly reliable ICAs filled with silver-coated copper flakes.

5.1.3 Copper Oxidation and Galvanic Corrosion

As is well known, copper is susceptible to oxidation. Oxidation occurs under both dry and wet conditions and usually becomes more serious under high temperatures. However, a galvanic corrosion happens only when the following conditions are met: (a) two metals with different electrochemical potentials (see Table 5.1) are present and

connected; (b) an aqueous phase with electrolyte exists; and (3) one of the two metals has electrochemical potential lower than the potential of the reaction ($H_2O + O_2 + 4e^- = 4OH^-$), which is 0.4 V under the standard condition. Since the plating of silver on the surface of copper particles is not integral, galvanic corrosion of silver-coated copper flakes can occur when moisture and oxygen come in contact with the copper-silver interface. The difference in the electrical potential serves as the driving force for the electron flow between two metals. As a result, the copper acts as an anode and tends to corrode while the silver acts as a cathode and is protected. The reactions are shown as follows:

At the anode (i.e. exposed copper):

$$2Cu - 4e = 2Cu^{2+}$$

At the cathode (i.e. silver plating)

$$O_2 + 2H_2O + 4e = 4OH^-$$

The OH- produced at the cathode will migrate and diffuse to the anode and react with Cu^{2+} to form $Cu(OH)_2$. Consequently, the electrical conductivity of silver-coated copper flakes and thus ICAs filled with silver-coated copper flakes is degraded due to the formation of insulative $Cu(OH)_2$.

Table 5.1 Electrochemical potential values for selected metals.

Element	Reaction	Potential (V)
Gold	$Au^+ + e^- = Au$	1.691
	$Au^{3+} + 3e^- = Au$	1.50
Silver	$Ag^+ + e^- = Ag$	0.799
Copper	$Cu^+ + e^- = Cu$	0.521
Oxygen, water	$2H_2O + O_2 + 4e^- = 4OH^-$	0.401
Copper	$Cu^{2+} + 2e^- = Cu$	0.342
Hydrogen	$2H^+ + 2e^- = H_2$	0
Lead	$Pb^{2+} + 2e^- = Pb$	-0.126

Table 5.1 continued

Tin	$Sn^{2+} + 2e^- = Sn$	-0.138
Nickel	$Ni^{2+} + 2e^- = Ni$	-0.257
Chromium	$Cr^{3+} + 3e^- = Cr$	-0.744
Zinc	$Zn^{2+} + 2e^- = Zn$	-0.762
Magnesium	$Mg^{2+} + 2e^- = Mg$	-2.372

5.1.4 Copper Corrosion Prevention Using Corrosion Inhibitors

Copper, one of the most important metals, has a wide variety of industrial applications due to its excellent electrical, thermal and mechanical properties. Corrosion of copper plays a very important role in the diverse applications and consequently, studying the corrosion prevention of copper has attracted much attention. Corrosion inhibitor, defined as a chemical compound that decreases the corrosion rate of a material, typically a metal or an alloy [185], remains an effective approach to protect the copper from corrosion in various aggressive environments. There are several types of corrosion inhibitors [185].

- *Anodic corrosion inhibitors*. Anodic inhibitors usually act by forming a protective oxide film on the surface of the metal (where metal is corroded) and thus directly control corrosion by preventing the reaction that causes corrosion.
- *Cathodic corrosion inhibitors.* Cathodic inhibitors form a protective film coating of the cathodic metal (where metal is not lost) and thus indirectly prevent corrosion by limiting the diffusion of reducing species to the cathodic metal surface. As every oxidation requires the reduction to occur at the same time, the slow diffusion reduces the corrosion rate. Oxygen scavengers can react with the dissolved oxygen in the system to reduce the corrosion rate.

- *Mixed corrosion inhibitors.* Mixed inhibitors are organic materials that absorb on the surface and thus block both anodic and cathodic reactions.
- *Volatile corrosion inhibitors.* Volatile corrosion inhibitors (VCI), also called vapor phase inhibitors (VPI), are compounds transported in a closed environment to the site of corrosion by volatilization from a source.

Various organic corrosion inhibitors have been widely used to retard or prevent the oxidation and corrosion of copper. These corrosion inhibitors include azoles [186-187], amines [188-192], amino acids [193], triphenylmethane derivatives [194], thiol group compounds [195], phosphates [196] and other organic compounds [197]. Figure 5.3 shows some examples of effective copper corrosion inhibitors in various environments. These effective organic corrosion inhibitors typically contain a π-system and/or heteroatoms such as nitrogen (N), sulfur (S), or phosphorus (P), which improves the inhibitor efficiency. This has been explained by the formation of coordinative bonds between vacant d orbitals in Cu atom and atoms able to donate electrons [197]. Among these organic corrosion inhibitors, benzotriazole (BTAH, Figure 5.3, 1) has been reported to be one of the most effective copper corrosion inhibitors.

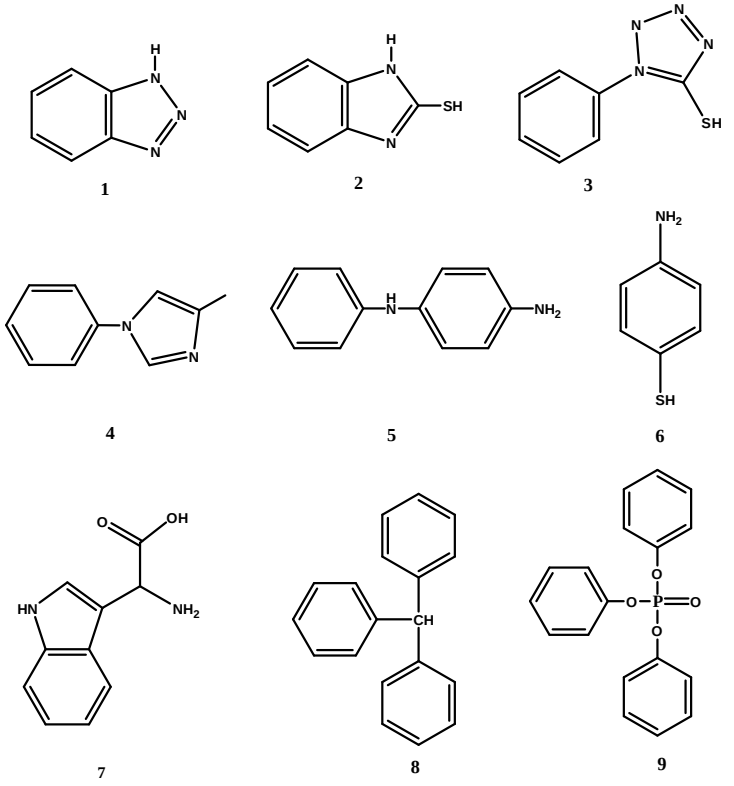

Figure 5.3 Examples of copper corrosion inhibitors. 1: benzotriazole; 2: 2-mecaptobenzothiazole; 3: 1-phenyl-5-mercapto-1,2,3,4-tetrazole; 4: 1-phenyl-4-methylimidazole; 5: N-phenyl-1,4-phenylenediamine; 6: 4-aminobenzenethiol; 7: Tryptophan; 8: triphenylmethane; 9: Triphenyl phosphate.

However, contradictory inhibitor mechanisms have been proposed and the mechanism by which BATH interact with copper surface remains to be elucidated. Generally, BATH acts as a mixed corrosion inhibitor, but the predominant effect is on inhibition of anodic reaction. The inhibition process generally involves (i) the absorption of the corrosion inhibitor on the surface of copper where copper undergoes oxidation to Cu^{+}; (ii) the formation of protective insoluble copper complex on the surface, preventing the copper

surface from corrosion [197-199]. Cotton and his co-workers pioneered research of using BTAH as a copper corrosion inhibitor and postulated that the complex existed in a linear polymeric form (Figure 5.4) [200]. In this proposed structure, copper was bonded by coordination involving a lone pair of electrons from one nitrogen atom and a Cu-N bond formed by replacement of the H atom from the N-H group. It is generally believed that the superior corrosion inhibition efficiency of BTAH is attributed to both the formation of strong Cu-N chemical bond and the formation of $[Cu\text{-}BTA]_n$ polymeric complex. The formation of polymeric complex not only improve the stability of the protective film on the copper surface but also increase the packing density, making the protective film an effective barrier against diffusion of aggressive ions from the surrounding to the copper surface and passage of metal ion into the surrounding.

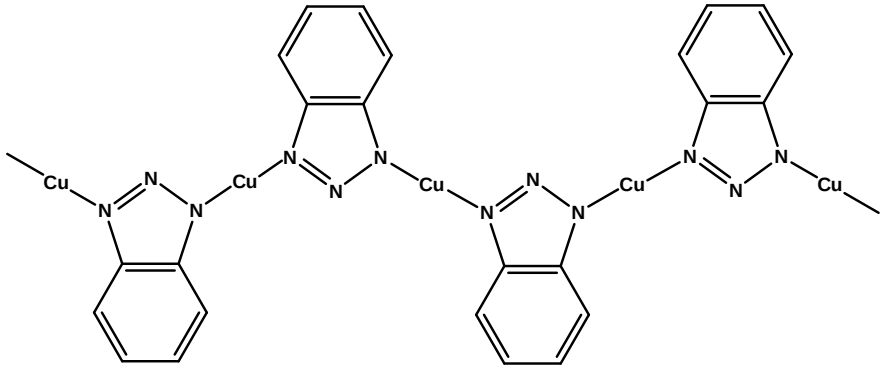

Figure 5.4 Copper-benzotriazole complex chemisorbed on the copper surface as postulated by Cotton [200].

Despite high corrosion inhibition efficiency of BTAH, it should be emphasized there is no universal solution for effective copper corrosion inhibition. For example,

thiazoles and benzotriazole show a good protection except in strongly acidic media, where tetrazoles and imidazoles show a high inhibition efficiency. Benzotriazole loses its high efficiency where sulfide ions are present in the environment. The efficiency of a corrosion inhibitor depends strongly on the factors causing corrosion such as concentration of corrosion inhibitor, pH and temperature. In most cases, effective corrosion inhibitors were determined experimentally from a large set of organic compounds and the experiments provides only the information whether a specific corrosion inhibitor is effective or not in a given environment. Therefore, a specific corrosion inhibitor has to be selected or tailored for a specific application.

Although the formation of dense layers of polymeric complex improves the corrosion inhibition efficiency, these dense layers could prevent the electron transport across conductive fillers within ICAs. Another disadvantage is the low thermal stability of benzotrizole on the copper surface. It was reported that in oxygen containing environment, benzotriazole was quickly lost from the surface at temperatures above 150 ^{o}C. Recently, many papers have been published on the use of intrinsically conductive polymers [201-203] and their derivatives [202, 204-205] as a corrosion inhibitor for copper. These polymers may function as macromolecular corrosion inhibitors as they reduce the number of active sites on the metal surface through adsorption and may act as a physical barrier by decreasing the transport of corrosive agents [206]. But their low processability, poor mechanical properties and inadequate thermal stability significantly limit their use as corrosion inhibitors [207]. Moreover, their insolubility with epoxy resins may further restrict their applications in electronic industry [208].

In this chapter, N-phenylaminopropyltrimethoxylsilane (NPAPTMS) has been selected as copper corrosion inhibitor. Previous studies in our research group indicated that, in contrast with other molecules studied, NPAPTMS can prevent the oxidation of copper flakes effectively during thermal curing at 150 ^{o}C and subsequent reliability tests. Moreover, the reaction of the secondary amine groups with epoxy leading to the formation of tertiary amine groups enables an effective protection of copper surface at high temperatures as the tertiary amine groups are linked to the highly cross-linked polymer matrix, which decompose at temperatures higher than 300 ^{o}C. Additional advantage may involve the adhesion improvement between conductive adhesives and silicon chips as the reaction between NPAPTMS and silicon chips occurs.

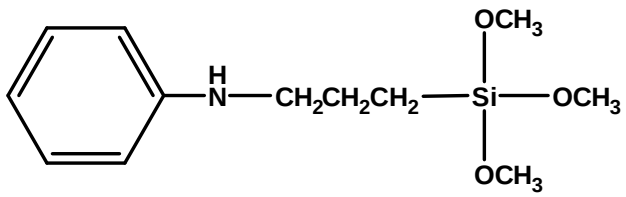

Figure 5.5 Molecular structure of N-phenylaminopropyltrimethoxylsilane.

5.2 Experimental

5.2.1 Materials

Diglycidyl ether of bisphenol F (DGEBF) having an epoxide equivalent weight of 165-173 was supplied by Shell Chemical Company. The curing agent, Lindride 52D (methylhexahydrophthalic anhydride), was provided by Lindau Chemical Inc. Silver-coated copper flakes and the catalyst, 1-cyanoethyl-2-ethyl-4-methylimidazole (2E4MZCN), were donated by Ferro Corp. and Shikoku Chemicals Corp. (Japan),

respectively. Silver-coated copper flakes (RDAGCU) have an aspect ratio of 3 and silver thickness of about 150 nm.

5.2.2 Surface Modification of Silver-coated Copper Flakes

Silver-coated copper flakes (5 g) were dispersed in 10 mM NPAPTMS in ethanol and were stirred at room temperature for 24 hours. Then the mixture was centrifuged and the flakes were re-dispersed in ethanol four times in an effort to remove non-adhering molecules. Finally, the modified silver-coated copper flakes were dried in vacuum before further use.

5.2.3 Preparation of ICAs Filled with Silver-coated Copper Flakes

ICAs filled with silver-coated copper flakes were prepared by curing the mixture of DGEBF, curing agent, catalyst, and 80 wt% untreated silver-coated copper flakes (or silver-coated copper flakes modified by NPAPTMS) at 150 ^{o}C for 1 hour. It was found that silver-coated copper flakes were easily dispersed in the epoxy resin after surface modification with NPAPTMS. For comparison, NPAPTMS (1 wt% of the mixture) was also in-situ incorporated into the ICAs filled with the untreated silver-coated copper flakes.

5.2.4 Characterization

A thermogravimetric analyzer (TGA) from TA Instruments, model 2050 was used to study the oxidation of silver-coated copper flakes in air. The temperature was raised from 25 ^{o}C to 600 ^{o}C at a heating rate of 10 ^{o}C/min.

The resistivity of ICAs was measured according to the method described in chapter 2. Contact resistance of ICAs in a circuit was studied on the test coupon depicted

in Figure 5.6. The test coupon consisted of etched metal patterns and a FR-4 organic substrate fabricated by Standley Circuit (Englewood, CO). Then the ICA was stencil-printed on the gaps between every two metal patterns. After the ICA was cured, the contact resistance of the patterned circuit was measured with the multimeter attached to the two ends of the pattern.

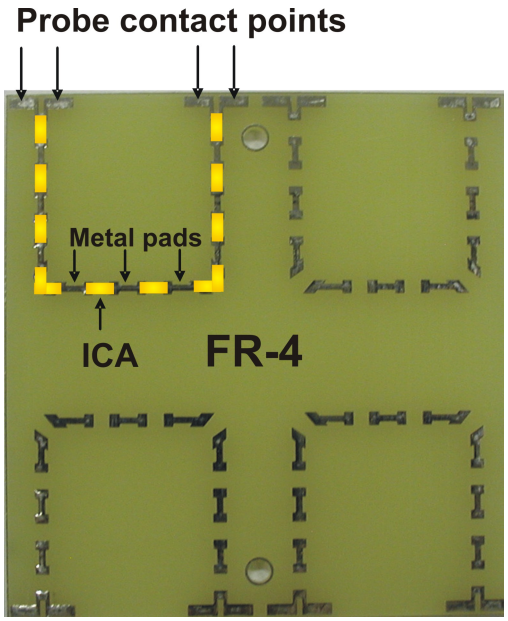

Figure 5.6 Test coupon for contact resistance measurement.

The specimens were exposed to 85 ^{o}C/85% RH in a temperature/humidity chamber (Lunaire Environmental, model CEO932W-4) and were exposed to dry heat at 85 ^{o}C in a thermal oven.

The resistance of each specimen was measured periodically for more than 1000 hours. Reflow tests were conducted in a BTU oven (BTU International). The reflow oven

has seven chambers and one cooling station. The temperatures for each chamber were set as 75, 110, 156, 198, 221, 255 and 175 ^{o}C, characteristic of a typical lead-free reflow profile. After each reflow, resistance of the specimens was measured and resistivity was calculated accordingly.

5.3 Results and Discussion

5.3.1 Characterization of Silver-coated Copper Flakes

Figure 5.7 shows the SEM images of the untreated silver-coated copper flakes. The size of silver-coated copper flakes is mainly about 5-10 μm (Figure 5.7 (a)). It was observed taht some pits exist on the surface of silver-coated copper flakes, which may be due to the incomplete plating of copper flakes with silver. As shown in Figures 5.7, 5.8 and 5.9, some flakes showed a relatively smooth surface while others were coated with nanoparticles. Energy-dispersive X-ray spectroscopy (EDX) of the smooth regions indicated that these smooth surfaces had a little amount of silver (Figure 5.8) and some relatively dark region shows the present of a fair amount of oxygen indicating that copper oxides forms in the detected area (Figure 5.9). EDX of the surface decorated with nanoparticles indicates the presence of a relatively large amount of silver. Therefore, these nanoparticles are silver nanoparticles plated on the surface of copper flakes. Figure 5.10 shows the XRD spectrum of the silver-coated copper flake. In addition to copper, silver crystaline phase was clearly identified.

Oxidation of silver-coated copper flakes was characterized by TGA (Figure 5.11). The TGA result indicates that oxidation of silver-coated copper flakes occurred at around 150 ^{o}C in air (Figure 5.11, inset) and continued up to 600 ^{o}C, by which temperature the weight gain was 22.2%. For silver-coated copper flakes modified by NPAPTMS, the

weight loss occurred from 110 ^{o}C and continued up to 300 ^{o}C with a weight loss of 0.75% (Figure 5.11, inset), which verifies the presence of NPAPTMS on the surface of silver-coated copper flakes. It could be possible that, during the heating in the temperature range of 150-300 ^{o}C, the weight loss of NPAPTMS on the silver-coated copper flakes and the weight increase of the silver-coated copper flakes due to oxidation both occurred. However, comparing the amount of the weight increase of untreated silver-coated copper flakes (20.44%) with that of the modified one (15.85%) in the temperature range of 300-600 ^{o}C, it can be concluded that the onset of oxidation of silver-coated copper flakes modified by NPAPTMS has been significantly delayed.

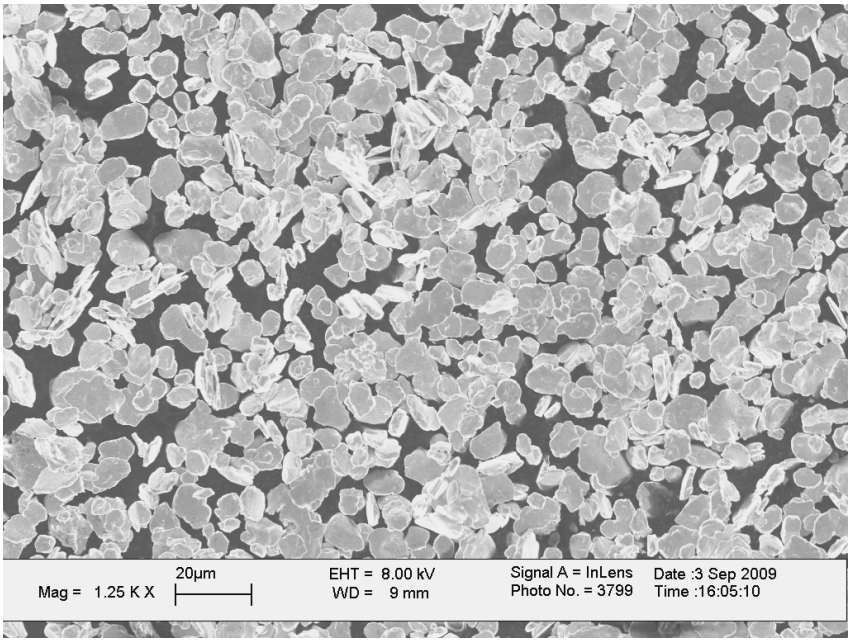

(a)

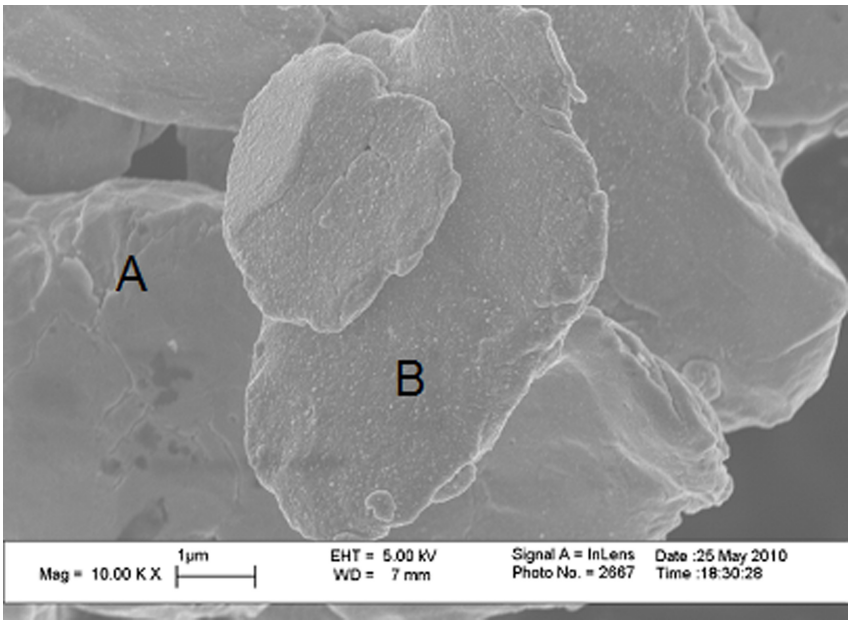

(b)

Figure 5.7 SEM images of silver-coated copper flakes (a) and (b).

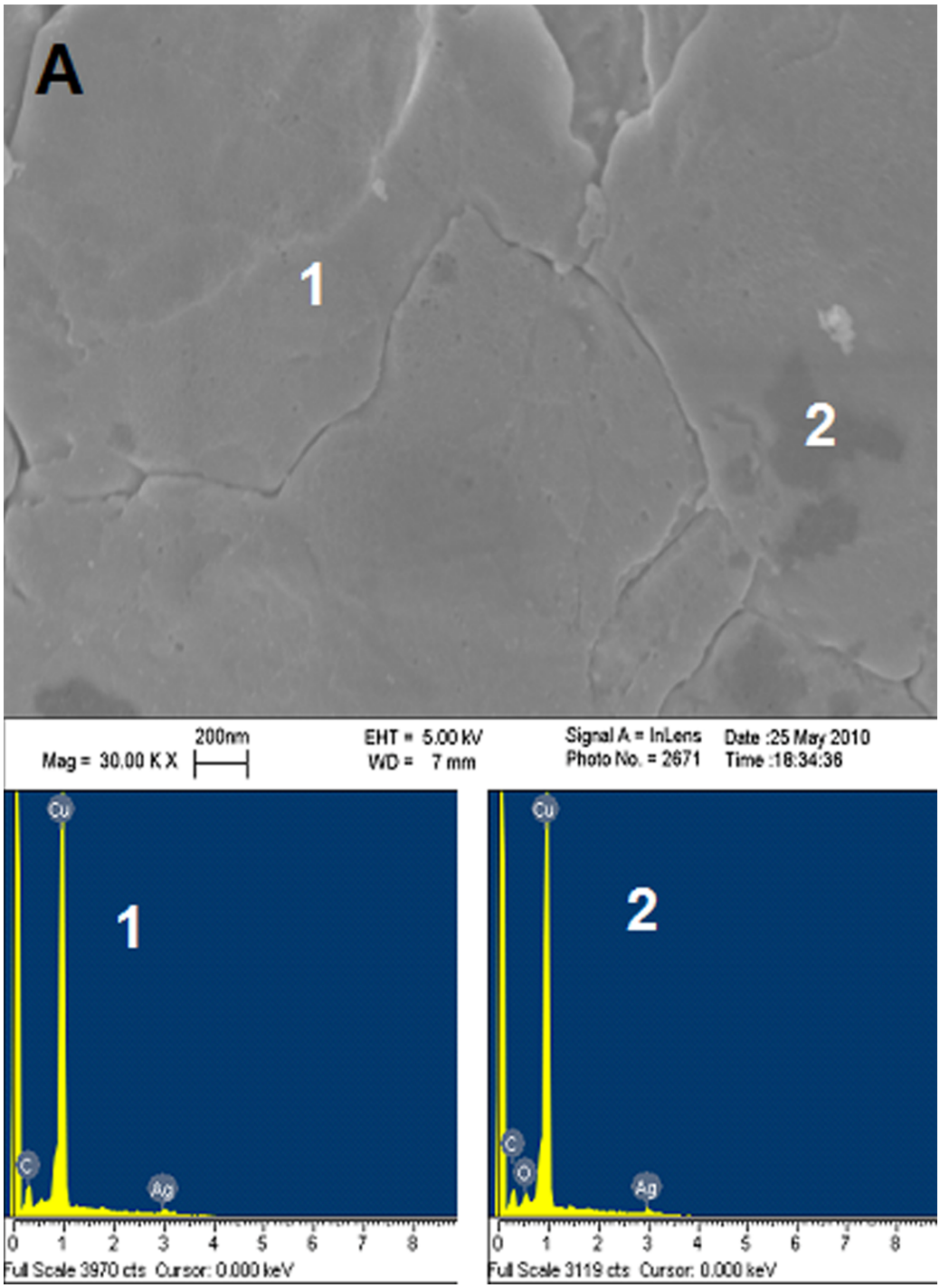

Figure 5.8 SEM-EDX of silver-coated copper flakes in the region A in Figure 5.7.

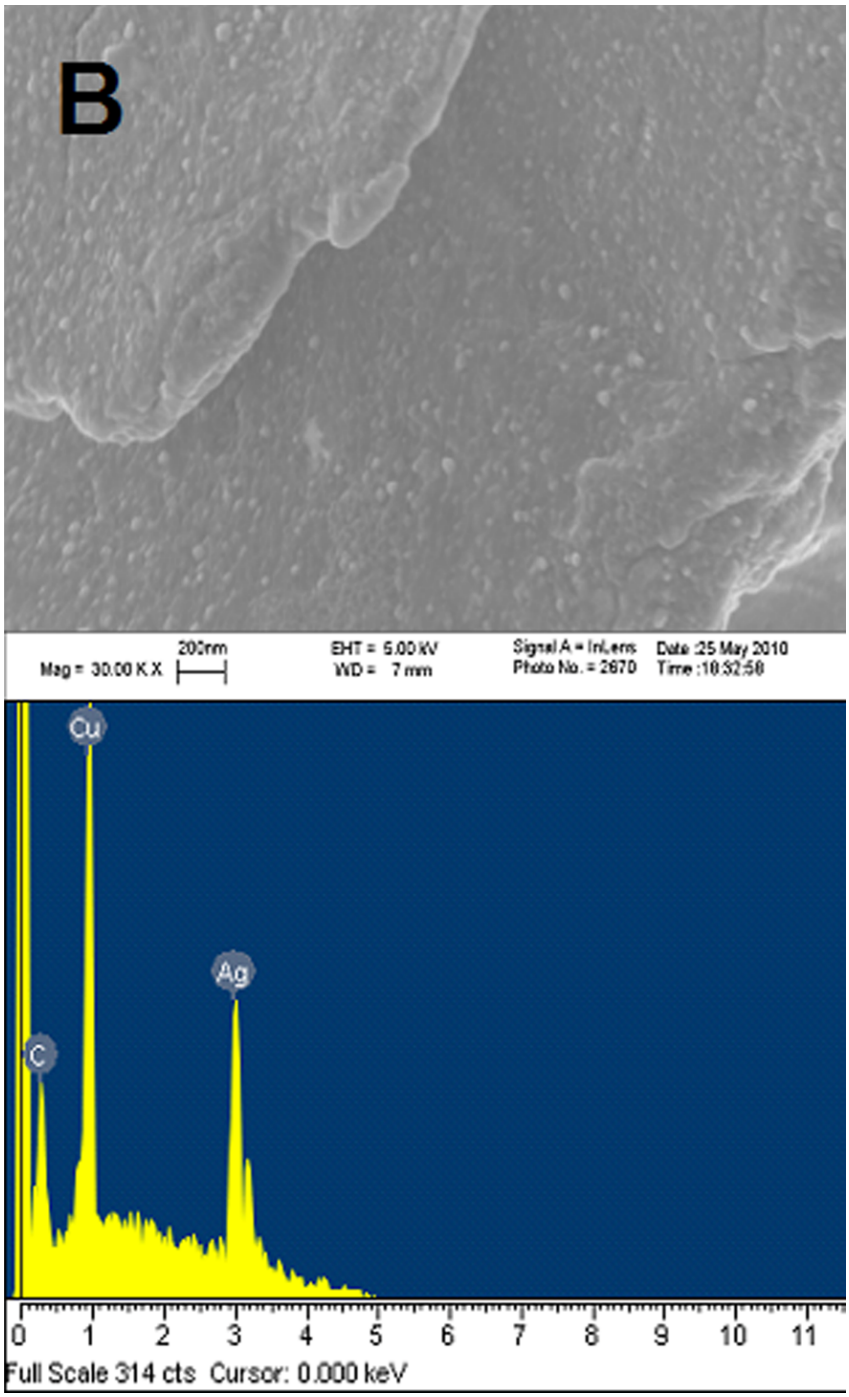

Figure 5.9 SEM-EDX of silver-coated copper flakes in the region B in Figure 5.7.

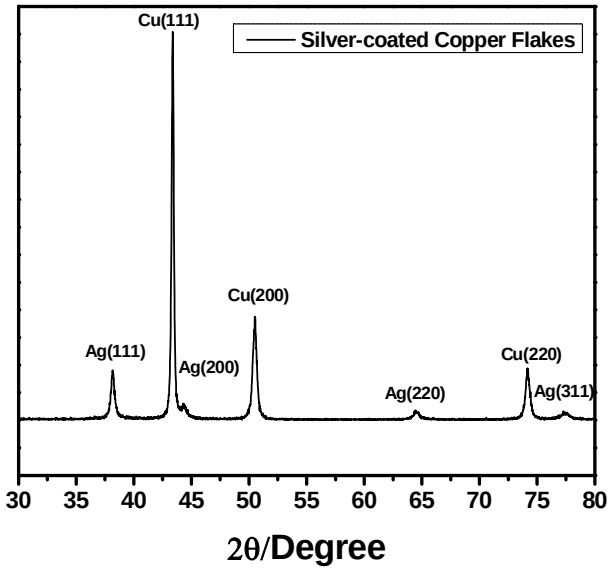

Figure 5.10 XRD of silver-coated copper flakes.

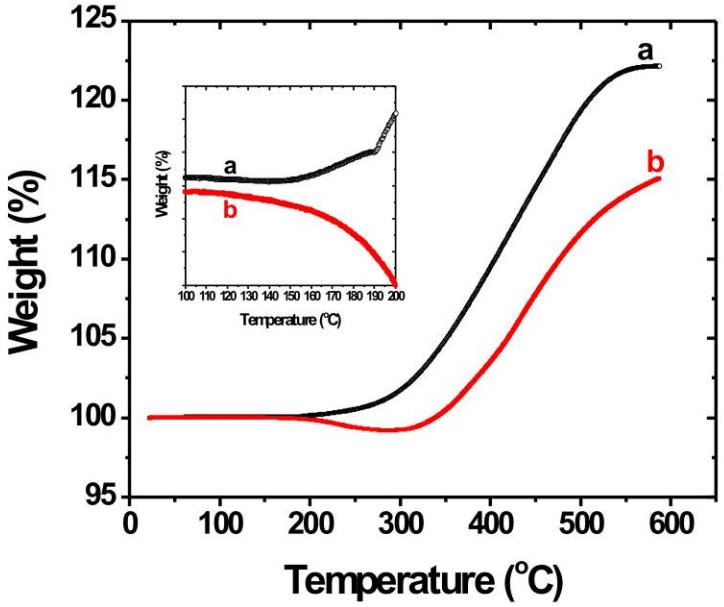

Figure 5.11 TGA of silver-coated copper flakes in air (a) untreated and (b) treated with NPAPTMS. Inset shows the temperature range from 100 to 200 ^{o}C.

5.3.2 Electrical Properties of ICAs Filled with Silver-coated Copper Flakes

Figure 5.12 shows the electrical resistivity of ICAs filled with silver-coated copper flakes with different processes. Bulk resistivity of ICAs filled with 80 wt% untreated silver-coated copper flakes is about 1.3×10^{-3} Ω cm, similar to the value of 1.6×10^{-3} Ω cm reported in the literature [24]. By *in situ* incorporation of NPAPTMS, bulk resistivity of ICAs filled with untreated silver-coated copper flakes was decreased to 7×10^{-4} Ω cm. The ICA filled with silver-coated copper flakes modified by NPAPTMS showed the lowest bulk resistivity of 2.4×10^{-4} Ω cm, similar to that of commercially available silver-filled ICAs (~10^{-4} Ω cm). Tan et al. reported that bulk resistivity of silver flake-filled ICAs was decreased from about 6.9×10^{-4} to about 5.5×10^{-4} Ω cm with addition of a silane coupling agent (KH-570 SCA) [209]. Improvement of electrical conductivity was also observed for composites filled with silver nanopartiles modified by 3-aminopropyl triethoxysilane, compared with the untreated one [210]. It is believed that the remarkable improvement in the dispersion of silver fillers in the polymer matrix and the enhanced adhesion between fillers and polymer matrix contributed to the improved electrical conductivity [209-210]. In the present study, the improved dispersion of silver-coated copper flakes modified by NPAPTMS in the polymer matrix could also contribute to the better electrical conductivity. However, the main reason could be the coordination of nitrogen on NPAPTMS to the exposed copper [211] of silver-coated copper flakes, thus protecting copper from oxidation during curing at 150 ^{o}C. This explanation is supported by the TGA result (Figure 5.11) indicating that silver-coated copper began oxidation at the curing temperature (150 ^{o}C) in the absence of oxidation prevention.

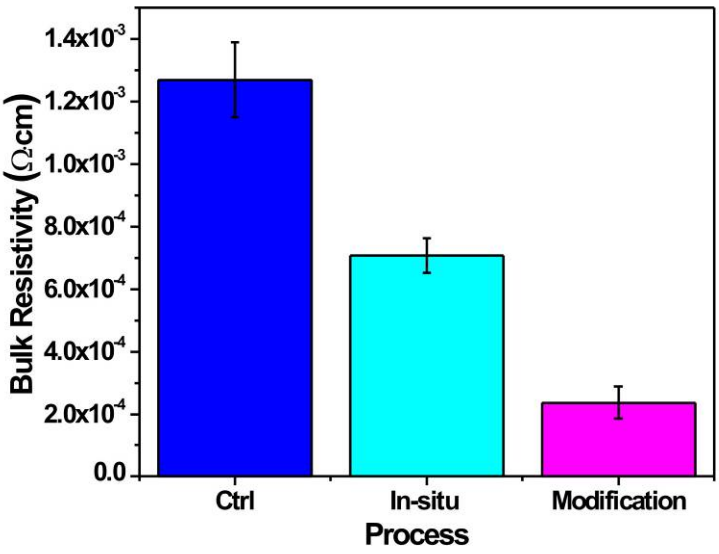

Figure 5.12 Electrical resistivity of ICAs filled with (a) untreated silver-coated copper flakes, (b) untreated silver-coated copper flakes with *in-situ* incorporation of NPAPTMS and (c) silver-coated copper flakes modified by NPAPTMS.

5.3.3 Reliability Tests of ICAs

The National Center for Manufacturing Sciences (NCMS) has set a standard for conductive adhesives intended to replace solder that if the shift in contact resistance is less than 20% after 500 hours of aging at 85 ^{o}C/85% RH, then contact resistance is defined as "stable" [212]. The contact resistance shifts of ICAs filled with untreated and treated silver-coated copper flakes aging at 85 ^{o}C/85% RH are compared and the results are shown in Figure 5.13. Obviously, the ICAs filled with silver-coated copper flakes that are modified by NPAPTMS showed much more stable contact resistance than the ICA containing the untreated silver-coated copper flakes. It was found that bulk resistivity of the ICA filled with untreated silver-coated copper flakes dramatically increased during aging. Therefore the contact resistance of ICAs filled with untreated silver-coated copper

flakes was not stable. However, the increase in contact resistance of the ICAs filled with silver-coated copper flakes modified by NPAPTMS on a Ni/Au surface was less than 10% during aging for more than 1000 hours. The effective stabilization of contact resistance resulted from the chemical coordination of NPAPTMS to the exposed copper of silver-coated copper flakes, and thus NPAPTMS acted as a protective layer, preventing the galvanic corrosion.

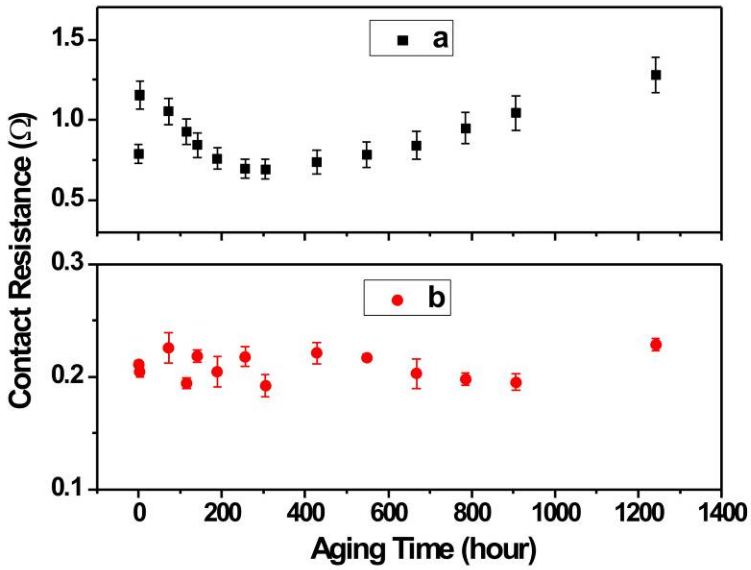

Figure 5.13 Contact resistance shifts of ICAs filled with (a) untreated silver-coated copper flakes and (b) silver-coated copper flakes modified by NPAPTMS aging at 85 ^{o}C/85% RH.

Figure 5.14 shows the contact resistance shifts of ICAs filled with untreated and treated silver-coated copper flakes on a Ni/Au surface after reflows. As silver-coated copper flakes started to be oxidized at 150 ^{o}C (Figure 5.11), the oxidation of exposed copper of silver-coated copper flakes led to the increase in contact resistance of ICAs

filled with untreated silver-coated copper flakes by more than 90% after 3 reflows. However, ICAs filled with silver-coated copper flakes modified by NPAPTMS showed decreased contact resistance. Although NPAPTMS started to detach from the surface of silver-coated copper flakes at 110 ^{o}C, the reaction of the SCA with the epoxy matrix during cross-linking will prevent oxidation of the exposed copper of silver-coated copper flakes during reflow process with a peak reflow temperature of 255 ^{o}C. The decreased contact resistance may result from the post curing effect of ICAs [65, 213].

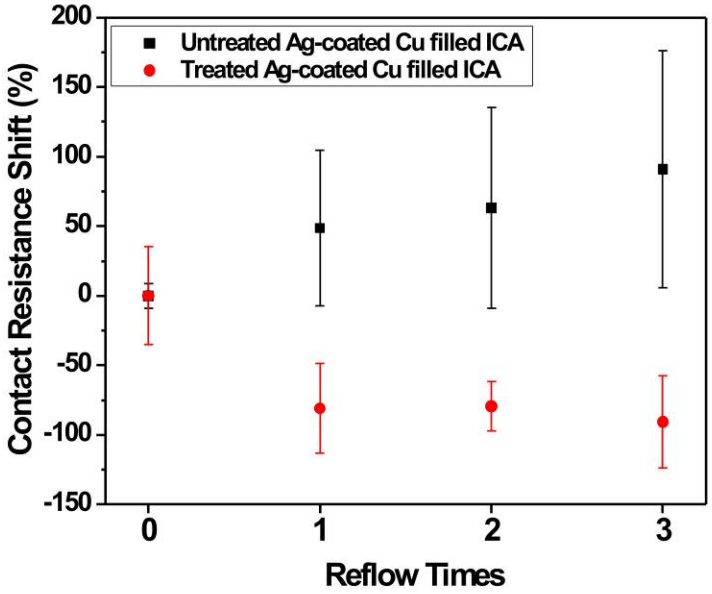

Figure 5.14 Contact resistance shifts of ICAs filled with (a) untreated silver-coated copper flakes and (b) silver-coated copper flakes modified by NPAPTMS during reflow processes.

5.4 Conclusions

In summary, by surface modification of silver-coated copper flakes with NPAPTMS, the ICAs with bulk resistivity as low as $2.4\times10^{-4}\,\Omega$ cm has been formulated.

The resistivity is comparable to that of commercially available silver-filled ICAs (~10^{-4} Ω cm). The reduced resistivity of the ICAs filled with the modified silver-coated copper flakes compared with the ICAs filled with untreated silver-coated copper flakes was attributed to the oxidation prevention of the silver-coated copper flakes by NPAPTMS during curing. More importantly, contact resistance of the ICAs filled with the modified silver-coated copper flakes on a Ni/Au surface was stabilized for more than 1000 hours of aging at 85 ^{o}C/85% RH and after three reflows with a peak reflow temperature of 255 ^{o}C. The development of highly reliable, highly conductive and low cost ICAs filled with silver-coated copper flakes will allow them to be widely used in electronic packaging.

CHAPTER 6

PREPARATION OF HIGHLY RELIABLE LOW COST ICAS USING AMINE CURING AGENT AS CORROSION INHIBITOR

This chapter investigates the development of highly conductive, highly reliable and low cost ICAs by the in situ protection of silver-coated copper flakes with an amine curing agent. First, the epoxy resin cured with an anhydride or amine curing agent is characterized by Fourier Transform Infrared Spectroscopy (FT-IR). This chapter compares the electrical resistivity of between ICAs cured with an anhydride and ICA cured with an amine and their resistivity stability during reliability tests. The reasons why ICAs cured with the amine have lower resistivity and better reliability than ICAs cured with the anhydride are discussed.

6.1 Introduction

In chapter 5, it has been found that copper surface modified with amine silane coupling agent (N-phenylaminopropyltrimethoxylsilane, NPAPTMS) can effectively prevent the oxidation of silver-coated copper flakes during curing at 150 ^{o}C and subsequent corrosion during 85 ^{o}C/85% RH aging and triple reflow test. It was also found that in situ incorporation of NPAPTMS into formulation is not as effective as surface modification of silver-coated copper flakes with NPAPTMS. In many industrial applications, it would be more desirable to formulate ICAs without a complicated process (such as surface modification).

In this chapter, an amine curing agent is selected for the preparation of highly reliable, highly conductive, and low-cost ICAs filled with silver-coated copper flakes. This is because amines have been reported as effective copper corrosion inhibitors, including primary, secondary and tertiary amines. The coordination of the amine curing agent to the exposed copper of silver-coated copper flakes prevents the oxidation of the exposed copper during the ICA curing at 150 ^{o}C. After curing, the formed ample secondary and tertiary amine groups could further protect the exposed copper surface from oxidation/corrosion effectively in harsh environments.

6.2 Experimental

6.2.1 Materials

Diglycidyl ether of bisphenol F (DGEBF) with an epoxide equivalent weight of 165-173 was supplied by Shell Chemical Company. Isophorone diamine (IPDA) was purchased from Sigma-Aldrich. Silver-coated copper flakes (RDAGCU) with an aspect ratio of 3 and silver thickness of about 150 nm were donated by Ferro Corp. The catalyst, 1-cyanoethyl-2-ethyl-4-methylimidazole (2E4MZCN), and methylhexahydrophthalic anhydride (MHHPA) were donated by Shikoku Chemicals Corp. (Japan) and Lindau Chemicals Corp., respectively.

6.2.2 Preparation of ICAs Filled with Silver-coated Copper Flakes

ICAs filled with silver-coated copper flakes were prepared by curing the mixture of DGEBF, the curing agent, the catalyst and 80 wt% silver-coated copper flakes at 150 ^{o}C for 1 hour. Two curing agents, MHHPA and IPDA were used.

6.2.3 Characterization

FT-IR spectra of anhydride- and amine-cured epoxies were recorded using Nicolet FT-IR spectrometer (Magna IR 560) at room temperature after curing. All the spectra were obtained in the spectral range of 400-4000 cm^{-1} at a resolution of 2 cm^{-1} and 256 repetitive scans were averaged per spectrum.

The specimens were exposed to 85 ^{o}C/85% RH in a temperature/humidity chamber (Lunaire Environmental, model CEO932W-4) and 85 ^{o}C/dry in a thermal oven. The resistance of each specimen was measured periodically for more than 1000 hours. Reflow tests were conducted in BTU oven (BTU International). The reflow oven has seven chambers and one cooling station. The temperatures for each chamber were set as 75, 110, 156, 198, 221, 255 and 175 ^{o}C, characteristic of a typical lead-free profile. After each reflow, resistance of the specimens was measured and resistivity was calculated accordingly.

6.3 Results and Discussion

6.3.1 Curing Mechanism and FT-IR Spectra of an Epoxy Cured with Anhydride or Amines

Figure 6.1 shows FT-IR spectra of MHHPA (Figure 6.1 (a)), DGEBF (Figure 6.1 (b)) and MHHPA-cured DGEBF (Figure 6.1 (c)). Peak assignments of the spectra are summarized in Table 6.1. The major differences in the spectrum before and after curing are as follows: (1) a broad feature of the stretching of –OH at 3527 cm^{-1} was observed after curing; (2) the disappearance of the bands at 1861 and 1784 cm^{-1} assigned to stretching of C=O and at 1219 cm^{-1} to the stretching of C-O indicated that the reaction of anhydride with DGEBF occurred; (3) the intensity at 915 cm^{-1} decreased, indicative of

the reduction in the amount of epoxide groups; (4) appearance of the peaks at 1737 and 1175 cm^{-1} due to the stretching of C=O and C-O verified the formation of ester linkages.

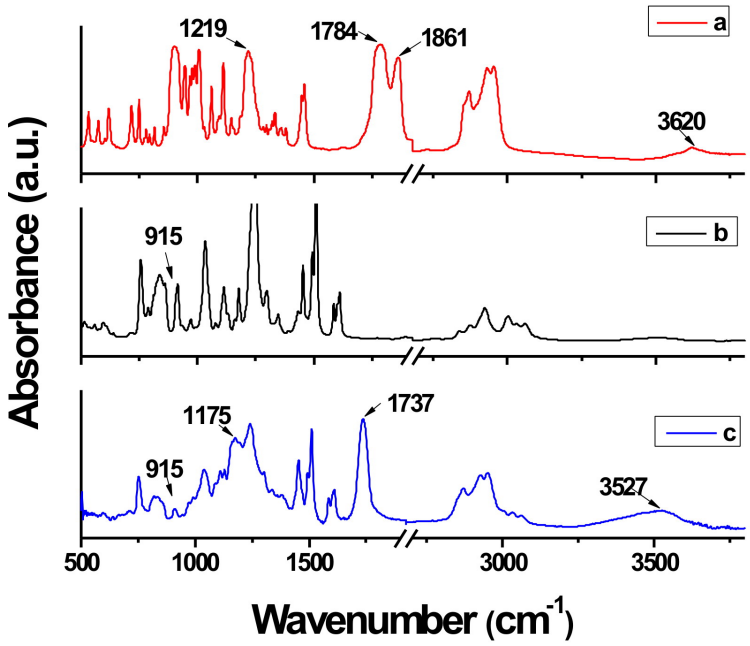

Figure 6.1 FT-IR Spectra of (a) MHHPA, (b) DGEBF and (c) MHHPA-cured DGEBF.

Table 6.1 Peak assignments in the FT-IR spectra of DGEBF, MHHPA, MHHPA- and IDPA- cured DGEBF [214-220].

DGEBF	MHHPA	MHHPA-cured DGEBF	IPDA	IPDA-cured DGEBF	Assignments
	3620				$\nu_{(O-H)}$, free
3503		3527		3550	$\nu_{(O-H)}$, hydrogen bonded
			3382 3351 3280 3184		$\nu_{(N-H)}$, primary amine

Table 6.1 continued

				3421	ν(N-H), secondary amine
3060		3061		3060	ν(φ-H)
3032		3032		3032	ν(φ-H)
2950	2954		2950		$\nu_{as}(CH_3)$
2924	2926		2903		$\nu_{as}(CH_2)$
	2871	2869			$\nu_s(CH_3)$
			2838		$\nu_s(CH_2)$
2836					$\nu_s(OCH_2)$
	1861				ν_s(C=O), anhydride
	1784				ν_{as}(C=O), anhydride
		1737			ν(C=O), ester
1611		1609		1609	ν(C=C)φ
			1604		δ(N-H), primary amine
1583		1586		1585	ν(C=C)φ
		1510			ν(C=C)φ
1452	1458			1452	$\delta_{(CH2)}$ scissors
1243		1242		1242	$\nu_{C(\varphi)\text{-}OC(alkyl)}$
		1175			$\nu_{(C\text{-}O)}$, ester
1108		1111		1113	$\nu_{(C\text{-}OH)}$, alcohol $\nu_{(C\text{-}O\text{-}C)}$, ether
1040		1040		1034	$\nu_{C(\varphi)O\text{-}C(alkyl)}$
	1219				$\nu_{(C\text{-}O)}$, anhydride
	947				anhydride ring
915		915		915	epoxide
	901				anhydride ring
838		836			$\delta_{(\varphi\text{-}H)}$ out of plane $\delta_{(C\text{-}O\text{-}C(\varphi))}$, ether

ν: stretching, ν_{as}: asymmetric stretching, ν_s: symmetric stretching, δ: deformation, φ: benzene ring.

The mechanism of addition of amines to an epoxy ring is complicated as inter- and intra-molecularly complexes may form in the starting substance [220]. Moreover, the

addition of hydroxyl group containing compounds (water/moisture, alcohols, phenols and acids) facilitates nucleophilic attack of amine to the carbon atoms of epoxy rings. The following equations (Figure 6.2) briefly describe the main reactions of an epoxy resin with the amine [215, 221-223]. The initial step involved the addition of active hydrogen to the epoxy group and formed a secondary amine. The secondary amine may further react with an epoxy resin to form a tertiary amine. In addition, the etherification of a hydroxyl group with epoxide groups may occur. As a result, a cross-linked polymer network is generated since both epoxy and amine are multifunctional. Amines are more reactive than anhydride and can react with epoxy resins at room temperature. It should be pointed out that the diffusivity of the reactive functional groups are seriously restricted as the reaction of amine with epoxy resins proceeds and the glass transition temperature of the mixture approaches the reaction temperature, although there is a significant amount of reactive functional groups available. Consequently, the available functional groups such as amino groups dramatically increase moisture absorption. Therefore, a high curing temperature (150 ^{o}C) is employed to achieve low moisture absorption of the resulting polymer. Figure 6.3 shows FT-IR spectra of DGEBF, IPDA and IPDA-cured DGEBF. The peak assignments are also generalized in Table 6.1. After curing, a very small band at 915 cm^{-1} indicated that epoxide groups were almost reacted. The peaks at 3382, 3351, 3280 and 3184 cm^{-1} due to the stretching of N-H were changed to the broad absorption at 3421 cm^{-1}, which was assigned to the stretching of secondary amine (N-H) [219]. Meanwhile, the band at 1604 cm^{-1} assigned to $–NH_2$ scissor disappeared indicating the reaction of the primary amine.

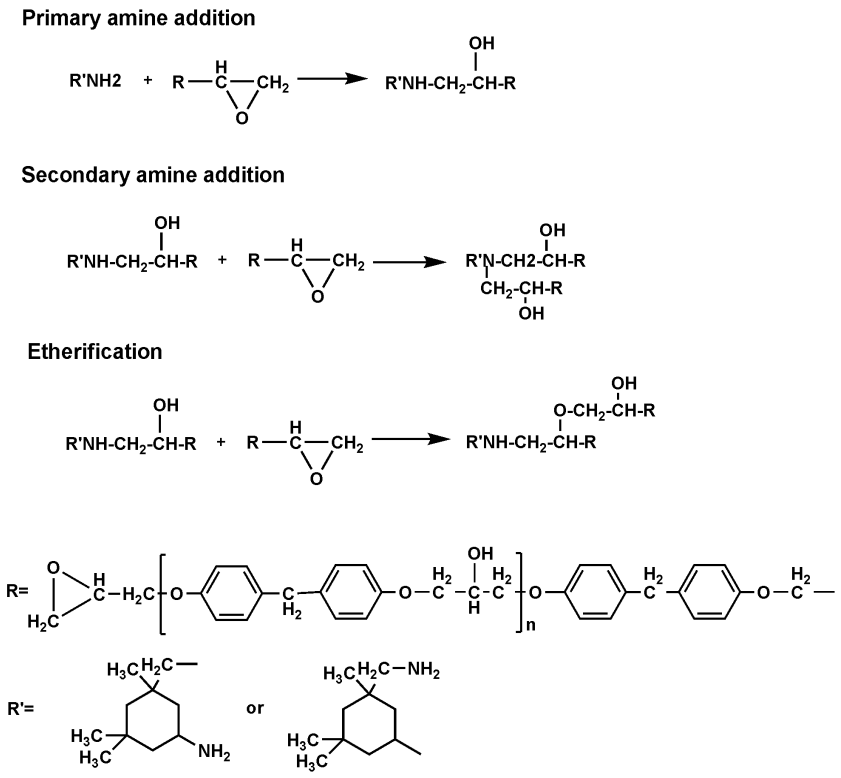

Figure 6.2 Curing mechanism of IPDA with DGEBF [215, 221-223].

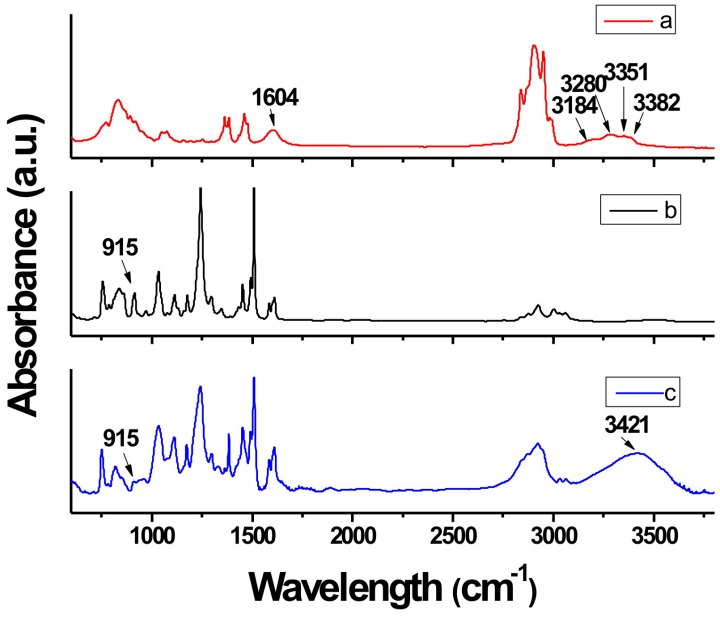

Figure 6.3 FT-IR spectra of (a) IPDA, (b) DGEBF and (c) IPDA-cured DGEBF.

6.3.2 Electrical Properties of ICAs Filled with Silver-coated Copper Flakes

During curing of ICAs, the polymer matrix shrinks due to the conversion of non-covalent interactions (such as van der Waals force) to covalent bonds between an epoxy resin and a curing agent. Shrinkage of the polymer matrix causes more intimate contacts among the fillers in the composite and thus conductive networks are established within the polymer matrix after curing [64]. Bulk resistivity of anhydride-cured ICAs filled with 80 wt% silver-coated copper was about 1.3×10^{-3} Ω cm, similar to the reported value of 1.6×10^{-3} Ω cm [24]. Compared with anhydride-cured ICAs, amine-cured ICAs show a much lower bulk resistivity (2×10^{-4} Ω cm). This resistivity is comparable to that of commercially available silver-filled ICAs (~10^{-4} Ω cm). In last chapter, that bulk resistivity of ICAs filled with the same silver-coated copper flakes modified by NPAPTMS (2.4×10^{-4} Ω cm) was much lower than that of ICAs filled with untreated silver-coated copper flakes (1.3×10^{-3} Ω cm). The reduced resistivity was attributed to the oxidation prevention of the silver-coated copper flakes by NPAPTMS during curing at 150 ^{o}C. Yim et al. reported that the oxidation of copper flakes occurred during the curing of copper-filled ICAs. With the incorporation of a corrosion inhibitor, the contact resistance of copper-filled ICAs dramatically reduced (about 0.3 Ω), compared with copper-filled ICAs without a corrosion inhibitor (about 100 MΩ) [23]. In the present study, the main reason that amine-cured ICAs have a much lower resistivity could be due to the coordination of nitrogen on the curing agent to the exposed copper of silver-coated copper flakes, protecting the exposed copper from oxidation during curing at 150 ^{o}C. This explanation is supported by the TGA result (Figure 5.11), which indicates that silver-coated copper flakes begin oxidation at the curing temperature if there is no

protection. Wokaun et al. investigated the coordination of m-toluidine to a copper surface concluded that the primary amine bound to a copper surface via the nitrogen lone pair, i.e. the amine donated electron density to metal, as verified by surface enhanced Raman scattering studies [211]. Therefore, the coordination of amines to the exposed copper surface of silver-coated copper flakes could protect the exposed copper of silver-coated copper flakes from oxidation during curing.

6.3.3 Reliability Tests of ICAs Filled With Silver-coated Copper Flakes

Bulk resistivity changes of the samples during 85 ^{o}C/dry and 85 ^{o}C/85% RH aging are shown in Figures 6.4 and 6.5, respectively. As can be seen from Figure 6.4, anhydride-cured ICAs showed a small increase in bulk resistivity while bulk resistivity of amine-cured ICAs decreased at first and then was stable. The decrease in bulk resistivity of amine-cured ICAs may result from post-annealing effect [213, 224]. However, during 85 ^{o}C/85% RH aging, bulk resistivity of anhydride-cured ICAs increased dramatically with time while that of amine-cured ICAs was stable for more than 1000 hours (Figure 6.5). One of the critical requirements for galvanic corrosion to occur is water and therefore, galvanic corrosion can be neglected and only simple oxidation occurred during 85 ^{o}C/dry aging. The stable bulk resistivity of both anhydride- and amine-cured ICAs indicated that the oxidation of silver-coated copper flakes was not significant at 85 ^{o}C. However, the dramatic increase in bulk resistivity of the anhydride-cured ICAs indicated that galvanic corrosion came to play and was dominant during 85 ^{o}C/85% RH since ester groups formed during the curing of anhydride with epoxy could not protect the exposed copper of silver-coated copper flakes. Unlike anhydrides, amines which can chemically adsorbe and coordinate to copper [28, 52] have been widely reported as copper corrosion

inhibitors in diluted HCl, H_2SO_4 and HNO_3 solutions. The amines include primary amine [189-192], secondary amine [188] and tertiary amine [225]. Therefore, considerable amounts of secondary and tertiary amines in the polymer network, as verified from FT-IR (Figures 6.3), can co-ordinatively bind to the exposed copper surface and prevent the galvanic corrosion of silver-coated copper flakes within the amine-cured ICAs effectively. The corrosion prevention maintained the stable bulk resistivity of amine-cured ICAs during the reliability test.

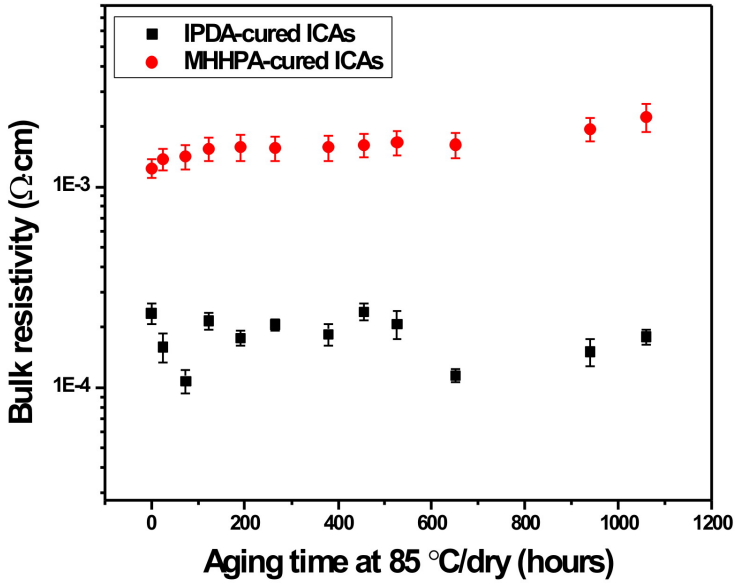

Figure 6.4 Bulk resistivity shifts of anhydride-cured ICAs and amine-cured ICAs during 85 ^{o}C/dry aging.

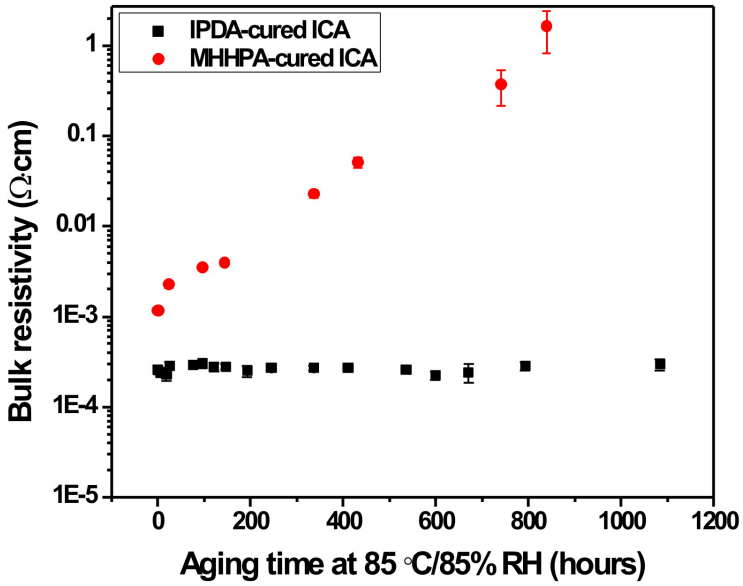

Figure 6.5 Bulk resistivity shifts of anhydride-cured ICAs and amine-cured ICAs during 85 ^{o}C/85% RH aging.

Most organic corrosion inhibitors may detach or decompose from the metal surfaces at elevated temperatures. Significant advantages of the novel approach in the present study for copper oxidation/corrosion prevention are the ample secondary and tertiary amines in amine-cured epoxy polymer networks available for multi-binding to copper surface and high decomposition temperatures of cross-linked polymers, enabling the effective protection of copper at high temperatures. Figure 6.6 shows bulk resistivity shifts of anhydride-cured and amine-cured ICAs during the triple reflow processes in air. After triple reflows, bulk resistivity of anhydride-cured ICAs increased by more than 90%. This increase was the result of oxidation of silver-coated copper flakes in anhydride-cured ICAs at temperatures higher than 150 ^{o}C in air (Figure 5.11). On the

contrary, the amine-cured ICAs filled with the silver-coated copper flakes showed even decreased bulk resistivities at a maximum reflow temperature of 255 ^{o}C in air during the reflow processes. The decreased bulk resistivity was due to the post-annealing effect [213, 224]. The results demonstrated the excellent protection of copper from oxidation with amine-cured epoxy at high temperatures.

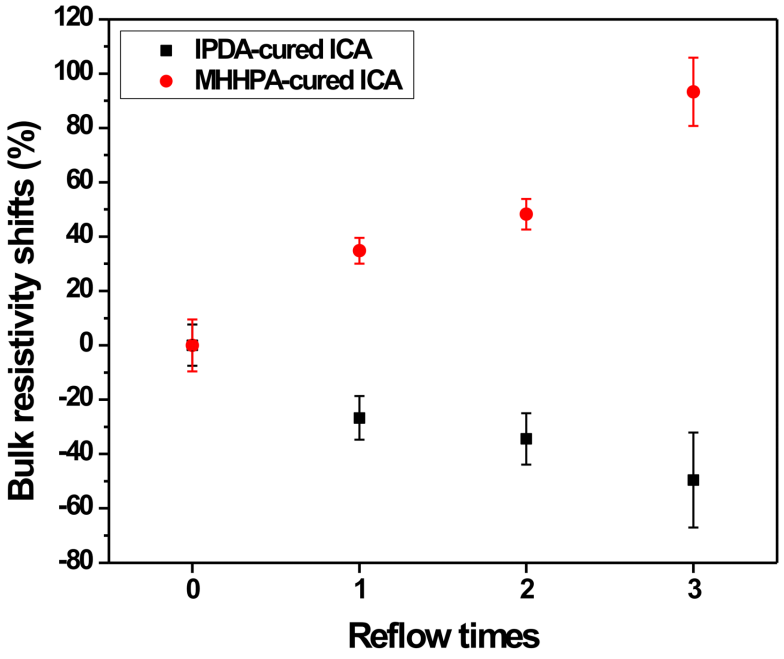

Figure 6.6 Bulk resistivity shifts of anhydride-cured and amine-cured ICAs during reflow processes.

6.4 Conclusions

In summary, by selecting the amine as a curing agent, silver-coated copper flake filled ICAs with bulk resistivity as low as commercially available silver-filled ICAs have been prepared. More importantly, the amine-cured ICAs showed stable bulk resistivity during 85 ^{o}C/85% RH aging for more than 1000 hours, and triple reflow tests indicated that the resistivity of the ICAs was stable at high temperatures (peak temperature: 255

^{o}C). Galvanic corrosion was identified as the dominant mechanism underlying unstable resistivity of silver-coated copper filled ICAs during 85 ^{o}C/85% RH aging. The key points for the design of amine-cured ICAs include (1) the effective protection of the exposed copper surface of silver-coated copper flakes from oxidation and corrosion by ample amines during curing and reliability tests; (2) high decomposition temperatures of cross-linked polymers containing amine groups enabling the excellent protection of the exposed copper surface at high temperatures. The novel approach will enable the lower cost ICAs to be widely used in electronic packaging.

CHAPTER 7

SUMMARY, CONCLUSIONS AND FUTURE WORK

7.1 Summary and Conclusions

Isotropically conductive adhesives (ICAs) have drawn much attention as an environmentally friendly solution for lead-free interconnects as they offer many advantages over traditional solder technology. These advantages include (1) environmental friendliness; (2) lower processing temperature (typically 150 ^{o}C or below) enabling the wide use of temperature-sensitive and low-cost components and substrates; (3) fewer processing steps reducing the processing cost; (4) low stress on a substrate; and (5) flexibility and stretchability enabling a more compliant interconnect; and (6) reduced cost. As the electronics follows the trend of higher performance at lower cost in a smaller size, two key features of ICAs, low temperature processing and ability to form flexibile (or stretchable) interconnects, have become increasingly important for emerging applications. However, compared with tin/lead solder (1.5-3$\times10^{-5}$ Ω cm), ICAs have lower conductivity (>1$\times10^{-4}$ Ω cm at 80 wt% loading of silver flakes). The low electrical conductivity limits the performance of device interconnected with ICAs. To improve the conductivity of ICAs, it is important to understand the electrical conduction in ICAs and develop higher performance ICAs to meet the requirements of emerging applications at a lower cost.

In this dissertation, an in-depth study of the interface between conductive fillers and electrical properties of ICAs has been carried out. This dissertation aims at gaining an insight into the interface between conductive fillers within a polymer matrix to

develop economical, highly conductive, reliable ICAs processable at low temperatures for electronic packaging applications. The research findings are summarized in the following paragraphs.

From the literature review in Chapter 1, it is evident that the interface between conductive fillers plays a key role in the electrical conductivity of ICAs. The high contact resistance existing between conductive fillers in ICAs causes ICAs to have high electrical resistivity. However, engineering the interface to obtain a low electrical resistivity ($<1\times10^{-4}$ Ω cm) remains a challenge. Chapter 2 introduces sintering technology to reduce the contact resistance between conductive fillers. It is found that the decomposition of the surface residues on silver nanoparticle plays a key role in the thermal sintering of silver nanoparticles. Silver nanoparticles synthesized by widely used wet-chemical methods may not be suitable for the preparation of highly conductive ICAs since stabilizers on the surface of silver nanoparticles are difficult to remove at a low temperature (<200 ^{o}C). Instead, silver nanoparticles in this study were synthesized by the combustion chemical vapor condensation (CCVC) method. CCVC offers many significant advantages over the most widely used wet-chemical methods to synthesize silver nanoparticles for highly conductive ICAs, including low decomposition temperatures of surface residues, low content of surface residues and increased production rates (up to 0.1-1 kg/h) [124]. The effects of the surface chemistry and the thermal behavior of silver nanoparticles were studied, which was correlated with the electrical properties of the resulting ICAs. It is found that silver nanoparticles with lower decomposition temperatures and lower content of surface residues are promising for the development of highly conductive ICAs. The formation of the metallurgical joints between the conductive fillers as a result of sintering

reduces the contact resistance effectively. This results in an ICA with electrical resistivity of 4.8×10^{-5} Ω cm when the ICA was cured at 180 ^{o}C.

Based on the experimental results and the understanding obtained in chapter 2, Chapter 3 further optimizes silver nanoparticles for the fast preparation of printable highly conductive ICAs. This fast preparation is important for industrial applications as the trend towards mixed assembly technologies, having components attached with both solders and ICAs on the same board requires uniformity of the curing profile/solder reflow processes. In this chapter, thermal behavior of silver flakes and silver nanoparticles are first investigated to provide a guideline for the processing temperature leading to highly conductive ICAs. It is found the fast sintering is attributed to: (1) the thermal decomposition of silver carboxylate-which is present on the surface of the incorporated silver flakes—to form in situ highly reactive silver nanoparticles; (2) the surface activation of the incorporated silver nanoparticles by the removal of surface residues. As a result, ICAs prepared at 230 ^{o}C for 5 minutes, at 260 ^{o}C for 10 minutes and using a typical lead-free solder reflow process show electrical resistivities of 8.1×10^{-5}, 6.0×10^{-6} and 6.3×10^{-5} Ω cm, respectively. The correlation between the rheological properties of the adhesive paste and the non-contact printing process has been discussed. With the optimal rheological properties, the formulated highly viscous pastes (221 mPa s at 2500 s^{-1}) can be non-contact printed into dot arrays with a radius of 130 μm. The non-contact printable ICA paste with superior electrical conductivity and fast processing are promising for the future of printed electronics.

Although ICAs with very low resistivities have been achieved, there are many problems associated with the incorporation of a large amount of silver nanoparticles.

These problems include (1) low dispersion efficiency of untreated nanoparticles in the epoxy matrix; (2) the relatively high cost of silver nanoparticles; (3) the complicated and expensive processes such as surface functionalization limiting their industrial applications; and (4) difficulties in printing pastes filled with nanomaterials. Chapter 4 describes a novel method to solve these problems and develops flexible highly conductive ICAs at a low temperature (150 ^{o}C) by in situ reduction of silver carboxylates on the surface of silver flakes into highly surface reactive silver nanoparticles. The formation of highly surface reactive nanoparticles leads to the sintering between silver flakes. In this chapter, silver flakes are treated with epoxy resins and their surface morphologies and properties change induced by the treatment are characterized to explain the conductivity enhanced mechanism. It is found that the reduction of silver flakes by diglycidyl ether of polypropylene glycol (DGEPG) occurs and removes the surface lubricant, which allows the metallurgical joints and direct metal-metal contacts between the conductive fillers. The formation of the metallurgical joints and direct metal-metal contacts reduce and even eliminate the contact resistance effectively, enabling the preparation of flexible highly conductive ICAs at a low temperature. The approach developed offers many significant advantages such as (1) reduced materials cost; (2) low processing temperature compatible with low cost, flexible substrates such as paper and PET; (3) simple processing; (4) low viscosity of the formulated pastes with DGEPG, allowing the pastes to be used for low cost jet-dispensing technologies; (5) tunable mechanical properties; and (6) both flexibility and high electrical conductivity.

Chapters 5 and 6 describe the replacement of expensive silver flakes with low cost silver-coated copper flakes and develop highly reliable, highly conductive, and low

cost ICAs. Chapter 5 characterizes silver-coated copper flakes by SEM-EDX. It is found that the plating of silver on copper is not complete, which leads to the oxidation of silver-coated copper flakes at high temperatures (>150 ^{o}C) and corrosion of silver-coated coppers during the reliability tests. As a result, the degradation of electrical properties of ICAs occurs if there is no protection for silver-coated copper flakes. By surface modification of silver-coated copper flakes with N-phenylaminopropyltrimethoxylsilane, ICAs with bulk resistivity as low as 2.4×10^{-4} Ω cm has been formulated. The resistivity is comparable to that of commercially available silver-filled ICAs (~10^{-4} Ω cm). The reduced resistivity of the ICAs filled with the modified silver-coated copper flakes compared with the ICAs filled with untreated silver-coated copper flakes was attributed to oxidation prevention of the silver-coated copper flakes by N-phenylaminopropyltrimethoxylsilane during curing. More importantly, the contact resistance of the ICAs filled with the modified silver-coated copper flakes on a Ni/Au surface has been stabilized for more than 1000 hours during 85 ^{o}C/85%RH aging and after three reflows with a peak reflow temperature of 255 ^{o}C.

Chapter 6 introduces a novel approach for the development of highly conductive, highly reliable and low cost ICAs by in situ protection of silver-coated copper flakes with an amine curing agent. The coordination of the amine curing agent to the exposed copper of silver-coated copper flakes prevents the oxidation of the exposed copper during the ICA curing at 150 ^{o}C. After curing, the formed ample secondary and tertiary amine groups could further protect the exposed copper surface from oxidation/corrosion effectively in harsh environments. In comparison with an anhydride-cured ICA (resistivity: ~1.3×10^{-3} Ω cm), an amine-cured ICA exhibits a much lower bulk resistivity

(~2×10^{-4} Ω cm). This resistivity is comparable to that of commercially available silver-filled ICAs. Galvanic corrosion was identified as the dominant mechanism underlying unstable resistivity of silver-coated copper filled ICAs during 85 ^{o}C/85% RH aging. Moreover, amine-cured ICA shows very stable bulk resistivity during 85 ^{o}C/85% RH aging for more than 1000 hours and triple reflow tests with a peak reflow temperature at 255 ^{o}C. The key points for the design of amine-cured ICAs involve (1) the effective protection of the exposed copper surface of silver-coated copper flakes from oxidation and corrosion by ample amines during curing and reliability tests; (2) high decomposition temperatures of cross-linked polymers containing amine groups enabling the excellent protection of the exposed copper surface at high temperatures.

It is concluded that:

(1) engineering the interface between conductive fillers within the polymer matrix, that is, enabling the sintering between conductive fillers at a low temprerature, is the key to the development of highly conductive ICAs at a low temperature;

(2) Oxidation prevention of low cost conductive fillers during curing and the corrosion prevention of the conductive fillers in the reliability tests are crucial to achieve highly reliable, highly conductive, and low cost ICAs.

7.2 Future Work

7.2.1 Insights into ICAs with the Flexible Epoxy or Other Additives

In this dissertation, ICAs with the electrical resistivity of on the order of 10^{-5} Ω cm have been developed at 150 ^{o}C. It is very clear that the sintering of silver flakes leads to the significant decrease in the electrical resistivity. However, further research need to

be conducted. (1) The oxidation product of primary –OH should be verified. Instead of using commercial products like a mixture of compounds with different molecular weights, it is suggested to use pure compounds; Moreover, a systematic study of a series of molecules with different amount of –OH groups per mole of molecules, i.e. additives with –OH groups, can be further performed. (2) Study the effect of the additives on the curing of epoxy resins. It is important to know the gel point of the formulation with the novel additives and correlated the gel point with the electrical properties of the resulting ICAs. Since the curing brings silver flakes into intimate contacts because of cure shrinkage, it seems it is more desired to bring silver flakes into contact and subsequent sintering results in better necking between silver flakes. However, the problem is that the diffusion of –OH group to react with silver salts on the surface of silver flakes is significantly limited. On the contrary, if the reduction occurs while silver flakes are not in close contact, the reduction may not significantly contribute to the necking between silver flakes. Further studies need to be carried out to optimize the time to cure and to sinter. (3) The gel point can be controlled by using catalysts with different reactivities.

7.2.2 Preparation of Highly Conductive ICAs at Temperatures Below 150 ^{o}C

Printed electronics is an emerging field with a huge potential market approaching 10 billion US dollars in 2011, over 30 billion US dollars in 2015 and 96 billion US dollars in 2020, as forecasted [226]. The main requirements of this applications when applied to flexible substrates are: (1) low processing temperatures (<150 ^{o}C), to be compatible with organic substrates such as polyethylene terephthalate (PET, upper working temperature: 115-170 ^{o}C), polycarbonate (PC, working temperature: -40-130 ^{o}C) and paper (working temperature: <150 ^{o}C); (2) flexible (or stretchable) interconnects, to

allow for highly integrated systems to be light-weight, thin, bendable and potentially stretchable; (3) low viscosity and proper surface tension, allowing the solution to be properly jetted by a printer; (4) low cost, to allow the applicability to the organic disposable, recyclable electronics of the future. In this dissertation, the lowest temperature to achieve high conductivity is 150 ^{o}C, the upper limit temperatures for low cost substrates such as paper. The ICAs developed in this study meet most of the main requirements, thus very promising for emerging applications. Further works can be conducted to facilitate ICA applications in printed electronics. (1) It is more desirable to develop highly conductive ICAs at a temperature below 150 ^{o}C. If the current catalyst is replaced with a more reactive one, could it be possible to use the same formulation in this dissertation to develop highly conductive ICAs at temperatures lower than 150 ^{o}C? If not, it is important to figure out the reasons and to develop highly conductive ICAs at a lower temperature for printed electronics; (2) Further optimization and evaluation of flexibility on a device level or development of stretchable ICAs for stretchable interconnects is also suggested. Future electronic devices will require ICAs to be mechanically compliant. Traditionally, rigid epoxy resins (over 3 GPa in Young's modulus of the polymer matrix) are used as polymer matrices for ICAs to provide chemical bonding and excellent mechanical and adhesion strengths. However, with the popularity of flex circuits and flexible substrates, in particular for flexible printed electronics, there are some limitations when attaching the conventional rigid ICAs to the substrate due to the poor flexibility of the ICA joints. Another limitation is that the interconnection based on rigid ICAs tends to fracture under thermal cycling.

7.2.3 Preparation of Low Cost ICAs Filled With Copper Particles

Silver is expensive and will become more expensive in the future. Undoubtedly, replacement of silver with copper or other lower cost conductive fillers is a new trend. Although many efforts have been devoted to developing copper-filled ICAs, very limited progress has been made after several decades. There is an increasing interest in silver-coated copper particles (including spherical particles, flakes and other forms) for a variety of applications including silver-coated copper inks and adhesives. In this dissertation, highly conductive, highly reliable ICAs filled with low cost silver-coated copper flakes have been developed. The ICAs filled with low cost silver-coated copper flakes developed in this dissertation are comparable to commercial ICAs filled with silver flakes in regards of electrical conductivity and reliability. In particular, it is found that bare copper flakes exist in the low cost ICAs developed in this dissertation. This is a very promising result for future development of ICAs filled with copper particles. Further studies on ICAs filled with copper particles along with the methodology described in this dissertation can open tremendous opportunities.

APPENDIX A

AUTHOR'S PUBLICATIONS

A.1 Book Chapters

1. **R. W. Zhang**, Josh C. Agar, C. P. Wong, "Conductive polymer composites", *Encyclopedia of Polymer Science & Technology*, **invited**, 2011, 1-43.

A.2 Journal Publications

2. **R. W. Zhang**, K. S. Moon, W. Lin, C. P. Wong, "Preparation of highly conductive polymer nanocomposites by low temperature sintering of silver nanoparticles", *Journal of Materials Chemistry*, 2010, 20(10), 2018-2023.

3. **R. W. Zhang**, W. Lin, K. S. Moon, C. P. Wong, "Fast preparation of printable highly conductive polymer nanocomposites by thermal decomposition of silver carboxylate and low-temperature sintering of silver nanoparticles", *ACS Applied Materials & Interfaces*, 2010, 2(9), 2637-2645.

4. **R. W. Zhang,** K. S. Moon, W. Lin, J. C. Agar, C. P. Wong, "A simple and effective way to prepare highly conductive polymer composites by in situ reduction of silver carboxylate", *Composites Science and Technology*, 2011, 71(4), 528-534.

5. **R. W. Zhang**, W. Lin, K. Lawrence, C. P. Wong, "Highly reliable, low cost, isotropically conductive adhesives filled with Ag-coated Cu flakes for electronic packaging applications", *International Journal of Adhesion and Adhesives*, 2010, 30, 403-407.

6. **R. W. Zhang**, K. S. Moon, W. Lin, Y. Q. Duan, S. M. Lotz, C. P. Wong, "Interfacial design and understanding for enhancement of electrical conduction through ACA Joints", *IEEE Transactions on Advanced Packaging*, 2010, 33, 892-898.

7. **R. W. Zhang**, Y. Li, M. J. Yim, K. S. Moon, D. D. Lu, C. P. Wong, "Enhanced electrical properties of anisotropic conductive adhesive with π-conjugated self-assembled molecular wire junctions", *IEEE Transactions on Components and Packaging Technologies*, 2009, 32(3), 677-683.

8. **R. W. Zhang**, W. Lin, K. S. Moon, Q. Z. Liang, C. P. Wong, "Highly reliable, conductive silver-coated copper epoxy composites using amine curing agent for in situ corrosion protection", *IEEE Transactions on Advanced Packaging*, In press.

9. W. Lin, **R. W. Zhang**, S.-S. Jang, C. P. Wong, J. I. Hong, "Organic Aqua Regia"—Powerful Liquids for Dissolving Noble Metals", *Angewandte Chemie International Edition*, 2010, 49, 7929-7932. **Selected in *Nature Research Highlights* (*Nature* 467, 503 (2010)) and *Science Research Highlights* (*Science* 330, 153 (2010)). Reported by *Science Daily*, *Chemistry World*, etc.**

10. L. Yang, **R. W. Zhang**, D. Staiculescu, C. P. Wong, M. M. Tentzeris, "A novel conformal RFID-enabled module utilizing inkjet-printed antennas and carbon nanotubes for gas-detection applications", *IEEE, Antennas and Wireless Propagation Letters*, 2009, 8, 653-656.

11. W. Lin, **R. W. Zhang**, K. S. Moon, C. P. Wong, "Molecular phonon couplers at carbon nanotube/substrate interface to enhance interfacial thermal transport", *Carbon*, 2010, 48(1), 107-113.

12. C. P. Wong, W. Lin, L. Zhu, H. Jiang, **R. W. Zhang**, Y. Li, K. Moon, "Nano materials for microelectronic and photonic packaging", Frontiers of Optoelectronics in China, 2010, 3(2), 139-142.

13. W. Lin, **R. W. Zhang**, K. S. Moon, C. P. Wong, "Synthesis of vertically aligned carbon nanotubes on bulk copper substrates for thermal management: an insight into the significance of a conformal support layer by atomic layer deposition", *IEEE Transactions on Advanced Packaging*, 2010, 33(2), 370-376.

14. W. Lin, **R. W. Zhang**, C. P. Wong, "Modeling of thermal conductivity of graphite nanosheet composites", *Journal of Electronic Materials*, 2010, 39(3), 268-272.

15. W. Lin, Y. Xiu, H. Jiang, **R. W. Zhang**, O. Hildreth, K. Moon, C. P. Wong, "Self-assembled monolayer-assisted chemical transfer of in situ functionalized carbon nanotubes", *Journal of the American Chemical Society*, 2008, 130(30), 9636-9637.

16. M. X. Chen, W. Lin, **R. W. Zhang**, C. P. Wong, S. Liu, "Study on thermal contact resistance of highly conductive adhesives using orthogonal experiments", *IEEE Transactions on Component and Packaging Technology*, Submitted.

A.3 Conferences/Presentations

17. **R. W. Zhang**, Josh C. Agar, C. P. Wong, "Recent advances on electrically conductive adhesives", Proceedings of the IEEE 12th Electronic Packaging Technology Conference, Singapore, p. 696-704 (2010).

18. **R. W. Zhang**, C. P. Wong, "Low cost copper-based electrically conductive adhesives", Proceedings of the IEEE 12th Electronic Packaging Technology Conference, Singapore, p. 715-720 (2010).

19. **R. W. Zhang**, C. P. Wong, "Development of advanced interconnect materials for ink-jet printing by low temperature sintering", 59th Electronic Components and Technology Conference, California, SD, 151-154 (2009).

20. **R. W. Zhang**, Y. Q. Duan, W. Lin, K. S. Moon, C. P. Wong, "New electrically conductive adhesives (ECAs) for flexible interconnect applications", 59th Electronic Components and Technology Conference, California, SD, 1356-1360 (2009).

21. **R. W. Zhang**, K. S. Moon, W. Lin, C. P. Wong, "Electrical properties of ACA joints assisted by conjugated molecular wires", 59th Electronic Components and Technology Conference, California, SD, 2034-2038 (2009).

22. **R. W. Zhang**, K. S. Moon, W. Lin, H. J. Jiang, C. P. Wong, "Incorporation of self-assembly molecular wires into anisotropic conductive adhesive for high performance interconnection applications", 10th Electronic Packaging Technology Conference, 24-28 (2008).

23. **R. W. Zhang**, Y. Li, M. J. Yim, K. S. Moon, D. D. Lu, C. P. Wong, "Electrically conductive adhesive with π-conjugated self-assembled molecular wire junctions for enhanced electrical and thermal properties", IEEE Proceedings of 58th Electronic Components and Technology Conference, Orlando, FL, 1913-1918 (2008).

24. **R. W. Zhang**, Wei W, K. S. Moon, H. J. Jiang, W. Lin, C. P. Wong, "Development of transparent and flexible electrically conductive adhesives for microelectronics

applications", Portable Information Devices, 2008 and the 2008 7th IEEE Conference on Polymers and Adhesives in Microelectronics and Photonics, Germany, 1-5 (2008).

25. G. Orecchini, **R. W. Zhang**, J. Agar, A. Amaya, H-S Lee, D. Staiculescu, M. Tentzeris, C. P. Wong, L. Roselli, "Inkjet Printed Organic Transistors for Sustainable Electronics", Proceedings of the IEEE 60th Electronic Components Technology Conference, Las Vegas, NV, (2010).

26. J. C. Agar, K. J. Lin, **R. W. Zhang**, J. Durden, K. Lawrence, C. P Wong, "Novel PDMS(silicone)-in-PDMS(silicone): low cost flexible electronics without metallization", Proceedings of the IEEE 60th Electronic Components Technology Conference, Las Vegas, NV, (2010).

27. J. C. Agar, K. J. Lin, **R. W. Zhang**, J. Durden, K. Lawrence, C. P Wong, "Deconstruction of the myth of percolation in electrically conductive adhesives and it's implications", Proceedings of the IEEE 60th Electronic Components Technology Conference, Las Vegas, NV, (2010).

28. L. Yang, D. Staiculescu, **R. W. Zhang**, C. P. Wong, M. M. Tentzeris, "A novel 'green' fully-integrated ultrasensitive RFID-enabled gas sensor utilizing inkjet-printed antennas and carbon nanotubes", Antennas and Propagation Society International Symposium, APSURSI apos 09, IEEE, 1-4 (2009).

29. Y. Li, **R. W. Zhang**, L. B. Zhu, W. Lin, O. Hildreth, H. J. Jiang, J. X. Lu, Y. H. Xiu, Y. Liu, J. Moon, C. P. Wong, "Nano Materials and Composites for Electronic and Photo Packaging", Proceedings of the 9th Nanotechnology Conference, Garmanish, Germany, July 20-22, 4-6 (2009). (**Invited talk**)

30. A. Choudhury, N. Kumbhat, P.M. Raj, **R. W. Zhang**, G. Mehrotra, K. S. Moon, V. Sundaram, R. Dunne, M. Bolanos, C. P. Wong, R. R. Tummala, "Low temperature, low profile, ultra-fine pitch copper-to-copper chip-last embedded-active interconnection technology", Proceedings of the IEEE 60th Electronic Components Technology Conference, Las Vegas, NV, (2010).

31. W. Lin, R. Olivares, Q. Liang, **R. W. Zhang**, K. Moon, C. P. Wong, "Vertically aligned carbon nanotubes on copper substrates for applications as thermal interface materials: from synthesis to assembly", 59th Electronic Components and Technology Conference, California, SD, 441-447 (2009).

32. C. P. Wong, W. Lin, L. Zhu, H. Jiang, **R. W. Zhang**, Y. Li, K. Moon, "Nano materials for microelectronic and photonic packaging", World Journal of Engineering, 6(1), 1-4 (2009).

33. N. Kumbhat, A. Choudhury, M. Raine, G. Mehrotra, P.M. Raj, **R. W. Zhang**, K.S. Moon, R. Chatterjee, V. Sundaram, G. Meyer-Berg, C. P. Wong, R. R. Tummala, "Highly-reliable, 30μm pitch copper interconnects using nano-ACF/NCF", 59th Electronic Components and Technology Conference, California, SD, 1479-1485 (2009).

34. W. Lin, **R. W. Zhang**, C. P. Wong, "Chemical transfer of in-situ functionalized aligned carbon nanotube structures for microelectronic packaging applications", 10th Electronic Packaging Technology Conference, 115-120 (2008).

35. W. Lin, H. Jiang, **R. W. Zhang**, Q. Liang, J. Lu, Y. Xiu, K. Moon, O. Hildreth, C. P. Wong, "Nano Materials for microelectronic and photonic packaging", Portable Information Devices, 2008 and the 2008 7th IEEE Conference on Polymers and Adhesives in Microelectronics and Photonics, 1-5 (2008).

36. H. Jiang, K. Moon, **R. W. Zhang**, C. P. Wong, "In-situ reduced silver nanoparticles for highly conductive anisotropic conductive films applications", Portable Information Devices, 2008 and the 2008 7th IEEE Conference on Polymers and Adhesives in Microelectronics and Photonics, Germany, 1-5 (2008).

37. C. P. Wong, W. Lin, **R. W. Zhang**, Q. Liang, J. Lu, Y. Xiu, K. Moon, "Nano materials for microelectronic and photonic packaging", World Journal of Engineering, 5(3), 35-37 (2008).

38. W. Lin, H. Jiang, **R. W. Zhang**, Q. Liang, J. Lu, Y. Xiu, K. Moon, O. Hildreth, C. P. Wong, "Nano materials for microelectronic and photonic packaging", Portable Information Devices, 2008 and the 2008 7th IEEE Conference on Polymers and Adhesives in Microelectronics and Photonics, Germany (Garmish-Partenkirchen), Aug 17-20, 1-5 (2008)

A.4 Provisional Patents/Invention Disclosures

1. **R. W. Zhang**, W. Lin, K. S. Moon, C. P. Wong, "Ink-jettable electrically conductive adhesives", Invention Disclosure No. 4728 (2008), Provisional Patent Filed (2010).

2. **R. W. Zhang**, C. P. Wong, "Highly Reliable Low-Cost Electrically conductive Adhesives", Invention Disclosure No. 4770 (2009), Provisional Patent Filed (2010).

3. **R. W. Zhang**, K. S. Moon, W. Lin, Y. Liu , C. P. Wong, "Fluxless metal-metal bonding for 3D IC stacking", Invention Disclosure No. 5382, (2010).

4. **R. W. Zhang**, C. P. Wong, "Development of Highly Conductive Electrically Conductive Adhesives", Invention Disclosure No. 5486, (2010).

5. W. Lin, C. P. Wong, and **R. W. Zhang**, "Powerful solutions for selective dissolution and recovery of noble Metals", Invention Disclosure No. 5145, (2010).

6. K. Moon, H. Jiang, **R. W. Zhang** and C. Wong, "In-Situ Formed Nanoparticles in Polymer Matrix for Low Pressure Bonding", GTRC Invention Disclosure No. 4443 (2008).

REFERENCES

[1] Li, Y., Lu, D.D., and Wong, C.P., "*Electrically Conductive Adhesives with Nanotechnology*," Springer, New York, 2010.

[2] Kasap, S., Capper, P., and Editors, "*Springer Handbook of Electronic and Photonic Materials,*" Springer, 2006.

[3] Tummala, R.R., Rymaszewski, E.J., and Klopfenstein, A.G., "*Microelectronics Packaging Handbook*," Springer, p. 1027, 1997.

[4] Zhang, R., Agar, J.C., and Wong, C.P., "*Conductive Polymer Composites,*" Encyclopedia of Polymer Science and Technology, John Wiley & Sons, Inc., New York, in press.

[5] Li, Y. and Wong, C.P., "Recent advances of conductive adhesives as a lead-free alternative in electronic packaging: materials, processing, reliability and applications," *Materials Science & Engineering, R: Reports,* vol. R51, pp. 1-35, 2006.

[6] Lu, D., Luo, S., and Wong, C.P., *"Conductive polymer composites,"* Encyclopedia of Polymer Science and Technology, *Second Ed.,* John Wiley & Sons, Inc., New York, 2002.

[7] Lau, J.H., Wong, C.P., Lee, N.C., and Ricky, S.W., *"Electronics manufacturing with lead-free, halogen-free & Conductive-adhesive materials,"* Mcgraw-Hill Companies, Inc., 2003.

[8] Hwang, J.S., *"Environmental-friendly electronics: lead-free technology,"* Electrochemical publications Ltd, 2001.

[9] Liu, J., "*Conductive adhesives for electronics packaging,*" UK: Electrochemical Publications Ltd, 1999.

[10] Chen, K.-I. and Lin, K.-L., "Effects of gallium on wettability, microstructure and mechanical properties of the Sn-Zn-Ag-Ga and Sn-Zn-Ag-Al-Ga solder alloys," *Proceedings of the International Symposium on Electronic Materials and Packaging, 4th*, Kaohsiung, Taiwan, Dec. 4-6, pp. 49-54, 2002.

[11] Licari, J.J. and Swanson, D.W., "*Adhesives technology for electronic applications: materials, processes, reliability*," William Andrew, Norwich, NY, USA, 2005.

[12] Asai, S.i., Saruta, U., Tobita, M., Takano, M., and Miyashita, Y., "Development of an anisotropic conductive adhesive film (ACAF) from epoxy resins," *Journal of Applied Polymer Science,* vol. 56, pp. 769-77, 1995.

[13] Chang, D.D., Crawford, P.A., Fulton, J.A., McBride, R., Schmidt, M.B., Sinitski, R.E., and Wong, C.P., "An overview and evaluation of anisotropically conductive adhesive films for fine pitch electronic assembly," *IEEE Transactions on Components, Hybrids, and Manufacturing Technology,* vol. 16, pp. 828-35, 1993.

[14] Rocks, J., Halter, M., George, G., and Vohwinkel, F., "Calorimetric and rheological characterization of a high-performance epoxy curable at low temperatures," *Polymer International,* vol. 52, pp. 1749-1757, 2003.

[15] Leukel, J., Burchard, W., Krueger, R.-P., Much, H., and Schulz, G., "Mechanism of the anionic copolymerization of anhydride-cured epoxies analyzed by matrix-assisted laser desorption ionization time-of-flight mass spectrometry (MALDI-TOF-MS)," *Macromolecular Rapid Communications,* vol. 17, pp. 359-366, 1996.

[16] Fisch, W. and Hofmann, W., "The hardening mechanism of epoxy resins," *Journal of Polymer Science,* vol. 12, pp. 497-502, 1954.

[17] Fisch, W., Hofmann, W., and Koskikallio, J., "Curing mechanism of epoxy resins," *Journal of Applied. Chemistry,* vol. 6, pp. 429-41, 1956.

[18] Rocks, J., George, G.A., and Vohwinkel, F., "Curing kinetics and thermomechanical behaviour of co-anhydride cured aminoglycidyl epoxy resins," *Polymer International,* vol. 52, pp. 1758-1766, 2003.

[19] Rocks, J., Rintoul, L., Vohwinkel, F., and George, G., "The kinetics and mechanism of cure of an amino-glycidyl epoxy resin by a co-anhydride as studied by FT-Raman spectroscopy," *Polymer,* vol. 45, pp. 6799-6811, 2004.

[20] Teil, H., Page, S.A., Michaud, V., and Manson, J.A.E., "TTT-cure diagram of an anhydride-cured epoxy system including gelation, vitrification, curing kinetics model, and monitoring of the glass transition temperature," *Journal of Applied Polymer Science,* vol. 93, pp. 1774-1787, 2004.

[21] Zweifel, H. and Voelker, T., "Mechanism of anionic polymerization of maleic anhydride. 2," *Makromolekulare Chemie,* vol. 170, pp. 141-53, 1973.

[22] Palmese, G.R. and Gillham, J.K., "Time-temperature-transformation (TTT) cure diagrams: relationship between Tg and the temperature and time of cure for a polyamic acid/polyimide system," *Journal of Applied Polymer Science,* vol. 34, pp. 1925-39, 1987.

[23] Yim, M.J., Li, Y., Moon, K.S., and Wong, C.P., "Oxidation prevention and electrical property enhancement of copper-filled isotropically conductive adhesives," *Journal of Electronic Materials,* vol. 36, pp. 1341-1347, 2007.

[24] Lin, Y.-S. and Chiu, S.-S., "Electrical properties of copper-filled electrically conductive adhesives and pressure-dependent conduction behavior of copper particles," *Journal of Adhesion Science and Technology,* vol. 22, pp. 1673-1697, 2008.

[25] Lin, Y.-S. and Chiu, S.-S., "Effects of oxidation and particle shape on critical volume fractions of silver-coated copper powders in conductive adhesives for microelectronic applications," *Polymer Engineering and Science,* vol. 44, pp. 2075-2082, 2004.

[26] Park, S.-Y., Yoon, T.-W., Lee, C.-H., Jeong, I.-B., and Hyun, S.-H., "Surface modification of Ag coated Cu conductive metal powder for conductive silicone sealant gasket paste," *Materials Science Forum,* vol. 534-536, pp. 933-936, 2007.

[27] Huang, J.-C., "Carbon black filled conducting polymers and polymer blends," *Advances in Polymer Technology,* vol. 21, pp. 299-313, 2002.

[28] Zhang, R. and Liu, F., "Advances in Carbon Black-Polymer Composites," *Polymer Materials Science & Engineering,* vol. 21, pp. 45-49, 2005.

[29] Stankovich, S., Dikin, D.A., Dommett, G.H.B., Kohlhaas, K.M., Zimney, E.J., Stach, E.A., Piner, R.D., Nguyen, S.T., and Ruoff, R.S., "Graphene-based composite materials," *Nature,* vol. 442, pp. 282-286, 2006.

[30] Wang, X., Zhi, L., and Muellen, K., "Transparent, Conductive Graphene Electrodes for Dye-Sensitized Solar Cells," *Nano Letters,* vol. 8, pp. 323-327, 2008.

[31] Kim, Y., Cho, S.Y., Yun, Y.S., and Jin, H.-J., "Electroconductive adhesives based on polyurethane wtih multiwalled carbon nanotubes," *Modern Physics Letters B,* vol. 23, pp. 3739-3745, 2009.

[32] Heimann, M., Wirts-Ruetters, M., Boehme, B., and Wolter, K.-J., "Investigation of carbon nanotubes epoxy composites for electronics packaging," *IEEE Electronic Components and Technology Conference,* vol. 58th, pp. 1731-1736, 2008.

[33] Yu, X., Rajamani, R., Stelson, K.A., and Cui, T., "Carbon nanotube based transparent conductive thin films," *Journal of Nanoscience and Nanotechnology,* vol. 6, pp. 1939-1944, 2006.

[34] Moniruzzaman, M. and Winey, K.I., "Polymer Nanocomposites Containing Carbon Nanotubes," *Macromolecules,* vol. 39, pp. 5194-5205, 2006.

[35] Oh, Y., Suh, D., Kim, Y., Lee, E., Mok, J.S., Choi, J., and Baik, S., "Silver-plated carbon nanotubes for silver/conducting polymer composites," *Nanotechnology,* vol. 19, pp. 495602/1-495602/7, 2008.

[36] Wu, H.P., Wu, X.J., Ge, M.Y., Zhang, G.Q., Wang, Y.W., and Jiang, J., "Properties investigation on isotropical conductive adhesives filled with silver coated carbon nanotubes," *Composites Science and Technology,* vol. 67, pp. 1182-1186, 2007.

[37] Jang, J. and Ryu, S.K., "Physical property and electrical conductivity of electroless Ag-plated carbon fiber-reinforced paper," *Journal of Materials Processing Technology,* vol. 180, pp. 66-73, 2006.

[38] You, M., Zhang, L., Gong, Z., Liu, W., and He, A., "On the properties of conductive adhesive filled with electroless silver plated flake graphite," *Key Engineering Materials,* vol. 373-374, pp. 220-223, 2008.

[39] Lin, W., Xi, X., and Yu, C., "Research of silver plating nano-graphite filled conductive adhesive," *Synthetic Metals,* vol. 159, pp. 619-624, 2009.

[40] Liang, T., Guo, W., Yan, Y., and Tang, C., "Electroless plating of silver on graphite powders and the study of its conductive adhesive," *International Journal of Adhesion and Adhesives,* vol. 28, pp. 55-58, 2007.

[41] Lu, G., Li, X., and Jiang, H., "Electrical and shielding properties of ABS resin filled with nickel-coated carbon fibers," *Composites Science and Technology,* vol. 56, pp. 193-200, 1996.

[42] Zou, H., Zhang, L., Tian, M., Wu, S., and Zhao, S., "Study on the structure and properties of conductive silicone rubber filled with nickel-coated graphite," *Journal of Applied Polymer Science,* vol. 115, pp. 2710-2717, 2010.

[43] Kang, S.K., Rai, R.S., and Purushothaman, S., "Development of high conductivity lead (Pb)-free conducting adhesives," *IEEE Transactions on Components, Packaging, and Manufacturing Technology, Part A,* vol. 21, pp. 18-22, 1998.

[44] Kang, S.K. and Purushothaman, S., "Development of conducting adhesive materials for microelectronic applications," *Journal of Electronic Materials,* vol. 28, pp. 1314-1318, 1999.

[45] Lu, D. and Wong, C.P., "Isotropic conductive adhesives filled with low-melting-point alloy fillers," *IEEE Transactions on Electronics Packaging Manufacturing,* vol. 23, pp. 185-190, 2000.

[46] Gallagher, C., Matijasevic, G., and Maguire, J.F., "Transient liquid phase sintering conductive adhesives as solder replacements," *Proceedings - Electronic Components & Technology Conference,* vol. 47th, pp. 554-560, 1997.

[47] Gallagher, C., Matijasevic, G., and Capote, M.A., "Transient liquid phase sintering conductive adhesives for mechanical, electrical and thermal interconnects," Application: US Patent 5853622, 1998.

[48] Shearer, C., Shearer, B., Matijasevic, G., and Gandhi, P., "Transient liquid-phase sintering composites: polymer adhesives with metallurgical bonds," *Journal of Electronic Materials,* vol. 28, pp. 1319-1326, 1999.

[49] Kim, J.-M., Yasuda, K., and Fujimoto, K., "Isotropic conductive adhesives with fusible filler particles," *Journal of Electronic Materials,* vol. 33, pp. 1331-1337, 2004.

[50] Pandiri, S.M., "The behavior of silver flakes conductive epoxy adhesives," *Adhesives Age,* pp. 31-35, 1987.

[51] Lu, D. and Wong, C.P., "Thermal decomposition of silver flake lubricants," *Journal of Thermal Analysis and Calorimetry,* vol. 61, pp. 3-12, 2000.

[52] Lu, D. and Wong, C.P., "Characterization of silver flake lubricants," *Journal of Thermal Analysis and Calorimetry,* vol. 59, pp. 729-740, 2000.

[53] Dong, H., Li, Y., Yim, M.J., Moon, K.S., and Wong, C.P., "Investigation of electrical contact resistance for nonconductive film functionalized with p-conjugated self-assembled molecules," *Applied Physics Letters,* vol. 90, pp. 092102/1-092102/3, 2007.

[54] Ruschau, G.R., Yoshikawa, S., and Newnham, R.E., "Resistivities of conductive composites," *Journal of Applied Physics,* vol. 72, pp. 953-9, 1992.

[55] Holm, R., "Electric Contacts: Theory and Application", Springer-Verlag, New York, 1967.

[56] Zhang, R., Moon, K.S., Lin, W., and Wong, C.P., "Electrical properties of ACA joints assisted by conjugated molecular wires," *IEEE Electronic Components and Technology Conference,* vol. 59th, pp. 2034-2038, 2009.

[57] Chmutin, I.A., Letyagin, S.V., Shevchenko, V.G., and Ponamorcnko, A.T., "Conductive Polymer Composites: Structure, Contact Phenomena, and Anisotropy," *Vysokomol. Soedin. Ser. A,* vol. 36, 1994.

[58] Roldughin, V.I. and Vysotskii, V.V., "Percolation properties of metal-filled polymer films, structure and mechanisms of conductivity," *Progress in Organic Coatings,* vol. 39, pp. 81-100, 2000.

[59] Li, C., Thostenson, E.T., and Chou, T.-W., "Dominant role of tunneling resistance in the electrical conductivity of carbon nanotube-based composites," *Applied Physics Letters,* vol. 91, pp. 223114/1-223114/3, 2007.

[60] Agar, J.C., Lin, K.J., Zhang, R., Durden, J., Lawrence, K., Moon, K.-s., and Wong, C.P., "Deconstructing the myth of percolation in electrincally conductive adhesives and its implications," *Proceedings - Electronic Components & Technology Conference,* vol. 60th, pp. 1713-1718, 2010.

[61] Gul, V.E., *New concepts in polymer science: structure and properties of conducting polymer composites,* Utrecht, The Netherlands, 1996.

[62] Gilleo, K., "Assembly with conductive adhesives," *Soldering & Surface Mount Technology,* vol. 19, pp. 12-17, 1995.

[63] Harris, P.G., "Conductive adhesives: A critical review of progress to date," *Soldering & Surface Mount Technology,* vol. 20, pp. 19-21, 26, 1995.

[64] Lu, D., Tong, Q.K., and Wong, C.P., "Conductivity mechanisms of isotropic conductive adhesives (ICA's)," *IEEE Transactions on Electronics Packaging Manufacturing,* vol. 22, pp. 223-227, 1999.

[65] Lu, D. and Wong, C.P., "Effects of shrinkage on conductivity of isotropic conductive adhesives," *International Journal of Adhesion and Adhesives,* vol. 20, pp. 189-193, 2000.

[66] Miragliotta, J., Benson, R.C., and Phillips, T.E., "Vibrational analysis of a stearic acid adlayer adsorbed on a silver flake substrate," *Materials Research Society Symposium Proceedings,* vol. 445, pp. 217-222, 1997.

[67] Markley, D.L., Tong, Q.K., Magliocca, D.J., and Hahn, T.D., "Characterization of silver flakes utilized for isotropic conductive adhesives," *Proceedings - International Symposium on Advanced Packaging Materials: Processes, Properties and Interfaces, Braselton, Ga., Mar. 14-17, 1999,* pp. 16-20, 1999.

[68] Li, Y., Moon, K.-S., and Wong, C.P., "Electrical property improvement of electrically conductive adhesives through in-situ replacement by short-chain difunctional acids," *IEEE Transactions on Components and Packaging Technologies,* vol. 29, pp. 173-178, 2006.

[69] Li, Y., Moon, K.-S., Whitman, A., and Wong, C.P., "Enhancement of electrical properties of electrically conductive adhesives (ECAs) by using novel aldehydes," *IEEE Transactions on Components and Packaging Technologies,* vol. 29, pp. 758-763, 2006.

[70] Wu, H.P., Liu, J.F., Wu, X.J., Ge, M.Y., Wang, Y.W., Zhang, G.Q., and Jiang, J.Z., "High conductivity of isotropic conductive adhesives filled with silver nanowires," *International Journal of Adhesion and Adhesives,* vol. 26, pp. 617-621, 2006.

[71] Wu, H., Wu, X., Liu, J., Zhang, G., Wang, Y., Zeng, Y., and Jing, J., "Development of a novel isotropic conductive adhesive filled with silver nanowires," *Journal of Composite Materials,* vol. 40, pp. 1961-1969, 2006.

[72] Tao, Y., Xia, Y., Wang, H., Gong, F., Wu, H., and Tao, G., "Novel isotropical conductive adhesives for electronic packaging application," *IEEE Transactions on Advanced Packaging,* vol. 32, pp. 589-592, 2009.

[73] Chen, D., Qiao, X., Qiu, X., Tan, F., Chen, J., and Jiang, R., "Effect of silver nanostructures on the resistivity of electrically conductive adhesives composed of silver flakes," *Journal of Materials Science: Materials in Electronics,* vol. 21, pp. 486-490, 2010.

[74] Lin, X. and Lin, F., "The improvement on the properties of silver-containing conductive adhesives by the addition of carbon nanotube," *Proceedings of the IEEE CPMT Conference on High Density Microsystem Design and Packaging and Component Failure Analysis (HDP'04), 6th,* Shanghai, China, June 30-July 3, pp. 382-384, 2004.

[75] Kwon, O.H. and Messing, G.L., "A theoretical analysis of solution-precipitation controlled densification during liquid-phase sintering," *Acta Metallurgica et Materialia,* vol. 39, pp. 2059-68, 1991.

[76] Hou, M.M. and Eagar, T.W., "Low temperature transient liquid phase (LTTLP) bonding for Au/Cu and Cu/Cu interconnections," *Journal of Electronic Packaging,* vol. 114, pp. 443-447, 1992.

[77] Zhang, R., Moon, K.-s., Lin, W., and Wong, C.P., "Preparation of highly conductive polymer nanocomposites by low temperature sintering of silver nanoparticles," *Journal of Materials Chemistry.,* vol. 20, pp. 2018-2023, 2010.

[78] Zhang, R., Lin, W., Moon, K.-s., and Wong, C.P., "Fast Preparation of Printable Highly Conductive Polymer Nanocomposites by Thermal Decomposition of Silver Carboxylate and Sintering of Silver Nanoparticles," *ACS Applied Materials & Interfaces,* 2, 2637-2645, 2010.

[79] Moon, K.-S., Dong, H., Maric, R., Pothukuchi, S., Hunt, A., Li, Y., and Wong, C.P., "Thermal behavior of silver nanoparticles for low-temperature interconnect applications," *Journal of Electronic Materials,* vol. 34, pp. 168-175, 2005.

[80] Das, R.N., Egitto, F.D., and Markovich, V.R., "Nano- and micro-filled conducting adhesives for z-axis interconnections: new direction for high-speed, high-density, organic microelectronics packaging," *Circuit World,* vol. 34, pp. 3-12, 2008.

[81] Bai, J.G., Lei, T.G., Calata, J.N., and Lu, G.-Q., "Control of nanosilver sintering attained through organic binder burnout," *Journal of Materials Research,* vol. 22, pp. 3494-3500, 2007.

[82] Wang, T., Chen, X., Lu, G.-Q., and Lei, G.-Y., "Low-temperature sintering with nano-silver paste in die-attached interconnection," *Journal of Electronic Materials,* vol. 36, pp. 1333-1340, 2007.

[83] Jiang, H., Moon, K.-S., Lu, J., and Wong, C.P., "Conductivity enhancement of nano silver-filled conductive adhesives by particle surface functionalization," *Journal of Electronic Materials,* vol. 34, pp. 1432-1439, 2005.

[84] Jiang, H., Moon, K.-S., Li, Y., and Wong, C.P., "Surface Functionalized Silver Nanoparticles for Ultrahigh Conductive Polymer Composites," *Chemistry of Materials,* vol. 18, pp. 2969-2973, 2006.

[85] Ide, E., Angata, S., Hirose, A., and Kobayashi, K.F., "Metal-metal bonding process using Ag metallo-organic nanoparticles," *Acta Materialia,* vol. 53, pp. 2385-2393, 2005.

[86] Reinhold, I., Hendriks, C.E., Eckardt, R., Kranenburg, J.M., Perelaer, J., Baumann, R.R., and Schubert, U.S., "Argon plasma sintering of inkjet printed silver tracks on polymer substrates," *Journal of Materials Chemistry,* vol. 19, pp. 3384-3388, 2009.

[87] Perelaer, J., de Gans, B.-J., and Schubert, U.S., "Ink-jet printing and microwave sintering of conductive silver tracks," *Advanced Materials,* vol. 18, pp. 2101-2104, 2006.

[88] van Osch, T.H.J., Perelaer, J., de Laat, A.W.M., and Schubert, U.S., "Inkjet printing of narrow conductive tracks on untreated polymeric substrates," *Advanced Materials,* vol. 20, pp. 343-345, 2008.

[89] Perelaer, J., Klokkenburg, M., Hendriks, C.E., and Schubert, U.S., "Microwave Flash Sintering of Inkjet-Printed Silver Tracks on Polymer Substrates," *Advanced Materials,* vol. 21, pp. 4830-4834, 2009.

[90] Magdassi, S., Grouchko, M., Berezin, O., and Kamyshny, A., "Triggering the sintering of silver nanoparticles at room temperature," *ACS Nano,* vol. 4, pp. 1943-1948, 2010.

[91] Grouchko, M., Kamyshny, A., and Magdassi, S., "Formation of air-stable copper-silver core-shell nanoparticles for ink-jet printing," *Journal of Materials Chemistry,* vol. 19, pp. 3057-3062, 2009.

[92] Calvert, P., "Inkjet Printing for Materials and Devices," *Chemistry of Materials,* vol. 13, pp. 3299-3305, 2001.

[93] Greer, J.R. and Street, R.A., "Thermal cure effects on electrical performance of nanoparticle silver inks," *Acta Materialia,* vol. 55, pp. 6345-6349, 2007.

[94] Dearden, A.L., Smith, P.J., Shin, D.-Y., Reis, N., Derby, B., and O'Brien, P., "A low curing temperature silver ink for use in ink-jet printing and subsequent production of conductive tracks," *Macromolecular Rapid Communications,* vol. 26, pp. 315-318, 2005.

[95] Wakuda, D., Kim, K.-S., and Suganuma, K., "Room-temperature sintering process of Ag nanoparticle paste," *IEEE Transactions on Components and Packaging Technologies,* vol. 32, pp. 627-632, 2009.

[96] Lee, H.-H., Chou, K.-S., and Shih, Z.-W., "Effect of nano-sized silver particles on the resistivity of polymeric conductive adhesives," *International Journal of Adhesion and Adhesives,* vol. 25, pp. 437-441, 2005.

[97] Ye, L., Lai, Z., Liu, J., and Tholen, A., "Effect of Ag particle size on electrical conductivity of isotropically conductive adhesives," *IEEE Transactions on Electronics Packaging Manufacturing,* vol. 22, pp. 299-302, 1999.

[98] Zhang, R. and Wong, C.P., "Advanced Interconnect materials for ink-jet printing by low temperature sintering," *IEEE Electronic Components and Technology Conference,* vol. 59th, pp. 150-154, 2009.

[99] Gent, A.N. and Hamed, G.R., "Adhesion and bonding, adhesion," vol. 1, pp. 476-518, 1985.

[100] Good, R.J., "Theory of cohesive vs adhesive separation in an adhering system," *Journal of Adhesion,* vol. 4, pp. 133-154, 1972.

[101] Liong, S., Wong, C.P., and Burgoyne, W.F., Jr., "Adhesion improvement of thermoplastic isotropically conductive adhesive," *IEEE Transactions on Components and Packaging Technologies,* vol. 28, pp. 327-336, 2005.

[102] Moon, K., Rockett, C., Kretz, C., Burgoyne, W.F., and Wong, C.P., "Improvement of adhesion and electrical properties of reworkable thermoplastic conductive adhesives," *Journal of Adhesion Science and Technology,* vol. 17, pp. 1785-1799, 2003.

[103] Moon, K.-S., Rockett, C., and Wong, C.P., "Adhesion improvement of thermoplastic-based isotropic conductive adhesives under humid environment using self-assembled monolayer compounds," *Journal of Adhesion Science and Technology,* vol. 18, pp. 153-167, 2004.

[104] Li, Y., Yim, M.J., Moon, K., Zhang, R.W., and Wong, C.P., "Development of novel, flexible, electrically conductive adhesive for next-generation microelectronics interconnect applications," *IEEE Electronic Components and Technology Conference,* vol. 58th, pp. 1272-1276, 2008.

[105] Zhang, R., Wang, W., Moon, K.S., Jiang, H., Lin, W., and Wong, C.P., "Development of transparent and flexible electrically conductive adhesive for microelectronic applications," *Portable Information Devices, 2008 and the 2008 7th IEEE Conference on Polymers and Adhesives in Microelectronics and Photonics,* pp. 1-5, 2008.

[106] Zhang, R.W., Duan, Y., Lin, W., Moon, K., and Wong, C.P., "New electrically conductive adhesives (ECAs) for flexible interconnect applications," *IEEE Electronic Components and Technology Conference,* vol. 59th, pp. 1356-1360, 2009.

[107] Love, J.C., Estroff, L.A., Kriebel, J.K., Nuzzo, R.G., and Whitesides, G.M., "Self-Assembled Monolayers of Thiolates on Metals as a Form of Nanotechnology," *Chemical Reviews,* vol. 105, pp. 1103-1169, 2005.

[108] Jain, K., Klosner, M., Zemel, M., and Raghunandan, S., "Flexible electronics and displays: high-resolution, roll-to-roll, projection lithography and photoablation processing technologies for high-throughput production," *Proceedings of the IEEE,* vol. 93, pp. 1500-1510, 2005.

[109] Roncali, J., Leriche, P., and Cravino, A., "From one- to three-dimensional organic semiconductors: in search of the organic silicon?," *Advanced Materials,* vol. 19, pp. 2045-2060, 2007.

[110] Chiang, Y.-M., Birnie, D.P., and Kingery, W.D., "Physical Ceramics: Principles for Ceramic Science and Engineering," John Wiley & Sons, 1996.

[111] Kang, S. L., " Sintering densification, grain growth, and microstructure", Elsevier, 2005.

[112] Okuma, S., "The sintering mechanism of aluminum and the anodization of aluminum sintered bodies," *Electrocomponent Science and Technology,* vol. 6, pp. 23-9, 1979.

[113] Ashby, M.F., "Sintering diagrams," *Acta Metallurgica,* vol. 22, pp. 275-89, 1974.

[114] Pan, J., Le, H., Kucherenko, S., and Yeomans, J.A., "A model for the sintering of spherical particles of different sizes by solid state diffusion," *Acta Materialia,* vol. 46, pp. 4671-4690, 1998.

[115] Djohari, H., Martinez-Herrera, J.I., and Derby, J.J., "Transport mechanisms and densification during sintering: I. Viscous flow versus vacancy diffusion," *Chemical Engineering Science,* vol. 64, pp. 3799-3809, 2009.

[116] Djohari, H. and Derby, J.J., "Transport mechanisms and densification during sintering: II. Grain boundaries," *Chemical Engineering Science,* vol. 64, pp. 3810-3816, 2009.

[117] Kingery, W.D. and Berg, M., "Study of the initial stages of sintering solids by viscous flow, evaporation-condensation, and self-diffusion," *Journal of Applied Physics,* vol. 26, pp. 1205-12, 1955.

[118] Iwama, S. and Sahashi, T., "Sintering of ultrafine metal powders. I. Coalescence growth stage of gold and silver," *Japanese Journal of Applied Physics,* vol. 19, pp. 1039-44, 1980.

[119] Cheng, K., Yang, M.-H., Chiu, W.W.W., Huang, C.-Y., Chang, J., Ying, T.-F., and Yang, Y., "Ink-jet printing, self-assembled polyelectrolytes, and electroless plating: low cost fabrication of circuits on a flexible substrate at room temperature," *Macromolecular Rapid Communications,* vol. 26, pp. 247-264, 2005.

[120] Kamyshny, A., Ben-Moshe, M., Aviezer, S., and Magdassi, S., "Ink-jet printing of metallic nanoparticles and microemulsions," *Macromolecular Rapid Communications,* vol. 26, pp. 281-288, 2005.

[121] Yamamoto, M., Kashiwagi, Y., and Nakamoto, M., "Size-Controlled Synthesis of Monodispersed Silver Nanoparticles Capped by Long-Chain Alkyl Carboxylates from Silver Carboxylate and Tertiary Amine," *Langmuir,* vol. 22, pp. 8581-8586, 2006.

[122] Dong, T.-Y., Chen, W.-T., Wang, C.-W., Chen, C.-P., Chen, C.-N., Lin, M.-C., Song, J.-M., Chen, I.-G., and Kao, T.-H., "One-step synthesis of uniform silver nanoparticles capped by saturated decanoate: direct spray printing ink to form metallic silver films," *Physical Chemistry Chemical Physics,* vol. 11, pp. 6269-6275, 2009.

[123] Nguyen, B.T., Gautrot, J.E., Nguyen, M.T., and Zhu, X.X., "Nitrocellulose-stabilized silver nanoparticles as low conversion temperature precursors useful for inkjet printed electronics," *Journal of Materials Chemistry,* vol. 17, pp. 1725-1730, 2007.

[124] Oljaca, M., Maric, R., Shanmugham, S., and Hunt, A., "Nanomaterials for solid oxide fuel cells," *American Ceramic Society Bulletin,* vol. 82, pp. 38-40, 2003.

[125] http://www.ngimat.com/technology/nanospray.html (Accessed Febuary 20, 2011).

[126] Oljaca, M., Xing, Y., Lovelace, C., Shanmugham, S., and Hunt, A., "Flame synthesis of nanopowders via combustion chemical vapor deposition," *Journal of Materials Science Letters,* vol. 21, pp. 621-626, 2002.

[127] Hunt, A.T., Carter, W.B., and Cochran, J.K., Jr., "Combustion chemical vapor deposition: a novel thin-film deposition technique," *Applied Physics Letters,* vol. 63, pp. 266-8, 1993.

[128] Stark, W.J., Maedler, L., Maciejewski, M., Pratsinis, S.E., and Baiker, A., "Flame synthesis of nanocrystalline ceria-zirconia: effect of carrier liquid," *Chemical Communications (Cambridge, United Kingdom),* pp. 588-589, 2003.

[129] Xiong, Y., Siekkinen, A.R., Wang, J., Yin, Y., Kim, M.J., and Xia, Y., "Synthesis of silver nanoplates at high yields by slowing down the polyol reduction of silver nitrate with polyacrylamide," *Journal of Materials Chemistry,* vol. 17, pp. 2600-2602, 2007.

[130] Chen, M., Wang, L.-Y., Han, J.-T., Zhang, J.-Y., Li, Z.-Y., and Qian, D.-J., "Preparation and Study of Polyacryamide-Stabilized Silver Nanoparticles through a One-Pot Process," *Journal of Physical Chemistry B,* vol. 110, pp. 11224-11231, 2006.

[131] Kotthaus, S., Guenther, B.H., Haug, R., and Schaefer, H., "Study of isotropically conductive bondings filled with aggregates of nano-sized Ag-particles," *IEEE Transactions on Components, Packaging, and Manufacturing Technology, Part A,* vol. 20, pp. 15-20, 1997.

[132] Waterhouse, G.I.N., Bowmaker, G.A., and Metson, J.B., "The thermal decomposition of silver (I, III) oxide: A combined XRD, FT-IR and Raman spectroscopic study," *Physical Chemistry Chemical Physics,* vol. 3, pp. 3838-3845, 2001.

[133] http://cnx.org/content/m34549/latest/ (Accessed Febuary 20, 2011)

[134] Weaver, J.F. and Hoflund, G.B., "Surface Characterization Study of the Thermal Decomposition of AgO," *Journal of Physical Chemistry,* vol. 98, pp. 8519-24, 1994.

[135] Weaver, J.F. and Hoflund, G.B., "Surface Characterization Study of the Thermal Decomposition of Ag_2O," *Chemistry of Materials,* vol. 6, pp. 1693-9, 1994.

[136] Singh, M., Haverinen, H.M., Dhagat, P., and Jabbour, G.E., "Inkjet Printing - Process and Its Applications," *Advanced Materials*, vol. 22, pp. 673-685, 2010.

[137] Chabinyc, M.L. and Salleo, A., "Materials Requirements and Fabrication of Active Matrix Arrays of Organic Thin-Film Transistors for Displays," *Chemistry of Materials,* vol. 16, pp. 4509-4521, 2004.

[138] Kolbe, J., Arp, A., Calderone, F., Meyer, E.M., Meyer, W., Schaefer, H., and Stuve, M., "Inkjettable conductive adhesive for use in microelectronics and microsystems technology," *Microelectronics Reliability,* vol. 47, pp. 331-334, 2007.

[139] Jang, D., Kim, D., Lee, B., Kim, S., Kang, M., Min, D., and Moon, J., "Nanosized glass frit as an adhesion promoter for ink-jet printed conductive patterns on glass substrates annealed at high temperatures," *Advanced Functional Materials,* vol. 18, pp. 2862-2868, 2008.

[140] Fuller, S.B., Wilhelm, E.J., and Jacobson, J.M., "Ink-jet printed nanoparticle microelectromechanical systems," *J. Microelectromech. Syst.,* vol. 11, pp. 54-60, 2002.

[141] Perelaer, J., de Laat, A.W.M., Hendriks, C.E., and Schubert, U.S., "Inkjet-printed silver tracks: low temperature curing and thermal stability investigation," *Journal of Materials Chemistry,* vol. 18, pp. 3209-3215, 2008.

[142] Perelaer, J., Hendriks, C.E., de Laat, A.W.M., and Schubert, U.S., "One-step inkjet printing of conductive silver tracks on polymer substrates," *Nanotechnology,* vol. 20, pp. 165303/1-165303/5, 2009.

[143] Lu, D.D., Li, Y.G., and Wong, C.P., "Recent advances in nano-conductive adhesives," *Journal of Adhesion Science and Technology,* vol. 22, pp. 815-834, 2008.

[144] Yamamoto, S., Fujiwara, K., and Watarai, H., "Surface-enhanced Raman scattering from oleate-stabilized silver colloids at a liquid/liquid interface," *Analytical Sciences,* vol. 20, pp. 1347-1352, 2004.

[145] Moskovits, M. and Suh, J.S., "Conformation of mono- and dicarboxylic acids adsorbed on silver surfaces," *Journal of the American Chemical Society,* vol. 107, pp. 6826-9, 1985.

[146] Ishioka, T., Wakisaka, H., Saito, T., and Kanesaka, I., "Vibrational study on structural transitions of potassium pelargonate CH3(CH2)7CO2K," *Spectrochimica Acta, Part A: Molecular and Biomolecular Spectroscopy,* vol. 57A, pp. 129-135, 2001.

[147] Abe, K., Hanada, T., Yoshida, Y., Tanigaki, N., Takiguchi, H., Nagasawa, H., Nakamoto, M., Yamaguchi, T., and Yase, K., "Two-dimensional array of silver nanoparticles," *Thin Solid Films,* vol. 327-329, pp. 524-527, 1998.

[148] Lee Seung, J. and Kim, K., "Development of silver film via thermal decomposition of layered silver alkanecarboxylates for surface-enhanced Raman spectroscopy," *Chemical communications (Cambridge, England),* pp. 212-3, 2003.

[149] Yang, N., Aoki, K., and Nagasawa, H., "Thermal metallization of silver stearate-coated nanoparticles owing to the destruction of the shell structure," *Journal of Physical Chemistry B,* vol. 108, pp. 15027-15032, 2004.

[150] Uvarov, N.F., Burleva, L.P., Mizen, M.B., Whitcomb, D.R., and Zou, C., "Conductivity of long-chain silver carboxylates and their thermal decomposition products," *Solid State Ionics,* vol. 107, pp. 31-40, 1998.

[151] Liu, X., Lu, S., Zhang, J., and Cao, W., "Thermal decomposition process of silver behenate," *Thermochimica Acta,* vol. 440, pp. 1-6, 2006.

[152] Lee, S.J., Han, S.W., Choi, H.J., and Kim, K., "Structure and Thermal Behavior of a Layered Silver Carboxylate," *Journal of Physical Chemistry B,* vol. 106, pp. 2892-2900, 2002.

[153] Yamamoto, M. and Nakamoto, M., "Novel preparation of monodispersed silver nanoparticles via amine adducts derived from insoluble silver myristate in tertiary alkylamine," *Journal of Materials Chemistry,* vol. 13, pp. 2064-2065, 2003.

[154] Tekin, E., Smith, P.J., and Schubert, U.S., "Ink-jet printing as deposition and patterning tool for polymers and inorganic particles," *Soft Matter,* vol. 4, pp. 703-713, 2008.

[155] Bell, G.C., Jr., Rosell, C.M., and Joslin, S.T., "Rheology of silver-filled glass die attach adhesive for high-speed automatic processing," *IEEE Transactions on Components, Hybrids, and Manufacturing Technology,* vol. CHMT-10, pp. 507-10, 1987.

[156] Barnes, H.A., "Thixotropy-a review," *Journal of Non-Newtonian Fluid Mechanics,* vol. 70, pp. 1-33, 1997.

[157] Durairaj, R., Ekere, N.N., and Salam, B., "Thixotropy flow behaviour of solder and conductive adhesive pastes," *Journal of Materials Science: Materials in Electronics,* vol. 15, pp. 677-683, 2004.

[158] Durairaj, R., Mallik, S., Seman, A., Marks, A., and Ekere, N.N., "Rheological characterisation of solder pastes and isotropic conductive adhesives used for flip-chip assembly," *Journal of Materials Processing Technology,* vol. 209, pp. 3923-3930, 2009.

[159] Koltay, P.Z., R.;, "Non-contact nanoliter&picoliter liquid dispensing," *The 14th International Conference on Solid-State Sensors, Actuators and Microsystems,* Lyon, France, p. 6, 2007.

[160] Li, Y., Moon, K.-s., and Wong, C.P., "Electronics without lead," *Science*, vol. 308, pp. 1419-1420, 2005.

[161] Zhang, R., Lin, W., Lawrence, K., and Wong, C.P., "Highly reliable, low cost, isotropically conductive adhesives filled with Ag-coated Cu flakes for electronic packaging applications," *International Journal of Adhesion and Adhesives,* vol. 30, pp. 403-407, 2010.

[162] Morris, J.E., *Nanopackaging: Nanotechnologies and Electronics Packaging,* Springer, 2008.

[163] Wakuda, D., Kim, K.-S., and Suganuma, K., "Room temperature sintering of Ag nanoparticles by drying solvent," *Scripta Materialia,* vol. 59, pp. 649-652, 2008.

[164] Zhang, R.W., Duan, Y., Lin, W., Moon, K., and Wong, C.P., "New electrically conductive adhesives (ECAs) for flexible interconnect applications," *IEEE Electron. Compon. Technol. Conf.,* vol. 59th, pp. 1356-1360, 2009.

[165] Sekitani, T. and Someya, T., "Stretchable, Large-area Organic Electronics," *Advanced Materials,* vol. 22, pp. 2228-2246, 2010.

[166] Cong, H. and Pan, T., "Photopatternable conductive PDMS materials for microfabrication," *Advanced Functional Materials,* vol. 18, p. 3871, 2008.

[167] Lutz, M.A. and Cole, R.L., "Flexible silicone adhesive with high electrical conductivity," *Proceedings - Electronic Components Conference,* vol. 39th, pp. 83-87, 1989.

[168] Sivaramakrishnan, S., Chia, P.-J., Yeo, Y.-C., Chua, L.-L., and Ho, P.K.H., "Controlled insulator-to-metal transformation in printable polymer composites with nanometal clusters," *Nature Materials,* vol. 6, pp. 149-155, 2007.

[169] Thostenson, E.T., Li, C., and Chou, T.-W., "Nanocomposites in context," *Composites Science and Technology*, vol. 65, pp. 491-516, 2005.

[170] Klosterman, D., Li, L., and Morris, J.E., "Materials characterization, conduction development, and curing effects on reliability of isotropically conductive adhesives," *IEEE Transactions on Components,Packaging and Manufacturing Technology., Part A*, vol. 21, pp. 23-31, 1998.

[171] Li, L. and Morris, J.E., "Electrical conduction models for isotropically conductive adhesive joints," ," *IEEE Transactions on Components,Packaging and Manufacturing Technology., Part A,* vol. 20, pp. 3-8, 1997.

[172] Li, C., Thostenson, E.T., and Chou, T.-W., "Dominant role of tunneling resistance in the electrical conductivity of carbon nanotube-based composites," *Applied Phyasics Letter,* vol. 91, pp. 223114/1-223114/3, 2007.

[173] Wu, H.P., Wu, X.J., Ge, M.Y., Zhang, G.Q., Wang, Y.W., and Jiang, J.Z., "Effect analysis of filler sizes on percolation threshold of isotropical conductive adhesives," *Composites Science and Technology,* vol. 67, pp. 1116-1120, 2007.

[174] Lu, D., Tong, Q.K., and Wong, C.P., "A study of lubricants on silver flakes for microelectronics conductive adhesives," *IEEE Transactions on Components and Packaging Technologies,* vol. 22, pp. 365-371, 1999.

[175] Oh, Y., Chun, K.-Y., Lee, E., Kim, Y.-J., and Baik, S., "Functionalized nano-silver particles assembled on one-dimensional nanotube scaffolds for ultra-highly conductive silver/polymer composites," *Journal of Materials Chemistry,* vol. 20, pp. 3579-3582, 2010.

[176] Shi, L.T., Saraf, R., and Huang, W.S., "Processing solder/polymer composite pastes for surface mount technology," *Processing of Advanced Materials,* vol. 3, pp. 57-62, 1993.

[177] Kang, S.K., Buchwalter, S.L., LaBianca, N.C., Gelorme, J., Purushothaman, S., Papathomas, K., and Poliks, M., "Development of conducting adhesive materials for via fill applications," *IEEE Transactions on Components and Packaging Technology,* vol. 24, pp. 431-435, 2001.

[178] H. Nishikawa, S. Mikami, N. Terada, K. Miyake, A. Aoki, and Takemoto, T., "Electrical property of conductive adhesives using silver-coated copper filler," *IEEE, 2nd Electronics Systemintegration Technology Conference,* pp. 825-828, 2008.

[179] Ho, L.-N., Nishikawa, H., Natsume, N., Takemoto, T., Miyake, K., Fujita, M., and Ota, K., "Effects of Trace Elements in Copper Fillers on the Electrical Properties of Conductive Adhesives," *Journal of Electronic Materials,* vol. 39, pp. 115-123, 2010.

[180] Gong, Y.S., Lee, C., and Yang, C.K., "Atomic force microscopy and Raman spectroscopy studies on the oxidation of Cu thin films," *Journal of Applied Physics,* vol. 77, pp. 5422-5, 1995.

[181] Hu, Y.Z., Sharangpani, R., and Tay, S.-P., "Kinetic investigation of copper film oxidation by spectroscopic ellipsometry and reflectometry," *Journal of Vacuum Science & Technology, A: Vacuum, Surfaces, and Films,* vol. 18, pp. 2527-2532, 2000.

[182] Takeshima, E., Takatsu, K., Kojima, Y., and TFujii, T., "Electroplating of fine particles with metal," *US Pat. 4954235,* 1990.

[183] Djokic, S., Dubios, M., and Lepard, R.H., "Process for the production of silver coated particles," *US Pat. 5945158,* 1999.

[184] Xu, X., Luo, X., Zhuang, H., Li, W., and Zhang, B., "Electroless silver coating on fine copper powder and its effects on oxidation resistance," *Materials Letters,* vol. 57, pp. 3987-3991, 2003.

[185] http://en.wikipedia.org/wiki/Corrosion_inhibitor

[186] Brusic, V., Frisch, M.A., Eldridge, B.N., Novak, F.P., Kaufman, F.B., Rush, B.M., and Frankel, G.S., "Copper corrosion with and without inhibitors," *Journal of the Electrochemical Society,* vol. 138, pp. 2253-9, 1991.

[187] Fenelon, A.M. and Breslin, C.B., "An electrochemical study of the formation of benzotriazole surface films on copper, zinc and a copper-zinc alloy," *Journal of Applied Electrochemistry,* vol. 31, pp. 509-516, 2001.

[188] Stupnisek-Lisac, E., Brnada, A., and Mance, A.D., "Secondary amines as copper corrosion inhibitors in acid media," *Corrosion Science,* vol. 42, pp. 243-257, 2000.

[189] Desai, M.N. and Rana, S.S., "Inhibition of the corrosion of copper in nitric acid. Aniline and other substituted aromatic amines," *Anti-Corrosion Methods and Materials,* vol. 20, pp. 16-20, 1973.

[190] Abd El Wanees, S., "Amines as inhibitors for corrosion of copper in nitric acid," *Anti-Corrosion Methods and Materials,* vol. 41, pp. 3-7, 1994.

[191] Sherif, E.M. and Park, S.-M., "Inhibition of Copper Corrosion in 3.0% NaCl Solution by N-Phenyl-1,4-phenylenediamine," *Journal of the Electrochemical Society,* vol. 152, pp. B428-B433, 2005.

[192] Sherif, E.M. and Park, S.-M., "Inhibition of copper corrosion in acidic pickling solutions by N-phenyl-1,4-phenylenediamine," *Electrochimica Acta,* vol. 51, pp. 4665-4673, 2006.

[193] Chakraborty, S.B., Bandyopadhyay, T.K., and Chaudhuri, S.R., "Amino acids as corrosion inhibitor for copper in nitric acid," *Bulletin of Electrochemistry,* vol. 8, pp. 111-13, 1992.

[194] Bastidas, J.M., Pinilla, P., Cano, E., Polo, J.L., and Miguel, S., "Copper corrosion inhibition by triphenylmethane derivatives in sulphuric acid media," *Corrosion Science,* vol. 45, pp. 427-449, 2003.

[195] Baeza, H., Guzman, M., Ortega, P., and Vera, L., "Corrosion inhibition of copper in 0.5 M hydrochloric acid by 1,3,4-thiadiazole-2,5-dithiol," *Journal of the Chilean Chemical Society,* vol. 48, pp. 23-26, 2003.

[196] Edwards, M., Hidmi, L., and Gladwell, D., "Phosphate inhibition of soluble copper corrosion by-product release," *Corrosion Science,* vol. 44, pp. 1057-1071, 2002.

[197] Antonijevic, M.M. and Petrovic, M.B., "Copper corrosion inhibitors. A review," *International Journal of Electrochemical Science,* vol. 3, pp. 1-28, 2008.

[198] Allam, N.K., Nazeer, A.A., and Ashour, E.A., "A review of the effects of benzotriazole on the corrosion of copper and copper alloys in clean and polluted environments," *Journal of Applied Electrochemistry,* vol. 39, pp. 961-969, 2009.

[199] Finsgar, M. and Milosev, I., "Inhibition of copper corrosion by 1,2,3-benzotriazole: A review," *Corrosion Science,* vol. 52, pp. 2737-2749, 2010.

[200] Dugdale, I. and Cotton, J.B., "An electrochemical investigation on the prevention of staining of copper by benzotriazole," *Corrosion Science,* vol. 3, pp. 69-74, 1963.

[201] Brusiz, V., Angelopoulos, M., and Graham, T., "Use of polyaniline and its derivatives in corrosion protection of copper and silver," *Journal of the Electrochemical Society,* vol. 144, pp. 436-442, 1997.

[202] Vera, R., Schrebler, R., Cury, P., Rio, R., and Romero, H., "Corrosion protection of carbon steel and copper by polyaniline and poly(ortho-methoxyaniline) films in sodium chloride medium. Electrochemical and morphological study," *Journal of Applied Electrochemistry,* vol. 37, pp. 519-525, 2007.

[203] Redondo, M.I. and Breslin, C.B., "Polypyrrole electrodeposited on copper from an aqueous phosphate solution: Corrosion protection properties," *Corrosion Science,* vol. 49, pp. 1765-1776, 2007.

[204] Redondo, M.I., Sanchez de la Blanca, E., Garcia, M.V., and Gonzalez-Tejera, M.J., "Poly(N-methylpyrrole) electrodeposited on copper: Corrosion protection properties," *Progress in Organic Coatings,* vol. 65, pp. 386-391, 2009.

[205] Chaudhari, S. and Patil, P.P., "Corrosion protective poly(o-ethoxyaniline) coatings on copper," *Electrochimica Acta,* vol. 53, pp. 927-933, 2007.

[206] Kilmartin, P.A., Trier, L., and Wright, G.A., "Corrosion inhibition of polyaniline and poly(o-methoxyaniline) on stainless steels," *Synthetic Metals,* vol. 131, pp. 99-109, 2002.

[207] Herrasti, P., Recio, F.J., Ocon, P., and Fatas, E., "Effect of the polymer layers and bilayers on the corrosion behaviour of mild steel: Comparison with polymers containing Zn microparticles," *Progress in Organic Coatings,* vol. 54, pp. 285-291, 2005.

[208] Tiitu, M., Talo, A., Forsen, O., and Ikkala, O., "Aminic epoxy resin hardeners as reactive solvents for conjugated polymers: polyaniline base/epoxy composites for anticorrosion coatings," *Polymer,* vol. 46, pp. 6855-6861, 2005.

[209] Tan, F., Qiao, X., Chen, J., and Wang, H., "Effects of coupling agents on the properties of epoxy-based electrically conductive adhesives," *International Journal of Adhesion and Adhesives,* vol. 26, pp. 406-413, 2006.

[210] Tee, D.I., Mariatti, M., Azizan, A., See, C.H., and Chong, K.F., "Effect of silane-based coupling agent on the properties of silver nanoparticles filled epoxy composites," *Composites Science and Technology,* vol. 67, pp. 2584-2591, 2007.

[211] Wokaun, A., Baiker, A., Miller, S.K., and Fluhr, W., "Adsorption on catalyst surfaces studied by enhanced Raman scattering," *Journal of Physical Chemistry,* vol. 89, pp. 1910-14, 1985.

[212] Zwolinski M, H.J., Rubon H, Zaks Y., "Electrically conductive adhesives for surface mount solder replacement,"*Proceedings of the second international conference o adhesive joining and coating technology in electronics manufacturing*, Stockholm, Sweden, , 1996.

[213] Inoue, M., Muta, H., Maekawa, T., Yamanaka, S., and Suganuma, K., "Temperature dependence of electrical and thermal conductivities of an epoxy-based isotropic conductive adhesive," *Journal of Electronic Materials,* vol. 37, pp. 462-468, 2008.

[214] Liu, Y., Du, Z., Zhang, C., Li, C., and Li, H., "Curing behavior and thermal properties of multifunctional epoxy resin with methylhexahydrophthalic anhydride," *Journal of Applied Polymer Science,* vol. 103, pp. 2041-2048, 2007.

[215] Karayannidou, E.G., Achilias, D.S., and Sideridou, I.D., "Cure kinetics of epoxy-amine resins used in the restoration of works of art from glass or ceramic," *European Polymer Journal,* vol. 42, pp. 3311-3323, 2006.

[216] Lin, R.-H. and Hsu, J.-H., "In situ FT-IR and DSC investigation on the cure reaction of the dicyanate/diepoxide/diamine system," *Polymer International,* vol. 50, pp. 1073-1081, 2001.

[217] Ngono, Y., Marechal, Y., and Mermilliod, N., "Epoxy-Amine Reticulates Observed by Infrared Spectrometry. I: Hydration Process and Interaction

Configurations of Embedded H2O Molecules," *Journal of Physical Chemistry B,* vol. 103, pp. 4979-4985, 1999.

[218] Sanchez-Soto, M., Pages, P., Lacorte, T., Briceno, K., and Carrasco, F., "Curing FTIR study and mechanical characterization of glass bead filled trifunctional epoxy composites," *Composites Science and Technology,* vol. 67, pp. 1974-1985, 2007.

[219] Carrasco, F., Pages, P., Lacorte, T., and Briceno, K., "Fourier transform IR and differential scanning calorimetry study of curing of trifunctional amino-epoxy resin," *Journal of Applied Polymer Science,* vol. 98, pp. 1524-1535, 2005.

[220] Dusek, K. and Editor, *Advances in Polymer Science,* Vol. 75*:* Epoxy Resins and Composites II Berlin: Springer-Verlag 1986.

[221] St John, N.A. and George, G.A., "Cure kinetics and mechanisms of a tetraglycidyl-4,4'-diaminodiphenylmethane/diaminodiphenyl sulfone epoxy resin using near IR spectroscopy," *Polymer,* vol. 33, pp. 2679-88, 1992.

[222] Rajagopalan, G., Immordino, K.M., Gillespie, J.W., Jr., and McKnight, S.H., "Diffusion and reaction of epoxy and amine in polysulfone studied using Fourier transform infrared spectroscopy: experimental results," *Polymer,* vol. 41, pp. 2591-2602, 1999.

[223] Rigail-Cedeno, A. and Sung, C.S.P., "Fluorescence and IR characterization of epoxy cured with aliphatic amines," *Polymer,* vol. 46, pp. 9378-9384, 2005.

[224] Inoue, M. and Suganuma, K., "The dependence on thermal history of the electrical properties of an epoxy-based isotropic conductive adhesive," *Journal of Electronic Materials,* vol. 36, pp. 669-675, 2007.

[225] Stupnisek-Lisac, E., Kopjar, D., and Mance, A.D., "The inhibition of copper corrosion in acid media," *Bulletin of Electrochemistry,* vol. 14, pp. 10-15, 1998.

[226] Leenen, M.A.M., Arning, V., Thiem, H., Steiger, J., and Anselmann, R., "Printable electronics: flexibility for the future," *Physica Status Solidi A: Applications and Materials Science,* vol. 206, pp. 588-597, 2009.